Bioinspired Jumping Locomotion for Miniature Robotics

THÈSE N^{O} 4742 (2010)

PRÉSENTÉE LE 9 JUILLET 2010

À LA FACULTÉ INFORMATIQUE ET COMMUNICATIONS

LABORATOIRE DE SYSTÈMES INTELLIGENTS

PROGRAMME DOCTORAL EN INFORMATIQUE, COMMUNICATIONS ET INFORMATION

ÉCOLE POLYTECHNIQUE FÉDÉRALE DE LAUSANNE

POUR L'OBTENTION DU GRADE DE DOCTEUR ÈS SCIENCES

PAR

Mirko KOVAC

acceptée sur proposition du jury:

Prof. B. Falsafi, président du jury
Prof. D. Floreano, Dr J.-C. Zufferey, directeurs de thèse
Dr F. Iida, rapporteur
Prof. A. Ijspeert, rapporteur
Dr R. Quinn, rapporteur

ÉCOLE POLYTECHNIQUE
FÉDÉRALE DE LAUSANNE

Suisse
2010

Abstract

In nature, many small animals use jumping locomotion to move in rough terrain. Compared to other modes of ground locomotion, jumping allows an animal to overcome obstacles that are relatively large compared to its size. In this thesis we outline the main design challenges that need to be addressed when building miniature jumping robots. We then present three novel robotic jumpers that solve those challenges and outperform existing similar jumping robots by one order of magnitude with regard to jumping height per size and weight. The robots presented in this thesis, called EPFL jumper v1, EPFL jumper v2 and EPFL jumper v3 have a weight between 7g and 14.3g and are able to jump up to 27 times their own size, with onboard energy and control. This high jumping performance is achieved by using the same mechanical design principles as found in jumping insects such as locusts or fleas.

Further, we present a theoretical model which allows an evaluation whether the addition of wings could potentially allow a jumping robot to prolong its jumps. The results from the model and the experiments with a winged jumping robot indicate that for miniature robots, adding wings is not worthwhile when moving on ground. However, when jumping from an elevated starting position, adding wings can lead to longer distances traveled compared to jumping without wings. Moreover, it can reduce the kinetic energy on impact which needs to be absorbed by the robot structure. Based on this conclusion, we developed the EPFL jumpglider, the first miniature jumping and gliding robot that has been presented so far. It has a mass of 16.5g and is able to jump from elevated positions, perform steered gliding flight, land safely and locomote on ground with repetitive jumps[1].

Keywords: jumping robot, hybrid locomotion, biological inspiration

[1]See the collection of the accompanying videos at http://lis.epfl.ch/microglider/moviesAll.zip

Résumé

Dans la nature, une multitude de petits animaux utilise le saut pour se déplacer sur les terrains accidentés. Si on le compare aux autres moyens de locomotion terrestre, le saut permet de surmonter des obstacles qui sont relativement grands par rapport à la taille de l'animal. Dans cette thèse, nous exposons les principaux défis de conception qui sont liés à la construction de robots miniatures sautants. Puis nous présentons trois robots sautants inédits qui répondent à ces défis et qui, au regard de la taille et du poids, effectuent un saut d'une distance dix fois plus grande que celle produite par des robots sauteurs similaires. Ceux présentés dans cette thèse, appelés EPFL jumper v1, EPFL jumper v2 et EPFL jumper v3, ont un poids compris entre 7g et 14,3g (avec batterie et contrôle) et sont capables de sauter jusqu'à 27 fois leur propre taille. Cette excellente performance de saut est accomplie grâce à l'utilisation des mêmes principes mécaniques trouvés chez les insectes sautants tells que les criquets ou les puces.

En outre, nous présentons un modèle théorique qui permet d'évaluer si l'ajout d'ailes pourrait potentiellement allonger le saut du robot. Les résultats du modèle et des expériences avec les ailes indiquent que pour les robots miniatures, cet ajout ne présente pas d'avantage quand ils se déplacent sur le sol. Cependant, quand le saut prend son départ depuis une position élevée, l'ajout des ailes peut allonger la distance parcourue, par rapport au vol dépourvu d'ailes. De plus, cela peut réduire l'énergie cinétique à l'impact qui doit être absorbée par la structure du robot. A partir de cette conclusion, nous avons développé le robot miniature "EPFL jumpglider", premier à ce jour à pouvoir sauter et planer. Il possède un masse de 16,5g et peut sauter à partir de positions élevées, effectuer un vol plané et dirigé, atterrir sans dommage, et se déplacer sur la terre au moyen de sauts répétés.[2]

Mots clés: robot sauteur, locomotion hybride, inspiration biologique

[2]Voir la liste des vidéos correspondantes: http://lis.epfl.ch/microglider/moviesAll.zip

Acknowledgements

Many people have contributed to the work presented in this thesis. First I would like to thank my two supervisors, Prof. Dario Floreano and Dr. Jean-Christophe Zufferey, for making me part of this project and thus giving me the opportunity to dive into this amazing research field and for giving me both guidance and freedom in the conduct of my PhD project. I thank Dario for his motivation, advices and for offering me countless opportunities where I could gain a foothold in the robotics universe. Jean-Christophe I'd like to thank especially for his honesty, constant support and many valuable discussions.

I would like to thank all my colleagues at the Laboratory of Intelligent Systems for providing the great, stimulating atmosphere. In particular, I would like to thank Mototaka Suzuki, Walter Karlen and Michal Dobrzynski for sharing the office together and the inspirational discussions. Further, I am very thankful for the opportunity to have worked with students during their bachelor and master projects. Their enthusiasm and many overtime hours of work have significantly contributed to the technical aspects of this thesis. As well, I'd like to express my gratitude to André Guignard, Jean-Daniel Nicoud, the Atelier de l'Institut de production et robotique de l'EPFL (ATPR) and the Atelier pour le routage et la fabrication de circuits imprimés de l'EPFL (ACI) for the invaluable help in the iterative fabrication process of the mechanical components for the robots.

A number of people have enriched my life in Lausanne. My special gratitude goes to my meditation friends, who are too numerous to name, for the many unforgettable memories and for living the sense between the lines.

In writing this thesis I have benefitted from comments and helpful discussion provided by a large number of people. I am particularly indebted to Jasminka

Kovač, Jean-Christophe Zufferey and Michal Dobrzynski for their truly tireless efforts in offering advice. I would also like to thank the members of the thesis committee, Prof. Roger Quinn, Prof. Auke Ijspeert, Prof. Fumiya Iida and Prof. Falsafi Babak for reviewing the manuscript. I would like to thank the administrative assistants Anouk Hein and Michelle Walti, for the magic that makes science possible. I would also like to express my gratitude to the EPFL and the Swiss National Science Foundation for their support and for funding my research.

I also thank all my friends for sharing all aspects of life, my parents, Djurdja and Zlatko for their inexhaustive support, trust and patience throughout my last two decades of education, and my sister Jasminka for her unfailing support in all life situations. Last but not least, I would like to thank Jam and Rubini for having been the star shine in the countless nights of thesis writing and for teaching me what really matters, besides a PhD.

Lausanne, July 2010

Contents

Abstract **i**

Résumé **iii**

Acknowledgements **v**

Contents **vii**

1 Introduction **1**

1.1 Jumping locomotion for miniature robotics 1

1.2 Main challenges of jumping locomotion 3

1.3 Jumping locomotion in living organisms 8

1.4 State of the art in robotics 14

1.5 Main contributions and thesis overview 22

2 Take-off **25**

2.1 Introduction 26

2.2 Design 27

2.2.1 Jump energy 28

2.2.2 Mechanical design 31

2.3 Results 32

2.3.1 Prototype 32

2.3.2 High power jumping performance 37

2.3.3 Variable take-off angle and ground force profile 38

2.4 Conclusion 39

3 Landing **43**
3.1 Introduction . . . 44
3.2 Design . . . 44
3.2.1 Protection on landing . . . 45
3.2.2 Uprighting . . . 45
3.2.3 Mechanical and electronic design . . . 46
3.2.4 Control strategy . . . 49
3.3 Results . . . 50
3.3.1 Uprighting and charging . . . 50
3.3.2 Jumping performance . . . 50
3.3.3 Protection on landing . . . 51
3.3.4 Rescue routine . . . 54
3.4 Conclusion . . . 54

4 Preparation for take-off **57**
4.1 Introduction . . . 58
4.2 Design . . . 59
4.2.1 Uprighting mechanism . . . 59
4.2.2 Steering mechanism . . . 62
4.3 Implementation . . . 64
4.3.1 Uprighting mechanism . . . 64
4.3.2 Steering mechanism . . . 64
4.3.3 Integration . . . 67
4.3.4 Adjustment of the jumping parameters . . . 68
4.4 Results . . . 70
4.4.1 The cost of the cage . . . 71
4.4.2 Adjustment of the jumping parameters . . . 71
4.4.3 Locomotion on an obstacle course . . . 74
4.5 Conclusion . . . 74

5 Flight **77**
5.1 Introduction . . . 78
5.2 Jumpgliding versus ballistic jumping . . . 78
5.3 Evaluation of adding wings to jumping robots . . . 86
5.4 Implementation of a jumpglider . . . 88

5.4.1 Jumpgliding performance 92
5.4.2 Discussion 94
5.5 Conclusion 99

6 Concluding remarks **103**

A Comparison to other robots **107**

B Wingfolding **115**

C Autonomous gliding and SMA actuated tail **127**
C.1 Introduction 128
C.2 Design 129
C.3 Results 136
C.4 Conclusion 143

D Perching to walls **145**
D.1 Introduction 146
D.2 Design 149
D.3 Results 161
D.4 Conclusion 168

Bibliography **173**

Publications **191**

Curriculum Vitae **193**

1 Introduction

The aim of this thesis is to describe the main design challenges for miniature jumping robots and to propose robotic solutions that address them. As a result, we present four novel prototypes that outperform existing similar jumping robots by one order of magnitude with regard to jumping height per size and weight.

This introductory chapter begins with the explanation why jumping is more promising than other modes of locomotion for robots to overcome large obstacles. It then describes the main challenges of jumping locomotion for miniature robots. Within this perspective, we summarize the solution to these challenges established in nature and existing jumping robots. Finally, we outline the main contributions of this thesis and give an overview in the following chapters.

1.1 Jumping locomotion for miniature robotics

One of the main challenges for mobile robots is to successfully move in the environment that they inhabit. As the robot decreases in size, it has to face the additional challenge of the obstacles in the environment being bigger relative to it compared to a larger robot. This effect is usually referred to as the 'Size Grain Hypothesis' [74], which is defined as an 'increase in environmental rugosity with decreasing body size'.

In this thesis, we focus on miniature robots, which we define as having a maximal body size between 3cm and 50cm and a mass between 3g and 500g. The interest of having such small robots is that they can be employed in situations such as the exploration of celestial bodies or for environmental monitoring,

where the mass and size of the equipment is a major constraint [160]. Deployed as a swarm, a collective system consisting of such small robots can potentially outperform an equally heavy single robot solution in application such as distributed sensing in rough terrain.

The most common solution to provide such miniature robots with locomotion ability is the addition of wheels to the robot's body as for example in the 'Robomote' [133] or the 'ALICE' robot [30]. This straight-forward approach has the advantage of being simple and robust because it can be realized using only one actuator to drive the wheels. However, it easily fails when encountering obstacles to overcome. The largest obstacle size that can be overcome using wheels are around 1.5 times the wheel diameter [23]. Alternative designs that use inflatable wheels or body hinges have been proposed enabling the robot to overcome bigger obstacles such as in [71]. Nonetheless, wheeled designs are fundamentally limited in the obstacle size compared to the body dimension that can be overcome. Wheels are therefore not the optimal solution for miniature robots that are intended to overcome large obstacles.

With a similar obstacle traversability performance to wheels, legs can be used to move in rough terrain, such as in the piezo-actuated hexapod runner [50]. The advantage of legs compared to wheels is that they offer improved ground traction and terrain adaptability which is advantageous in uneven and rough terrain [136]. However, the designs are mechanically more complex than wheels and need numerous joints, actuators and linkages. Recently, Birkmeyer et al. [16] presented a simpler solution for legged locomotion. It consists of a 10cm hexapod robot that employs an elegant mechanical design which collapses the dimensionality of the locomotion control to one motor only in order to perform running. With a similar control simplicity, the hybrid solution called 'whegs' uses a variation of segmented wheels to combine the simple implementation of wheels with the terrain adaptability of legs [101]. Although the control of these legged robots is reduced to a minimum, they remain limited to terrains with obstacles of only a few centimeters in height. In order to increase their capacity to overcome larger obstacles, a solution to add climbing capabilities would be needed. A possibility as observed in nature, for example in spiders could be added to legged or wheeled robots. Examples of such climbing robots were presented in e.g. [6, 103, 115, 125, 152]. However, they typically climb slowly

and are limited to relatively flat surfaces, which is currently the main drawback of climbing robots.

An alternative solution is to use flight to overcome ground obstacles such as in [46, 76, 119, 168]. However, flying locomotion is energetically more expensive compared to wheeled or legged locomotion.

One other possibility to tackle locomotion in rough terrain for small robots is to adopt jumping. In contrast to other ground locomotion methods, jumping offers the advantage that it allows the robot to overcome obstacles of several times its size by executing one, comparably simple, leg extension. The motion strategy known as 'pause and leap' can be employed to overcome large obstacles. It consists of a powerful jump which is altered with a pause phase where the jumper recharges for the next jump. This allows the robot to overcome comparably large obstacles which would not be possible with a legged or wheeled locomotion strategy.

Based on this rationale, we investigate in this thesis jumping locomotion in miniature robotics. The following section defines the main challenges that need to be addressed when using jumping locomotion for miniature robots.

1.2 Main challenges of jumping locomotion

A jumping sequence can be decomposed in several phases. We define these phases as (i) take-off, (ii) flight, (iii) landing and (iv) preparation for the next take-off (figure 1.1). In each of these phases, a number of challenges need to be addressed to use jumping as a successful form of locomotion. In this section we describe those phases in detail to pinpoint the implications that they have on the design of miniature jumping robots.

Take-off

The first phase that we consider is take-off, which refers to the initial propulsion of the robot into the air. The first challenge for the take-off phase is to keep the mass of the robot as low as possible. We provide here an overview of the basic underlying equations to illustrate this challenge. The jumping distance d and jumping height h of an object moving on a ballistic trajectory under gravity g

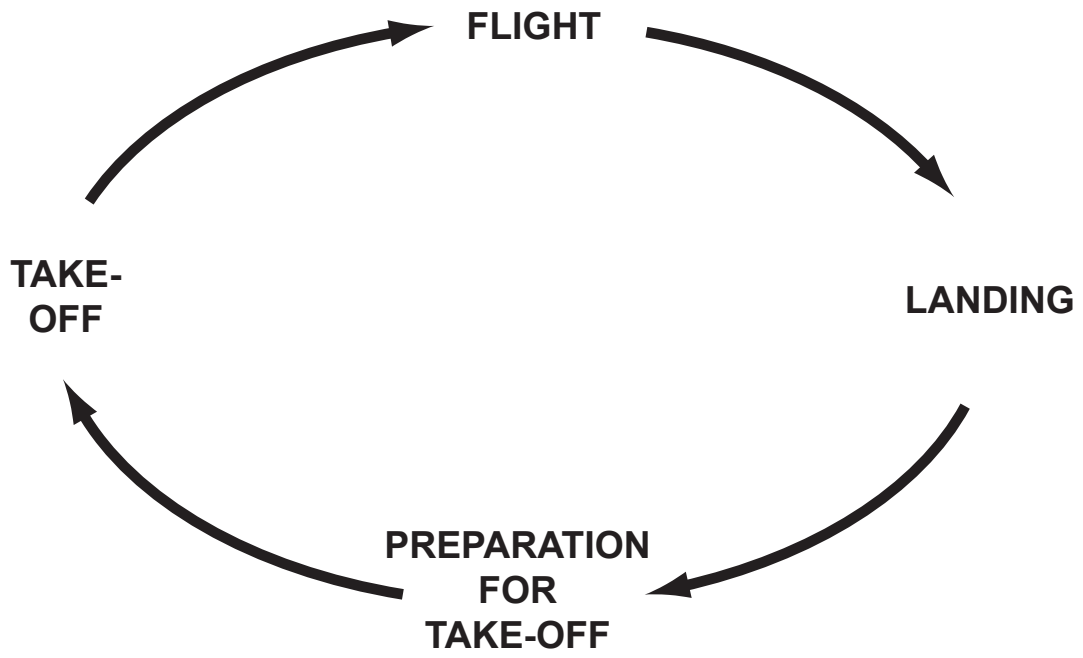

Figure 1.1: Four phases of jumping locomotion

when launched with a take-off velocity v_0 is given by [3]

$$v_0 = \sqrt{\frac{2E}{m}} \tag{1.1}$$

$$d = \frac{v_0^2 \sin 2\alpha_0}{g} \tag{1.2}$$

$$h = \frac{(v_0 \sin \alpha_0)^2}{2g} \tag{1.3}$$

In these equations we assume the ideal case with no air friction, an initial take-off energy E, take-off angle α_0 and a robot mass m. This means that the maximal jumping distance is reached at a take-off angle of $\alpha_0 = 45°$ and a maximal jumping height is reached at $\alpha_0 = 90°$. Furthermore, we see from these basic equations that both the jumping height and the jumping distance increase linearly with decreasing robot mass.

An important note related to this first challenge is the distribution of mass between the leg and the main body of the robot. Alexander [3] described this influence with the help of the so-called 'cost of transport' T which is defined as

the kinetic energy of a jumping system divided by the mass and distance of a jump. It can be used as an indicator for the jumping efficiency. With a being the fraction of the leg mass divided by the robot mass we can express the cost of transport as

$$T = \frac{g}{2(1-a)\sin(2\alpha_0)} \tag{1.4}$$

Reducing the fraction a allows to decrease the cost function T and obtain more efficient jumps. Consequently, to overcome larger obstacles per given jumping energy, one needs to reduce the entire robot mass (equation 1.2 and 1.3) and especially the weight of the legs (equation 1.4).

The second challenge is to perform a high power jump. This challenge increases in importance when the robot is scaled down. The power P of the actuation that needs to act on the robot to accelerate it to the take-off velocity is given by

$$P = \frac{E}{\Delta s} \cdot v_0 = \frac{m v_0^3}{2\Delta s} \tag{1.5}$$

with Δs being the acceleration distance to reach the take-off velocity v_0. Decreasing the size of the robot geometrically and assuming a constant robot mass and take-off velocity, the jumping energy has to be exerted within a shorter acceleration distance Δs, requiring a higher power jump. For example, a robot of 10g that is expected to jump a height of 1m at a take-off angle of 90°, needs a take-off energy of $E = mgh = 98.1mJ$. Assuming an acceleration distance of $\Delta s = 3cm$, this corresponds to a jumping power of 14.5W, which is very difficult to realize at a robot weight of only 10g. For comparison, a brushless DC servo-motor producing 11W weights 31g [64]. Therefore, we define the second challenge for the take-off phase to be the supply of such a high power actuation.

The third challenge is the ability to change the force profile which acts on the ground, while the system accelerates. From equation 1.5 we can derive the average force acting on the ground as:

$$F_{ave} = \frac{P}{v_0} \tag{1.6}$$

This force can be several times the weight of the robot. In the example given

above of the 10g robot exerting 14.5W, the average force is 3.27N, which corresponds to 33.3 times the robot's weight. One must ensure that this force is transmitted to the ground without slipping on the surface or prematurely taking off. Both would drastically decrease the jumping efficiency, which has been described in more detail in e.g. [5, 129, 164**?** , 165]. Therefore, the third challenge is the ability to adapt the ground force profile during the take-off phase.

The fourth and final challenge related to the take-off phase is the adaptability of the take-off angle. Depending on the environment in which the robot locomotes, it may be desirable to change the take-off angle [39, 145]. For example, in a terrain with many large obstacles, a higher take-off angle is preferable for locomotion because it allows for jumps over larger obstacles for the same jumping energy compared to a shallower take-off angle. In an environment with smaller obstacles, a take-off angle closer to 45° is preferred because it allows for a larger horizontal distance covered per jump.

Flight

Once the robot leaves the ground, it moves on a unpropelled trajectory through the air. The first challenge is to ensure a compact size to yield low aerodynamical friction. The aerodynamic friction can be described by the aerodynamical drag force as

$$F_{drag} = \frac{1}{2} c_d A_d \rho v^2 \tag{1.7}$$

with c_d being the aerodynamical friction coefficient, ρ the air density and A_d the robot's cross-sectional surface area in the direction of flight. The first challenge of the flight phase is therefore decreasing c_d by choosing an aerodynamical shape and decreasing A_d by keeping the jumping robot compact.

A possibility for jumping robots to increase the jumping distance is to use wings to prolong the jump by gliding. We call this concept 'jumpgliding'. As opposed to a jumping robot which moves on a ballistic trajectory in air and is completely passive during the flight phase, a jumpgliding robot can produce lift and could as well steer while airborne.

For jumpgliders, we define the second challenge during the flight phase as creating lift in order to reach further distances for the same energy. Similarly to

the aerodynamical drag, the aerodynamical lift force F_{lift} can be expressed as

$$F_{lift} = \frac{1}{2} c_l A_l \rho v^2 \tag{1.8}$$

with c_l being the lift coefficient and A_l the surface of the wings. To create lift, we need to increase the lift coefficient of the wing and have as large wings as possible.

The third challenge for the flight phase of jumpgliders is steering in air. Compared to jumping robots without wings, jumpgliders could use their wings to change the trajectory while airborne, which is an alternative solution to steering on ground.

Landing

The first challenge for the landing phase is to protect the robot from mechanical damage. The impact forces on landing can be relatively high and depend on the elasticity and damping coefficient of the robot structure [39]. The impact force can be expressed as

$$F_{impact} = \frac{m v_0^2}{2 \Delta s_{impact}} \tag{1.9}$$

with v_0 being the impact velocity and Δs_{impact} the elastic deformation on impact. Assuming that the 10g robot from our example drops from a height of 1m and experiences an elastic deformation on impact of $\Delta s_{impact} = 1mm$, the impact force F_{impact} is 98.1N, which is 1000 times the robot's weight. It is therefore essential to provide the robot with either protecting structures or wings to decelerate and decrease the impact force for a damage-free landing.

After impact with the ground, the robot needs to prepare for the next take-off sequence. When jumping from and landing on uneven surfaces, it is very difficult to ensure that the robot will land on its feet. Assuming that the robot lands on its side or upside down, the second challenge of the landing phase is to upright in order to take off again. This uprighting movement can happen actively using an uprighting mechanism or passively due to the shape or center of gravity position of the robot.

Table 1.1: Challenges for jumping locomotion

Take-off:	1) Small mass 2) High power actuation 3) Variable take-off angle 4) Variable ground force profile
Flight:	1) Compact size and low air friction 2) Aerodynamical lift 3) Steering in air
Landing:	1) Protection on impact with ground 1) Uprighting
Preparation for take-off:	1) Steering on ground 2) On board energy

Preparation for take-off

The first challenge for the preparation phase is the ability to steer on ground. As explained above, for jumpgliding robots, the steering could as well happen during the flight phase and does not necessarily need to be done during the preparation phase. For jumpers that do not influence the flight phase, a reorientation on ground prior to take-off is necessary to perform steered jumps.

The second challenge related to the preparation phase is on board energy. In order to operate by itself over longer periods of time, the robot should be able to perform several jumps with on board energy, without being connected with cables to a controller or a power supply.

These eleven challenges of jumping locomotion for miniature robots are summarized in table 1.1.

1.3 Jumping locomotion in living organisms

Jumping locomotion is widely used by a variety of animals. In this section we describe how jumping animals address the challenges for the four phases of jumping locomotion. We aim at extracting the biomechanical design principles that allow them to locomote by jumping in rough terrain and overcome obstacles of several times their own size. We do not focus on one particular animal. Instead, we attempt to summarize what has been presented in biological literature

that is relevant to the challenges of jumping locomotion for miniature robots.

Take-off

The mass of small jumping animals varies over several orders of magnitude and has to be kept as low as possible to yield high jumps [11]. For example, frogs range from a fraction of a gram for the 9mm Brazilian Gold Frog up to 3kg for the 33cm Goliath frog [146]. Fleas weigh around 0.2g [121] and large locusts up to 30g with a size of approximately 14.5cm [122]. There is evidence that locusts have legs that are optimized for light weight, due to their extremely low mechanical safety factors of only between one and two [108]. The safety factor indicates how much more force can be sustained by the leg structure relative to the force acting on it during an average jump [147].

Alexander [2] modeled and compared the jumping techniques of different jumping animals from insects to humans. He categorized them in three classes which he called 'squat jump', 'countermovement jump' and 'catapult jump'. In his model, the jumping animal is represented by a body that is actuated using two segmented legs as illustrated in figure 1.2.A. The leg consists of a muscle (a), connected in series with an elastic element (b). The main underlying condition for his model is that the muscle force is always in equilibrium with the elastic element. For the three jumping techniques, the coordination of muscle contraction, leg extension and the jumping movement is different. Therefore, it leads to different jumping heights depending on the employed technique. The distinctiveness of the catapult jump is that the legs are locked at an initial angle and the muscles can slowly charge the elastic element. Once the maximal isometric muscle force is build up and the elastic element is completely charged, the knees are unlocked using a click mechanism and start extending.

The criterion used to define the category of jumping in an animal is the fraction Fr of peak ground force in standing jumps divided by the body weight. The fraction of the peak ground force to body weight is typically around 1-3 for humans, about 18 for desert locusts and 135 for fleas [1]. Alexander distinguishes between 'human-like' ($Fr = 1$), 'bushbaby-like' ($Fr = 5$) and 'insect-like' ($Fr = 25$) jumping animals.

Based on the simulation results, Alexander concludes that for 'insect-like'

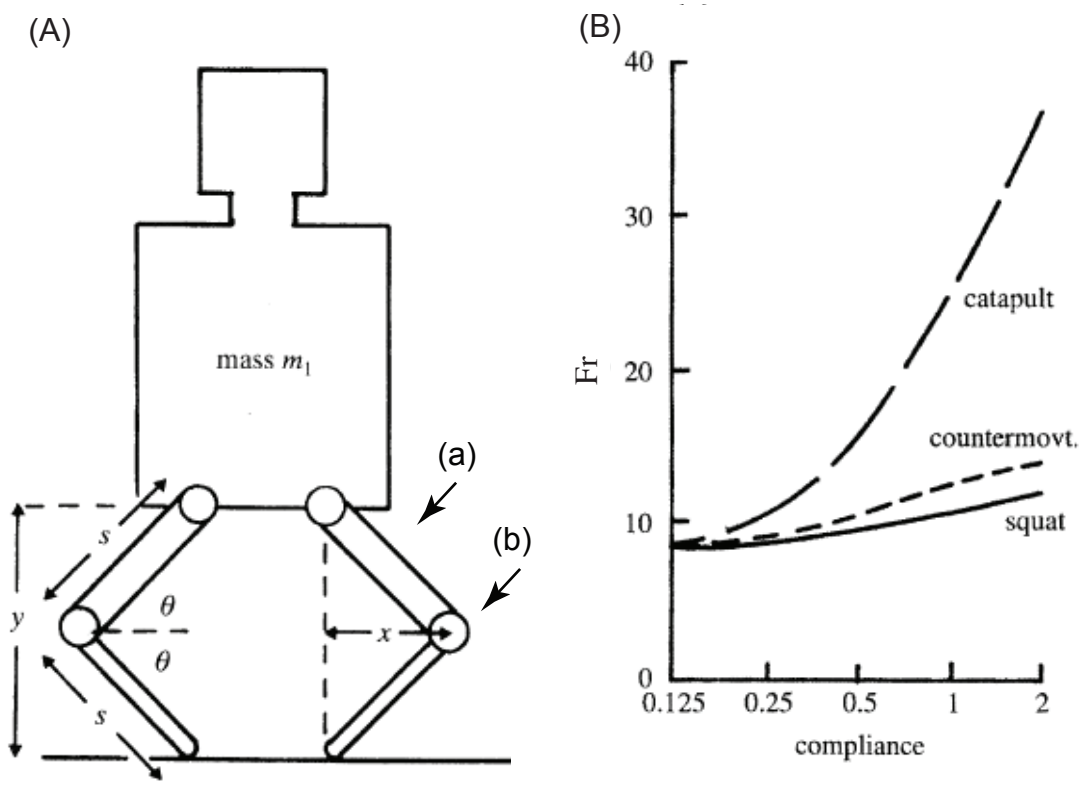

Figure 1.2: A: Two segmented leg and body model for the simulation of jumping performance as described in [2]. The leg consists of a muscle (a) connected in series with an elastic element (b). B: Simulated jumping height for the different jumping techniques and different compliances C for the elastic element in the leg

jumping animals, such as for locusts, the catapult jumping technique leads to a higher jumping height compared to squat jumps or countermovement jumps (figure 1.2.B). The reason for this is that for the catapult jump, the muscles can contract slowly, which allows them to develop their maximal force and charge more energy in the elastic element. The advantages of using the catapult jumping techniques for small animals has as well been described for trap jaw ants [54], stick insects [27], froghoppers [25] and fruit-fly larvae [95].

Regarding the underlying functional design principle for the legs, locusts use a four-bar mechanism [58]. The main advantages of a four-bar mechanism is that the trajectories of the links can be modified by changing the length of the four bars. When used for the leg design, this allows to change the take-off angle and the ground reaction force profile.

Flight

Although, to the best of our knowledge, there are no animals that use the combination of jumping and gliding flight on ground as their principal mode of locomotion, there are many examples of animals that combine jumping with gliding flight from elevated positions. It has evolved in a variety of different animal species. Gliding lizards, gliding geckoes, gliding ants, ballooning spiders, gliding squids, gliding frogs, gliding mammals, gliding snakes and many birds jump, typically from elevated positions such as trees and perform goal directed gliding flight. Jumping and gliding can also be found amongst extinct animals species such as the *Sharovipteryx* and some lizard like reptiles with similar wings to the *Draco* lizard. Figure 1.3 gives an overview of animals that use jumpgliding as part of their locomotion strategy along with scientific references. Furthermore, it has been argued [21, 40, 41, 96] that the combination of jumping from trees, combined with gliding may have been the precursor to flapping flight in insects and vertebrates due to its simplicity.

However, the role of jumping in these animals is not to overcome large obstacles and move over rough ground terrain, but to initiate the gliding phase [29]. As the focus of this thesis is of technological nature, the reader may be referred to [8, 40, 107, 141] for in-depth reviews of jumpgliding animals with detailed description of morphology and behavior. Nevertheless, two benefits of jumpgliding compared to jumping without gliding are important to mention for the application to miniature jumping robots. First, jumpgliding can reduce the potentially hazardous kinetic energy of landing. Second, a jumpgliding locomotion strategy allows the animal to cover larger horizontal distances when jumpgliding from elevated positions.

Besides these jumpgliding animals, there are many insects, such as fruit flies, locust or shore bugs that use jumping to initiate the flight phase [26, 31]. The jumping height of a system decreases with increasing mass and aerodynamical friction. Bennet-Clark and Alder [12] examined the effect of air friction on the jumping performance of insects. He concludes that the insect needs to reduce the fraction A/m, with A being the frontal area and m the mass of the jumping animal and that therefore the body of the jumping animal should be as compact as possible. Further, he states that the air friction increases in importance for

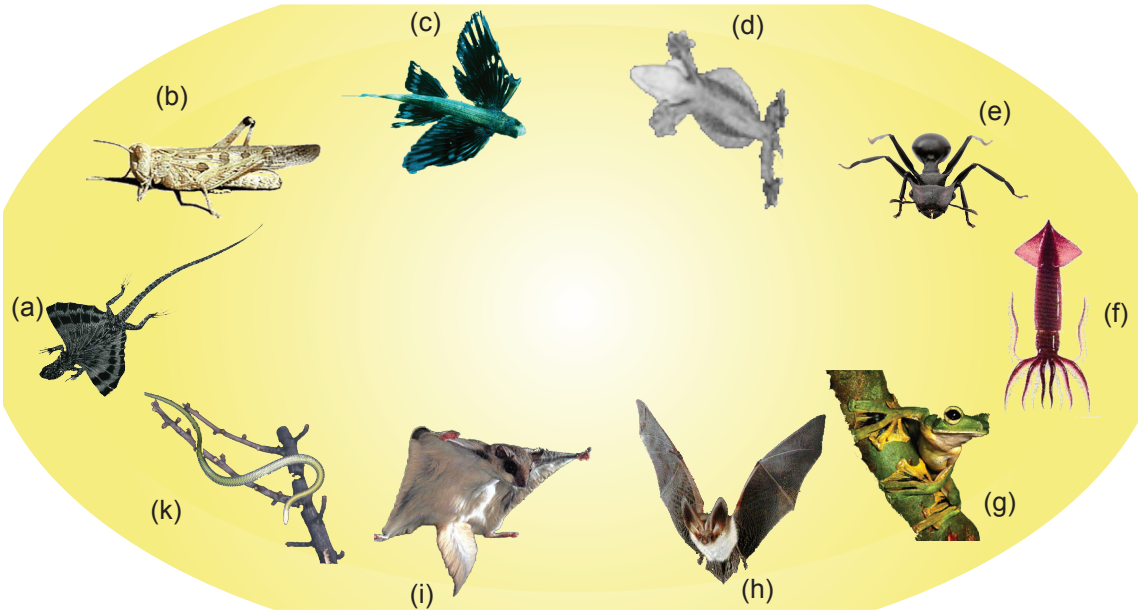

Figure 1.3: A selection of animals that use jumping and gliding as part of their locomotion strategy. (a) gliding lizards [89, 98, 99, 109], (b) locusts [123], (c) flying fish [8, 38], (d) gliding geckoes [72, 161], (e) gliding ants and spiders [36, 139, 158, 159], (f) gliding squid [8, 92], (g) gliding frogs [42, 97], (h) bats [143], (i) gliding mammals [17, 29, 100, 110], (k) gliding snakes [134, 135]

smaller animals. Locust that would reach a jumping height of 1m in vacuum, only reach around 0.65m in air, whereas fleas only reach around 0.4m in air for a 1m jump in vacuum.

Although wings increase the mass of the animal during jumping and therefore decrease the jumping performance, several animals use jumping to initiate winged flight. However, no correlation has been found between the exact moment when the flapping starts relative to the moment of take-off for shore bugs [26] and locusts [111]. This indicates that in such cases, it is sufficient if the wing flapping movements start about at the same time as the jump is executed and that the added friction of the open wings may not be important for the flight initiation jump [31].

Landing

Jumping insects often have an exoskeleton which protects them on landing allowing it to land in any position without major damage. It allows them to adopt a jumping strategy where they land in any position and upright for the next

take-off sequence. For example click beetles, fleas and other small animals such as the soft-bodied jumping springtail moths have been shown to land in any orientation after a jump [32, 121, 162].

This is very different in larger vertebrates such as kangaroos for example which typically try to land on their feet. It has been argued that this difference is due to the fact that the volume and mass scale to the power of three with the linear size of the animal [22, chap. 4]. This means that a larger animal generally has to support larger stresses and strains on its structure than a smaller one. As an illustrating example, we can imagine an animal which is scaled up to twice its size with the same shape. It will consequently be eight times as heavy and will have to support eight times higher forces with its skeleton. The same principle applies when the animal is moving at a velocity v; Its kinetic energy is defined as $E_{kin} = \frac{1}{2}mv^2$ which is a linear function of the mass m. If we assume that the deceleration distance on impact after a jump scales linearly with the body dimension of the jumping animal, it follows that the forces on landing are eight times higher for the animal of twice the size [112, chap. 10]. This fact may be a reason why it is not necessary for small jumping insects to land on their feet, since the impact forces on landing are much smaller for them than for larger animals. Additionally, the jumping strategy of not landing on the feet may be useful because of the above mentioned 'Size Grain Hypothesis' [74]. Locusts for example typically inhabited terrain which is very rugose relative to their size and makes it very difficult to stably land on their feet. After impact with the ground, insects perform righting movements using their legs as described for locust [47] and beatles [45].

Preparation for take-off

To steer the jumps, locust use their forelegs and lean towards the side where they want to jump [124]. This allows them to change the take-off direction by as much as 50° on each side, while the hind legs, which perform the jump, do not change their kinematics. Card and Dickinson [31] show that fruit flies use a similar strategy and shift their center of mass to steer the jump. Springtail morphs rotate their body on the spot, sometimes combined with short crawling to position themselves and perform steered jumps [162].

Table 1.2: Design principles used by desert locusts to address the challenges of jumping locomotion

Jumping phase	**Challenge**	**Design principle used by desert locusts**
Take-off:	1) Small mass	Legs are optimized for high strength and low weight
	2) High power actuation	Slowly charging an elastic element and releasing it quickly using a click mechanism
	3) Variable take-off angle	Using a four-bar mechanism for the legs
	4) Variable ground force profile	Using a four-bar mechanism for the legs
Flight:	1) Compact size and low air friction	Reached by having an elongated body shape
	2) Aerodynamical lift	Using wings
	3) Steering in air	Using aerodynamical appendages
Landing:	1) Protection on impact with ground	Using protecting structures
	2) Uprighting	Position of the center of gravity is shifted and using the legs to upright
Preparation for take-off:	1) Steering on ground	Rotating on the spot to perform steered jumps
	2) On board energy	Using stored chemical energy

Table 1.2 illustrates the design principles found in jumping animals. Although different jumping animals share these biomechanical design principles, we choose to illustrate them on the model of the desert locust (*Schistocerca gregaria*), due to its extensive coverage in biology literature.

1.4 State of the art in robotics

There is a relatively large body of work related to using jumping as a locomotion method for mobile robots for different applications and at different scales. Since the challenges and the fabrication methods vary significantly for different robot sizes, we limit our review to related work on miniature jumping robots with a size between 3cm and 50cm and a weight between 3g and 500g. Separate

literature may be consulted for larger robots such as the 2.5kg Sandia combustion powered jumpers [150], the 29.2kg quadruped 'AirHopper' [140], the 2.3kg Rescue robot [145], jumpers for applications in space [23] or humanoid jumpers [105]. Other projects explore and prototype the feasibility of jumping locomotion for millimeter scale robots [13][163]. Robots that use small sequential jumps as a continuous hopping gait for locomotion on ground have been presented in e.g. [14, 15, 69, 118].

The miniature jumping robots that we review in more detail are depicted in figure 1.4. We classify these robots in four classes which reflect their increasing locomotion capabilities. The first three robots (figure 1.4.A-C) belong to the class of jumping robots that focus on the actuation principle and are powered and controlled off-board. The second class consists of robots that are able to perform repetitive standing jumps with on board energy and control (figure 1.4.D). The third class includes robots that are able to perform repetitive standing jumps with onboard energy and control, but without the ability of steering (figure 1.4.E-F). To the fourth class we count robots that can perform repetitive steered jumps with onboard energy and control (figure 1.4.G-I). Jollbot (figure 1.4.G) can rotate its center of gravity around its axis, which allows for slow rolling and steering the jump. Scout and Mini-Whegs (figure 1.4.H and 1.4.I) are wheeled designs which are able to drive over flat surfaces and jump over obstacles. Compared to the other designs which use only jumping as their locomotion method, wheels allow them to propagate faster on surfaces when there are no large obstacles to overcome. However the added wheels potentially decrease the jumping height due to their added mass.

In the following four subsections, we will review the principles of how these existing robots address the challenges of jumping locomotion for the four phases as described above. A more detailed summary is given in table 1.3, along with a comparison of their jumping performance in table 1.4. As performance metrics we choose the mass, size, jumping height, jumping distance, jumping height per mass, the jumping height per size and the jumping height per mass and size. This last value is of particular interest because it indicates the roughness of the terrain that a robot can overcome for its size and weight. It is an indication of the energy density of the jumping robot.

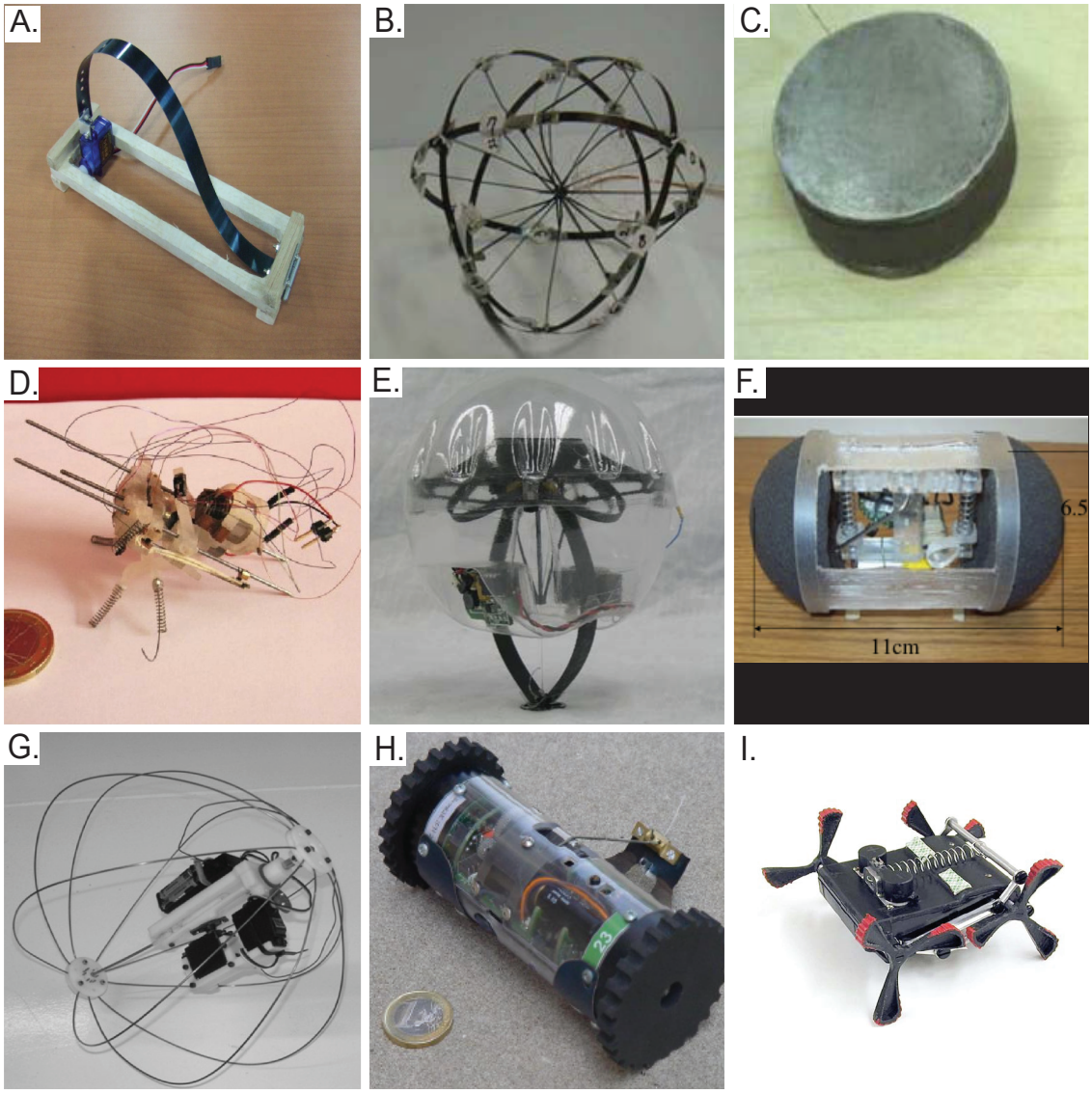

Figure 1.4: Existing miniature jumping robots. A: Closed elastica jumper [157], B: Spherical crawling/rolling robot [138], C: Voice coil jumper [163], D: Grillo [127], E: Microbot [39], F: Michigan jumper [165], G: Jollbot [5], H: Scout [137], I: Mini-Whegs [87]

Table 1.3: Summary of the solutions found in existing robots to address the challenges of jumping locomotion (continued on the next page). The flight phase is not included because its challenges are not addressed by any of the nine robots presented in the state of the art

	TAKE-OFF			LANDING		PREPARATION FOR TAKE-OFF	
Name	High power actuation	Variable take-off angle	Variable ground force profile	Protection	Uprighting	Steering	On board energy
Class 1: Able to perform standing jumps							
Closed elastica jumper Yamada et al. [157]	Using power amplification based on energy storage in an elastic buckling mechanism	Not addressed	Not addressed	Not addressed	Not addressed	Not addressed	Not addressed
Voice coil jumper [163]	Direct actuation based on voice coil	Not addressed	Not addressed	Not addressed	Not addressed	Not addressed	Not addressed
Spherical crawling/rolling robot [138]	Using SMA wires to charge elastic ribbons which are released to jump	Not addressed	Not addressed	Yes, using elastic ribbons as outer shell	Yes, when charging by changing its shape	Not addressed, but crawling ability allows it to propagate in a wanted direction	Not addressed
Class 2: Able to perform standing jumps with on board energy							
Grillo [127]	Using an electric motor to charge a spring which releases a piston to jump	Not addressed	Not addressed	Not addressed	Not addressed	Not addressed	Yes, using onboard batteries

	TAKE-OFF			LANDING		PREPARATION FOR TAKE-OFF	
Name	High power actuation	Variable take-off angle	Variable ground force profile	Protection	Uprighting	Steering	On board energy
Class 3: Able to perform repetitive standing jumps with on board energy							
Microbot [39]	Dielectric Elastomer Actuators (DEA) are used to charge a bistable snapping mechanism which is released to jump	Not addressed	Not addressed	Yes, using a plastic shell around the mechanism	Yes, passively through center of gravity position	Not addressed	Yes, using a miniature fuel cell
Michigan jumper [165]	Using an electric motor to charge a linear spring which is released to jump	Not addressed	Not addressed	Not addressed	Yes, passively through center of gravity position	Not addressed	Yes, using on-board batteries
Class 4: Able to perform repetitive steered standing jumps with on board energy							
Jollbot [5]	Using an electric motor to charge linear springs which are released to jump	Not addressed	Not addressed	Yes, using an elastic cage	Yes, by shifting the center of gravity position	Yes, by leaning prior to jumping. Additional ability of rolling by rotating a mass around its axis	Yes, using on-board batteries
Scout [137]	Using an electric motor to charge an elastic ribbons coiled around its body which is released to jump	Not addressed	Not addressed	Not addressed	Yes, passively through center of gravity position	Not addressed, but wheels allow it to propagate in a wanted direction	Yes, using on-board batteries
Mini-Whegs [87]	Using an electric motor to charge a linear spring which releases a four-bar mechanism to jump	Not addressed, but possible by changing the geometry of the four-bar mechanism	Not addressed, but possible by changing the geometry of the four-bar mechanism	Not addressed	Not addressed, but can run on its back and change its orientation by running into a wall	Not addressed, but wheels allow it to propagate in a wanted direction	Yes, using on-board batteries

Table 1.4: Performance of existing miniature jumping robots

Name	mass [g]	size [cm]	jump height [cm]	jump distance [cm]	jump height per mass[a] [cm/g]	jump height per size[a] [-]	jump height per mass and size[a] [cm/ (10^2·cm·g)]
Class 1: Able to perform standing jumps							
Closed elastica jumper [157]	30*	30.5	20	70	1.18*	1.16	3.86
Voice coil jumper [163]	42*	3	5	0	0.12*	1.67	3.97
Spherical crawling/rolling robot [138]	5*	9	20	5	4.02*	2.23	44.62
Class 2: Able to perform standing jumps with on board energy							
Grillo [127]	8	5	5	20[b]	1.25	2	25
Class 3: Able to perform repetitive standing jumps with on board energy							
Microbot [39]	11	46	38	0	3.45	0.83	7.51
Michigan jumper [165]	42	11	15	11	0.37	1.4	3.36
Class 4: Able to perform repetitive steered standing jumps with on board energy							
Jollbot [5]	465	29.4	18.4	0	0.04	0.63	0.13
Scout [137]	200	11	30	20	0.15	2.8	1.4
Mini-Whegs [101]	190	10.4	22	22	0.12	2.25	1.18

* Weight without batteries or control unit

[a] Jumping height at 90°, calculated using equation 1.1-1.3

[b] Value N/A, here calculated (equation 1.1-1.3), assuming a take-off angle of 45°

Take-off

The mass of the robots that have their power and control electronics on board ranges between 8g and 465g. The maximal jumping height per mass is 1.18 for class 1, 1.3 for class 2, 0.83 for class 3 and 0.12 for class 4 robots. These values indicate that the obstacle size that a robot can overcome for its mass is reduced for higher class robots which have more sophisticated locomotion capabilities.

The high power actuation is realized in eight out of the nine robots by first slowly charging an elastic element and releasing it quickly to jump. The only robot that uses direct actuation to jump is the voice coil jumper. It is as well the robot with the lowest jumping height per mass in the comparison. A variability of the take-off angle and ground force profile has not been shown for any of the robots in this review. However, for the Mini-Whegs it may be possible by changing the geometry of the four bar leg mechanism that it uses to perform the jump.

Flight

None of the nine miniature jumping robots address specifically the flight phase or create lift to prolong the jump. Armour et al. [5] have built a relatively heavy 0.7kg jumping robot of 50cm size called 'Glumper' that jumps and deploys membraneous wings with the intention to increase the jumping distance. However, the final prototype actually jumps further without wings than with them. Scarfogliero et al. [127] mention in their future work section eventual extensions of the Grillo robot with wings to prolong the jump but no realization has been presented so far. Another recent development is the hybrid locomotion platform MMALV [18]. Although it can not jump, it is mentioned here because it incorporates the transition from moving on elevated positions to flight, similar to the jumpgliding concept described above. It can crawl, fold its wings to enter narrow spaces and perform propelled steered flight after dropping down from roofs. Its main limitation is that it has a relatively high wing loading and needs a height loss of around 7m to transition to propelled flight. Since the flight phase has not been addressed by any miniature jumping robot, we leave it out in table 1.3.

Landing

Protection on landing has not been addressed specifically with modeling or experiments by any of the nine robots. The only exception is [39] which models the impact with the ground as a spring damper system and examines different terrain materials for Microbot, but without experimental results on the impact behaviour. Several robots protect the mechanism on landing by using a damping cage such as for the spherical crawling/rolling robot, Microbot, the Michigan jumper and Jollbot. However, no systematic characterization of mechanical robustness or forces acting on the systems when impacting with the ground has been presented so far.

Uprighting is achieved in the caged systems Microbot, the Michigan jumper and Jollbot by positioning the center of gravity in the lower part of the structure. The scout robot and Mini-Whegs have as well their center of gravity in the lower part of their body, but are not able to upright by rolling such as the caged systems. Therefore, for them it may be impossible to upright in case they land upside down.

Preparation for take-off

Steering is possible only in the class 4 robots. Jollbot shifts its center of gravity to change the take-off direction. Scout and Mini-Whegs use their wheels to orient themselves prior to jumping. On board energy is realized using batteries for all the robots except Microbot which uses Fuel cells to power its jumps.

Summarizing, the robots to date share some of the features that allow them to address the challenges of jumping locomotion. For the take-off phase, eight out of the nine robots use the motion strategy 'leap and pause' and charge slowly an elastic element and release it quickly to perform a high power jump. However, no characterization has been presented for a variation of take-off angle or ground force profile.

A further major limitation of current miniature jumping robots is their jumping performance. The maximal obstacle size that they can overcome is in average over all the nine robots only 1.66 their size, which is about the limit reachable with inflatable wheels. The flight phase has not been addressed by any of the robots and none have wings to create lift to prolong the jumps. For the landing

phase, the main limitation is that no systematic characterization of mechanical robustness or impact forces has been presented to date for the existing robots. For the preparation for take-off phase, the only robot that is able to upright after landing in any position and to perform steered jumps is Jollbot. However, its jumping performance is with a maximal jumping height of 0.67 times its size the lowest compared to other miniature jumping robots.

1.5 Main contributions and thesis overview

The main contribution of this thesis is to describe and solve the challenges of jumping locomotion for miniature robots in a much more effective way than other robots presented to date.

This introductory chapter has defined the main challenges of jumping locomotion for miniature robotics and has summarized how existing jumping robots and jumping animals address these challenges while being light-weight and able to overcome large obstacles. Also, we have defined the performance metric that is used to evaluate and compare the success of our solutions, namely the jumping height relative to the mass and size of the jumping robot.

The following four chapters describe how the challenges for the jumping phases 'take-off', 'landing', 'preparation for take-off' and 'flight' can be addressed. In each chapter we present a robotic prototype which represents our solution to the corresponding challenge, providing a tangible proof of concept. Chapter 2 introduces the 'EPFL jumper v1' a miniature jumping robot with a mass of 7g capable of performing standing jumps of more than 27 times its own height. It constitutes the propulsion unit for the prototypes presented in chapter 3, 4 and 5. Chapter 3 describes the development of our 'EPFL jumper v2', a caged system of 9.8g. It is capable of performing repetitive jumps autonomously and is featuring a control strategy which allows it to free itself from stuck situations. In chapter 4 we present the 'EPFL jumper v3', a 14.3g caged jumping robot capable of performing repetitive steered jumps. This robot successfully demonstrated its ability to repetitively move over several obstacles in series, such as three stairs of 45cm height each. In chapter 5 we evaluate whether the addition of wings to a jumping robot can prolong the jumping distance for miniature robots. We then present a novel robot called 'EPFL jumpglider' that can perform repetitive

jumps and goal directed gliding flight.

In chapter 6, we conclude the thesis and provide an outline of possible future directions. Appendix A compares the implementation and the jumping performance of the EPFL jumpers to the other previously presented miniature jumping robots. Finally, the appendices B-D discuss exploratory ideas of extensions, such as foldable wings, autonomous steering using Shape Memory Alloy (SMA) actuators and perching to walls that can be added to the prototypes presented in this thesis to enhance their locomotion capabilities.

2 Take-off

The main principles that are used to address the challenges of the take-off phase are (i) charging slowly an elastic element which is released to jump and (ii) using a four-bar linkage leg system for adjustment of the take-off angle and ground force profile during the acceleration phase. These design principles are represented in our first robotic prototype, called EPFL jumper v1. It is a novel 7g jumping robot that can perform standing jumps of 27 times its own size. This jumping robot forms the propulsion unit for the extended versions as introduced in the following chapters[1].

Note: This chapter is based on the publication (Kovac et al. [78])

[1]See accompanying video at http://lis.epfl.ch/microglider/EPFLjumperV1.mp4

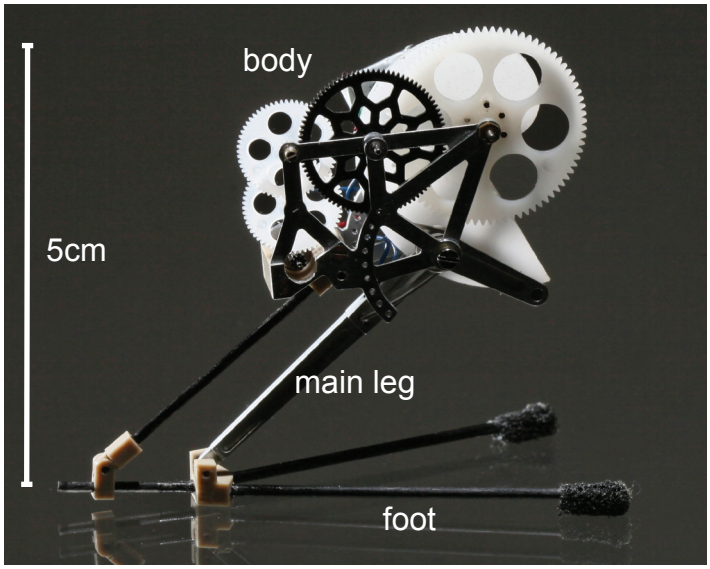

Figure 2.1: EPFL jumper v1 prototype capable of overcoming obstacles of up to 1.4m height (picture: Alain Herzog, EPFL)

2.1 Introduction

The main challenges of the take-off phase are (i) to keep the weight of the jumping system and especially its legs as light as possible, (ii) to keep the size compact, (iii) perform a high power actuation for the jump and (iv) to allow for variations of the take-off angle and ground force profile. In this chapter, we address these challenges by presenting the development and characterization of the realized prototype called EPFL jumper v1, which incorporates solutions to these challenges (figure 2.1). Since it only tackles the take-off phase, it is able to perform standing jumps but without the ability to upright on landing and jump again. It has a total weight of 7g including electronics and battery and can overcome obstacles of 1.4m height. It is adjustable in take-off angle, jumping height and force profile during the jump.

In the following sections, we first introduce the underlying calculations of jumping energy and the forces that act on the robot during the jump. We then present its conceptual design and implementation in Computer Aided Design (CAD) and its optimization using Finite Element Analysis (FEA). Finally we describe the working prototype and characterize its jumping performance.

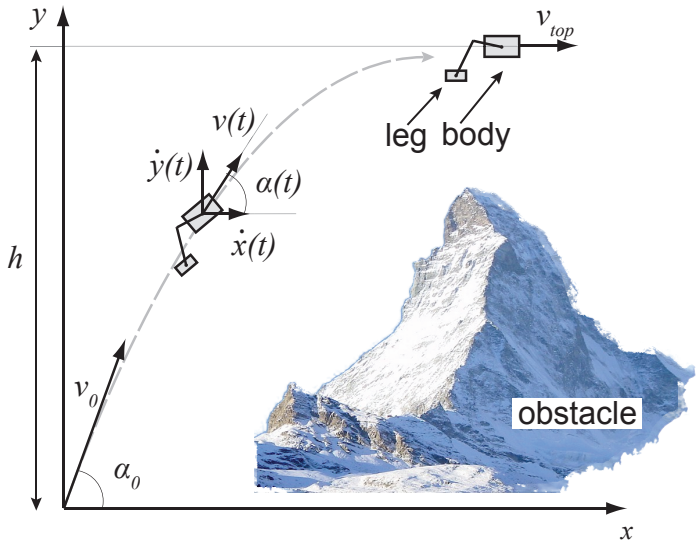

Figure 2.2: Sketch of the jump. Jumping height h, take-off angle α_0, take-off velocity v_0 horizontal $\dot{x}(t)$ and vertical $\dot{y}(t)$ velocity during flight and horizontal velocity on the top of the jumping trajectory v_{top}

2.2 Design

In order to design and adequately dimension the structural parts of our jumping robot, we estimated the required energy for jumping and the forces acting on the system. As a performance benchmark to calculate the forces, we dimension the system to be capable of overcoming an obstacle of 1m height h at a takeoff angle α_0 of 75° with a total system mass m of 10g (figure 2.2).

The working principle of the chosen design is illustrated in figure 2.3. First, a four-bar leg linkage, which is connected to the body on the ground link (a) is used to charge the torsion spring (c). To jump, the energy in the spring is released and extends the four-bar linkage to propel itself into the air.

Using a four-bar linkage for the legs offers the possibility to modify the take-off angle by adjustment of distance (d), the acceleration time by adjustment of distances (a) and (c) and the trajectory of the foot tip P to change the ground force profile by adjustment of the ratio (b)/(d) (figure 2.4).

Based on the calculations of the forces acting on the system we designed the components of the four-bar linkage and the body in CAD (figure 2.5) and optimized the critical part (main leg, figure 2.1) using FEA (figure 2.6).

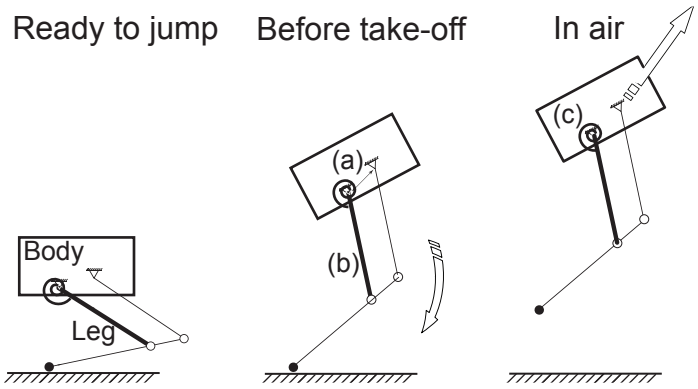

Figure 2.3: Working principle for the jumping mechanism. To jump, a four-bar leg linkage, which is connected to the body on the ground link (a) is extended via the input link (b) using a torsion spring (c)

2.2.1 Jump energy

Based on ballistic jump kinematics, the force balance on the system during jump (figure 2.2) can be expressed as:

$$F_x(t) = -F_{air}(t) \cdot \cos(\alpha(t)) \tag{2.1}$$

$$F_y(t) = -F_{air}(t) \cdot \sin(\alpha(t)) - F_g \tag{2.2}$$

with $F_x(t)$ being the horizontal and $F_y(t)$ the vertical force component, F_g the weight, $F_{air}(t)$ the air friction and $\alpha(t)$ the angle of the flight direction.

As a first model of the air friction force $F_{air}(t)$ we assume [85]

$$F_{air}(t) = \frac{1}{2}\rho v^2(t) A c_d \tag{2.3}$$

with ρ as the air density, $v(t)$ the velocity of the system, A the frontal area and c_d the drag coefficient.

Using these equations and the trigonometric relationship

$$\alpha(t) = \arctan(\frac{\dot{y}(t)}{\dot{x}(t)}) \tag{2.4}$$

we obtain a system of two nonlinear second order differential equations with $\dot{x}(t)$ being the horizontal and $\dot{y}(t)$ the vertical velocity. Accordingly, $\ddot{x}(t)$ is the

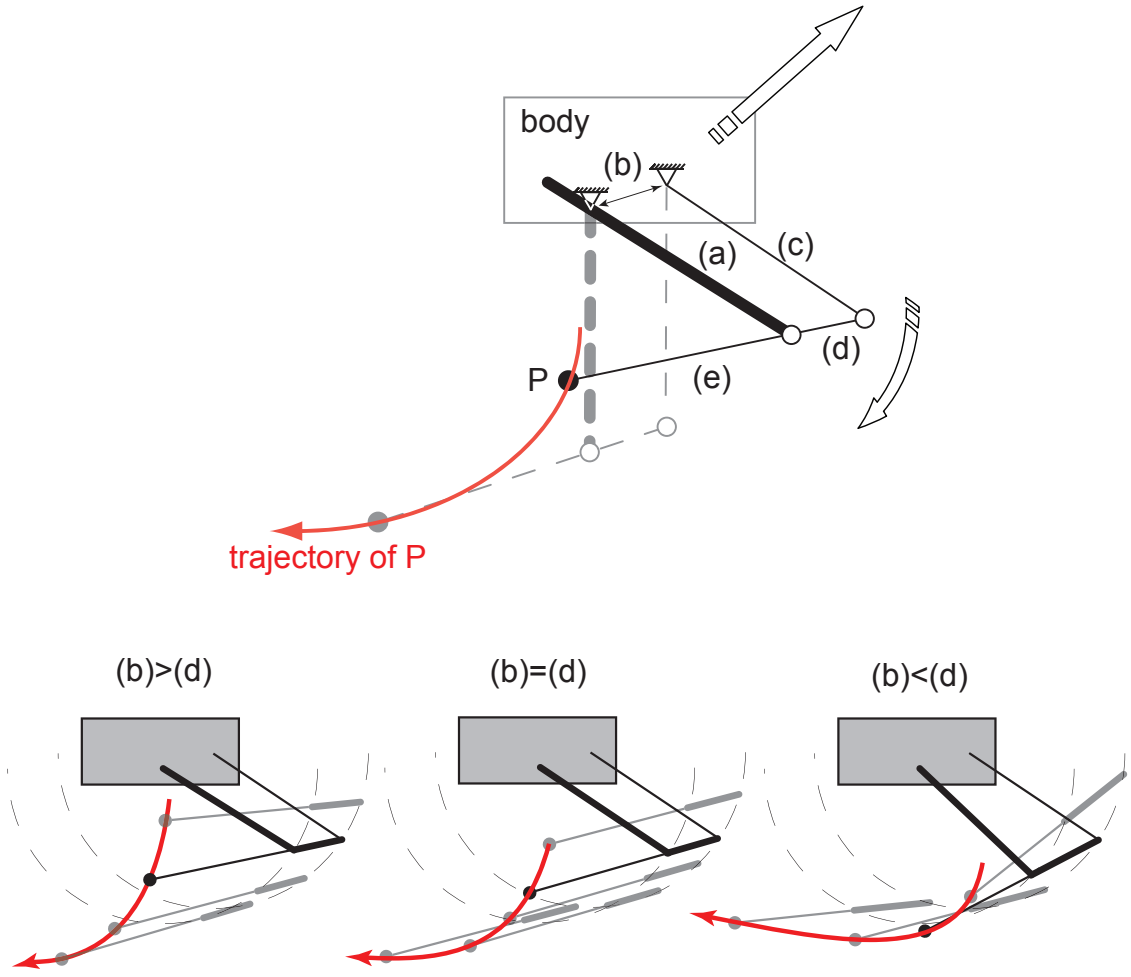

Figure 2.4: Sketch of the four-bar linkage jumping design and the foot tip P trajectory during take-off. (a) is the input link and (b) the ground link. Changing the lengths (a)-(d) allows to adjust the take-off angle (change distance (e)), acceleration time (change distance (a) and (c)) and trajectory of the foot tip P to alter the ground force profile (change ratio (b)/(d))

horizontal and $\ddot{y}(t)$ the vertical acceleration

$$\ddot{x}(t) = -\frac{1}{2m}\rho A c_d \cos(\arctan(\frac{\dot{y}(t)}{\dot{x}(t)})) \cdot (\dot{x}(t)^2 + \dot{y}(t)^2) \tag{2.5}$$

$$\ddot{y}(t) = -\frac{1}{2m}[2mg + \rho A c_d sin(\arctan(\frac{\dot{y}(t)}{\dot{x}(t)})) \cdot (\dot{x}(t)^2 + \dot{y}(t)^2)] \tag{2.6}$$

The initial conditions can be expressed as

$$\dot{x}(0) = \cos(\alpha_0) \cdot v_0 \tag{2.7}$$

$$\dot{y}(0) = \sin(\alpha_0) \cdot v_0 \tag{2.8}$$

$$x(0) = 0 \tag{2.9}$$

$$y(0) = 0 \tag{2.10}$$

However, the frontal area A and the drag coefficient c_d are not known exactly, a priori, and have to be estimated. As a first estimation we model the robot as a cylindrical body (length l of 100mm and radius r of 40mm), as suggested by Bennet-Clark [11] for jumping animals such as locusts. Assuming the flight direction in line with the body axis, a take-off angle α_0 of 75°, a friction coefficient c_d of 1.3 [11] and an air density ρ of 1.2kg/m^3 we solved this system of differential equations numerically using a Runge-Kutta (4,5) solver [28] and obtained a required take-off velocity v_0 of 4.05m/s.

This corresponds to an initial kinetic energy E_{kin0} of

$$E_{kin0} = \frac{1}{2}mv^2 = 82mJ \tag{2.11}$$

Introducing a safety factor which accounts for eventual additional losses in the leg structure and consulting available off the shelf components, we decided to design the system for an energy of up to 154mJ.

Based on this energy, the acceleration phase and forces acting on the system can be estimated. If we assume constant acceleration and an approximate acceleration distance of 3cm to discharge 154mJ, we obtain a force of 5.1N acting on

the system for a duration of 10.8ms. We used this approximation of force and energy for the dimensioning phase that follows.

2.2.2 Mechanical design

As calculated, releasing an energy of 154mJ in only 10.8ms, corresponds to an actuation power of 14.2W. Since there is no actuator capable of producing that much power at a weight of only a few grams, we decided to design a mechanism which can be charged slowly, store the energy in a spring and release it on demand using a click mechanism. This mechanical principle is used by several small jumping animals, such as frogs [120], locusts [11], springtails [19], click beatles [3] and fleas [54].

The basic principle is to charge a torsion spring and release its energy to extend a four-bar leg linkage to jump (figure 2.7). We use a 4mm DC motor (a) to turn an eccentric cam (b). The shape of the cam has been specifically designed to yield a constant torque on the motor. The motor turns the cam in counterclockwise direction, by way of a four stage gear box (c), in order to charge two torsion springs (d). These two springs are located around the axis of the leg (e) and are fixed to the frame (f) and the main leg (g). Once the most distal point of the cam is reached, the energy that is stored in the springs actuates the main leg which is the input link for the four-bar leg mechanism. In order to keep the weight as low as possible, we choose two 0.2mm gears with 60 teeth (figure 2.5 (1) and (2)) and a third stage 0.3mm gearwheel (3) with 81 teeth. This resulted in a total gear weight of 0.63g with an overall efficiency of 61% (assuming an efficiency of 85% for each stage). The total transmission ratio is 1266 and allows for motor speeds of around 8000t/min with a constant motor torque of only 0.038mNm.

Leg weight optimization using Finite Element Analysis (FEA)

According to structural mechanics [73], when using aluminum for the main leg material, we determined that a diameter of 2.2mm is needed to support the force of 5.1N where we assume a uni-axial stress condition, a leg length of 4cm and a safety factor of 1.2. In order to minimize the leg weight while keeping its required strength, we performed a 2D FEA on a simplified model of the

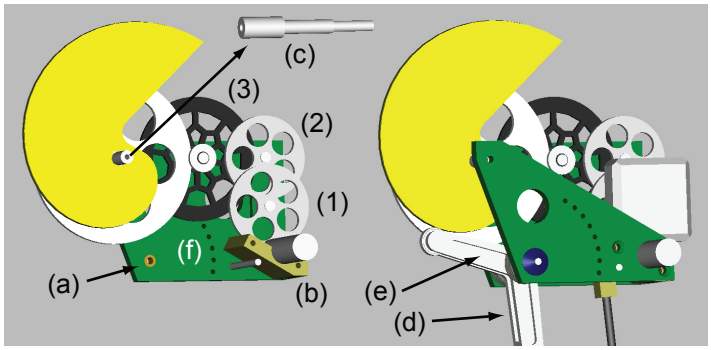

Figure 2.5: CAD model of the gearbox. (a) brass bearing to reduce friction, (b) distance piece to align the two body plates, (c) cam axis, (d) slot in main leg for the cam, (e) main leg and, (f) series of holes for spring setting. (1),(2) 0.2mm POM gears and (3) 0.3mm POM gear

main leg using commercial FEA software (ANSYS). The analysis indicates that the main stress lies close to the axis and on the surface perpendicular to the force vector (figure 2.6). Therefore, we removed the unnecessary material in the middle section of the leg to obtain a structurally beneficial H-shape which lead to a mass reduction of the main leg from 0.99g to 0.76g (23.2%). This also reduced the fraction a in the cost of transport equation 1.4 by 23.4% from 0.174 to 0.132. Thus, an improvement of the cost function T of 4.7% (figure 2.8) has been obtained for the jumping mechanism by optimizing the shape and weight of the main leg (figure 2.9.

2.3 Results

2.3.1 Prototype

The prototype (figure 2.7) consists of the gearbox including motor, gearwheels and cam, the main leg, 1.3mm carbon rods as feet, the infrared receiver and a 10mAh Lithium Polymer battery. As described earlier, changing the proportions of the feet leads to a change in take-off angle, acceleration time and ground force profile. The amount of energy that will be stored in the springs can be adjusted by changing the spring setting (figure 2.5.f) between 106mJ and 154mJ in steps of 6mJ. The body frame consist of Aluminum 7075, a relatively strong alloy that is commonly used as structural material in aeronautics. The cam and gears are

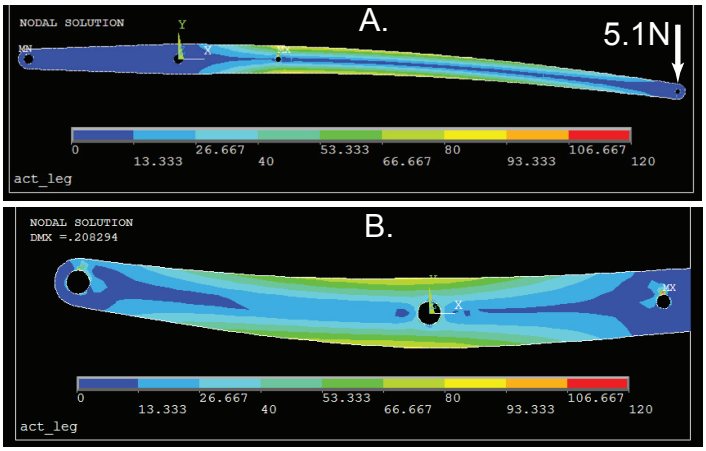

Figure 2.6: Results of the FEA on a simplified 2D model of the main leg. A: Stress at take-off, max. von Mises stress $\sigma_m \approx 90MPa$, max. deflection $d = 0.9mm$, B: Stress in charged position, max. von Mises stress $\sigma_m \approx 85MPa$, max. deflection $d = 0.21mm$.

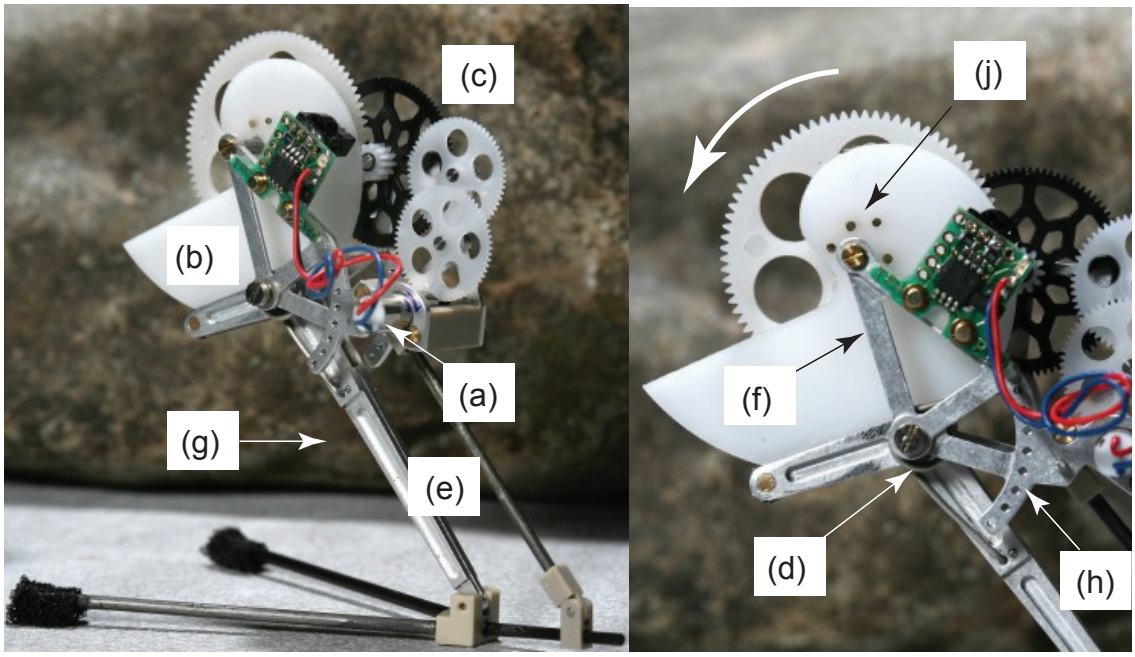

Figure 2.7: EPFL jumper v1 prototype. (a) 4mm DC pager motor, (b) cam, (c) four stage gear box, (d) two steel torsion springs, (e) four-bar linkage leg structure, (f) aluminum frame, (g) main leg as input link, (h) spring setting, (j) fixation of the cam to the last gear stage using five bolts (picture: Alain Herzog, EPFL)

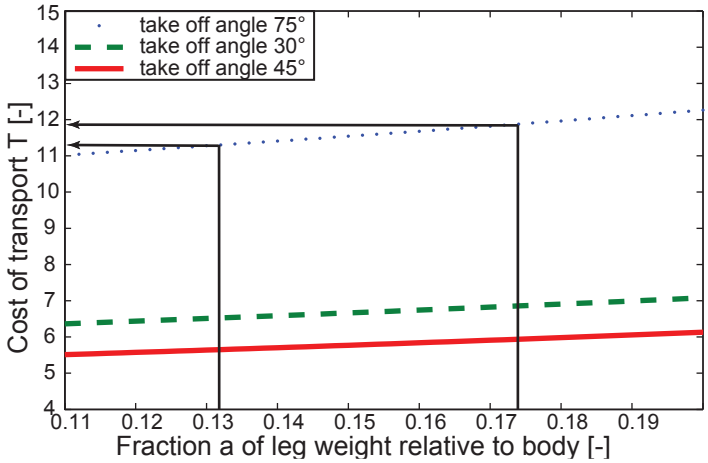

Figure 2.8: Cost function for different relative masses of the leg $a \cdot m$ in regard to the body mass $(1 - a) \cdot m$ at different take-off angles

Figure 2.9: Structurally optimized main leg

Table 2.1: Properties of the materials used

	Alu	PEEK	POM	Carbon
Density [g/cm^3]	2.7	1.3	1.56	1.55
E-Module [GPa]	69	3.5	5.2	130
Yield strength [MPa]	320	97	62	1400

Table 2.2: Weight budget for the EPFL jumper v1

Part	Material	Weight [g]
Body frame	Cibatool/PEEK	1.4
Cam	POM	0.78
Gears	POM	0.63
Main leg	Aluminium	0.76
Plastic parts on leg	PEEK/Carbon	0.32
Screws and axis	Steel/brass	0.79
2 springs	Spring steel	0.41
Motor		0.65
Total mass mechanism		**5.74**
LiPo Battery		0.48
IR receiver		0.76
Total mass prototype		**6.98**

manufactured from Polyoxymethylene (POM) due to its low weight and low surface friction coefficient. For critical structural parts in the body and legs we used Polyetheretherketone (PEEK) due to its very high strength-to-weight ratio (see table 2.1 for a selection of properties of the materials that have been used). Table 2.2 presents the weight budget of the robot. The entire and fully functional remote controlled prototype weighs 6.98g in its current form. Further weight reduction could be achieved by optimizing the body frame and by using a smaller infrared receiver and battery.

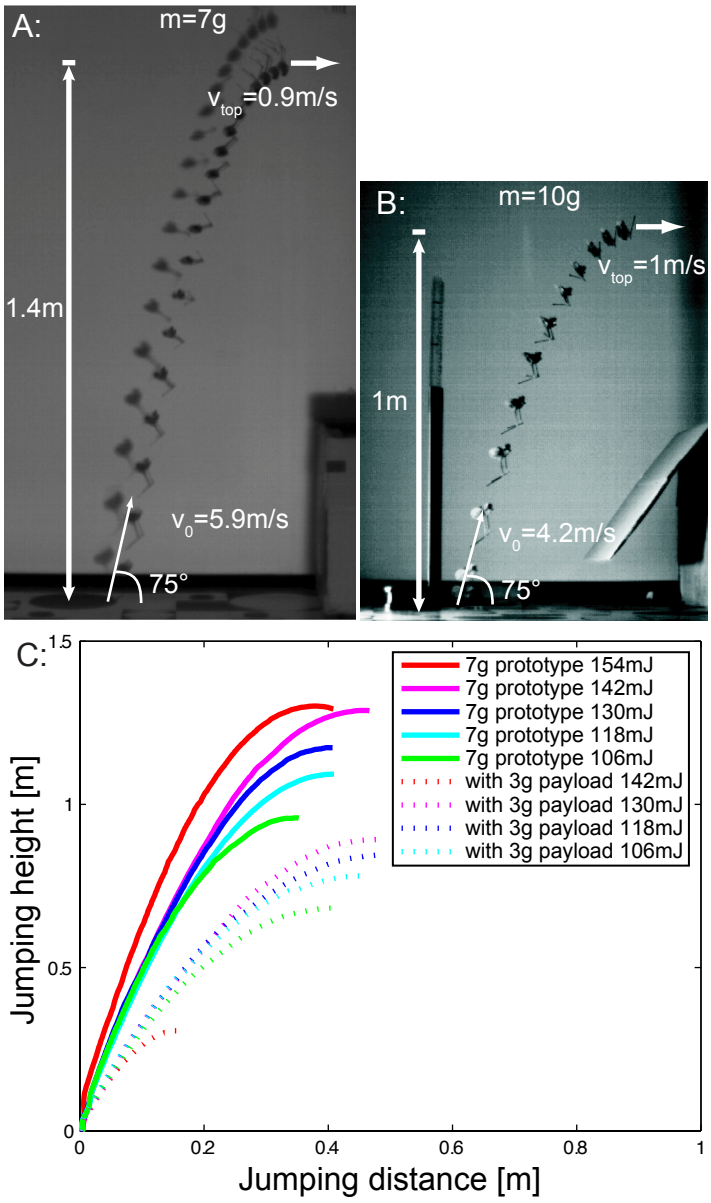

Figure 2.10: A. Jumping trajectory of the prototype without and B: With an additional payload of 3g, C: Jumping trajectories for the different spring settings, with and without payload of 3g

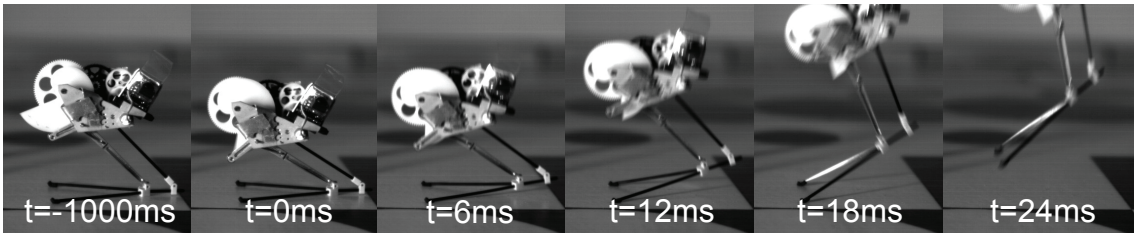

Figure 2.11: Takeoff sequence of the jumping mechanism including a payload of 3g

2.3.2 High power jumping performance

For the characterization of the jumping performance, we set the leg segment (a) and (c) to 40mm, (b) and (d) to 12.5mm and (e) to 44mm (figure 2.4) in order to obtain a take-off angle of 75° and we observed the jumps using a high speed camera [63] running at 1000 frames per second and track the robot during the jump using an adequate motion analysis software [67]. A jump of the 7g jumping prototype has been observed without additional mass (figure 2.10.A) and with additional 3g of lead in order to simulate a payload (figure 2.10.B).

The maximal height obtained without additional payload was 138cm. The acceleration time is 15ms, the initial take-off velocity 5.96m/s and the velocity at the top 0.9m/s. The complete jump duration is 1.02s and the traveled distance 79cm. This means that the prototype presented here is capable of overcoming obstacles of more than 27 times its own body size.

The prototype with an additional weight of 3g reached a height of 1.05m with a velocity of 1m/s at the top and an initial take-off velocity of 4.2m/s. This take-off velocity compares very well to the predicted 4.05m/s take-off velocity as modeled in the design phase. We characterize the change in jumping performance due to the different spring settings in figure 2.10.C and 2.12.The acceleration time t_{acc} of 19.1ms is much longer than the 10.8ms from the prediction. We argue that this is due to a slightly longer acceleration distance of 3.2cm instead of 3cm from the model, inertia effects and friction in the leg axis.

In order to provide an initial characterization of jumping with different payloads, we add a payload of 7.3g to the 7g jumping robot and measure the jumping height at a take-off angle of 75°(figure 2.13). The jumping height with a total robot mass of 7g is 138cm. At a total mass of 10g it is reduced by 24%. Adding

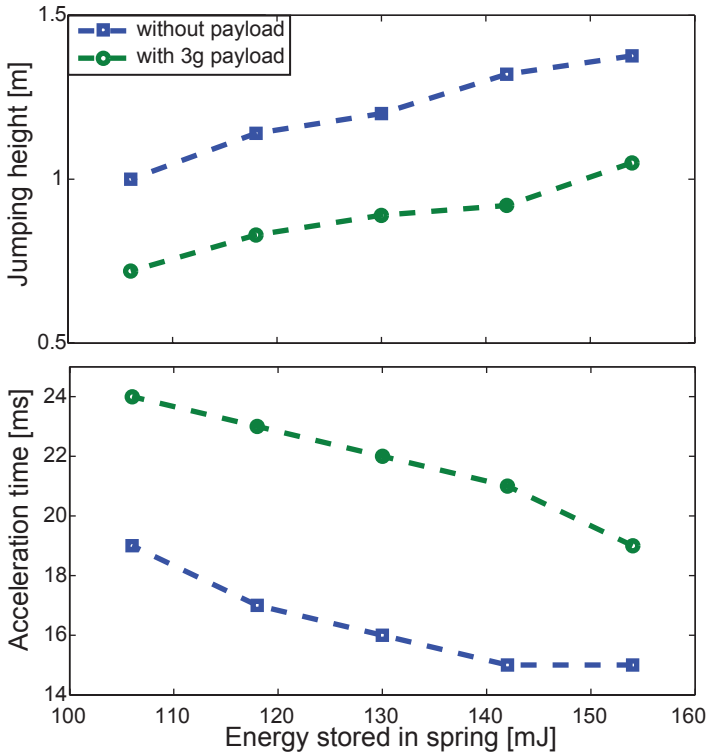

Figure 2.12: Jump height and acceleration time at different spring settings for the prototype with and without an additional payload of 3g

additional weight, leading to a total mass of 14.3g, the jumping height is reduced by 50% compared to the 7g jumping robot.

The motor recharges the mechanism for one jump cycle in 3s while sinking 95mA. This results in a power consumption of 352mW at 3.7V. The 10mAh provided by the LiPo battery would thus theoretically allow for 6.3min of continuous recharging or approximately 108 jumps.

2.3.3 Variable take-off angle and ground force profile

As described in section 2.2, changing the foot length (e) and the heel length (d) (figure 2.4) both change the take-off angle and the ground force profile. In order to characterize the capability of changing the take-off angle, we vary the foot length (e) between 2.9cm and 5.15cm in five steps and carry out four jumps for every foot length. The take-off angle is measured optically using a high speed camera at 500 frames per second and a feature tracking software (figure 2.14). The measured take-off angle ranges from α_0 =83.2° (SD=2.6) for a foot length

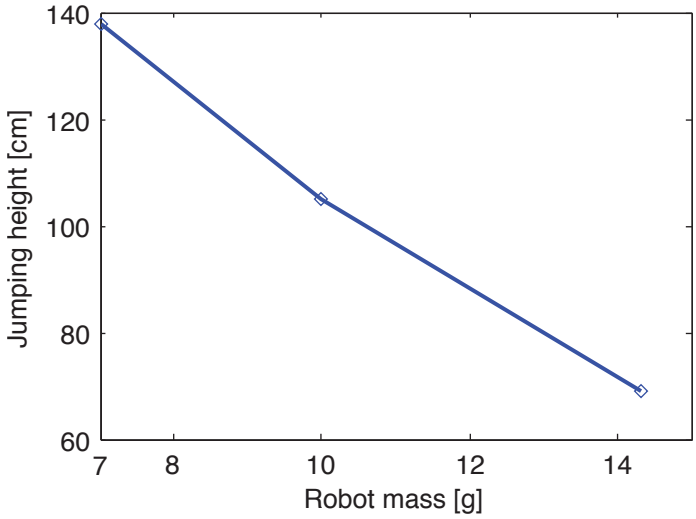

Figure 2.13: Jumping height for different robot weights

of 2.9cm to α_0 =55.9° (SD=0.78) for a foot length of 5.15cm. These experiments show that the take-off angle of the EPFL jumper v1 can be changed by varying the foot length (e).

In order to characterize the adjustability of the ground force profile, we change the heel length (d) between 0.85cm and 1.35cm in 6 steps at the maximal spring setting. We perform three jumps for every heel length and measure the ground force profile with a Nano17 6DOF force gauge at 5000Hz (figure 2.15). It can be seen that the peak ground force is largest with $F_{gf} = 3.92N$ (SD=0.20) for a heel length of 1.35cm and minimal with $F_{gf} = 1.8N$ (SD=0.18) for heel length of 0.85cm. Conclusively, changing the heel length allows a reduction of the peak ground force by 117%.

2.4 Conclusion

The jumping robot presented in this chapter represents our solutions to the main challenges of the take-off phase using bioinspired design principles. The first principle is to not use direct actuation of the legs, but to slowly charge an elastic element and release it quickly to jump. This principle allows the EPFL jumper v1 to reach a jumping height of more than 27 times its size with on board energy and control. With the current technology, we consider such high jumping performance as not feasible with direct actuation on a miniature robot with a

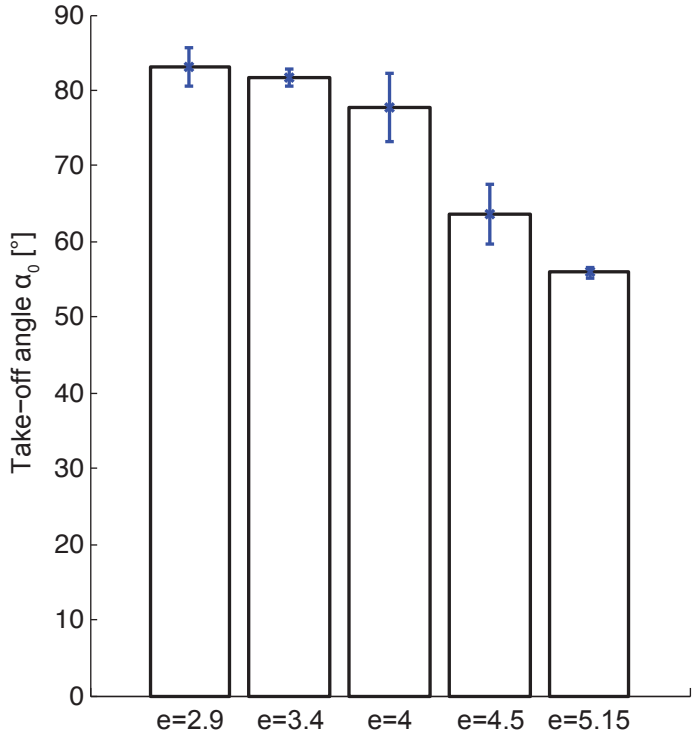

Figure 2.14: Take-off angle for different foot lengths with standard deviations (four runs for every foot length (e))

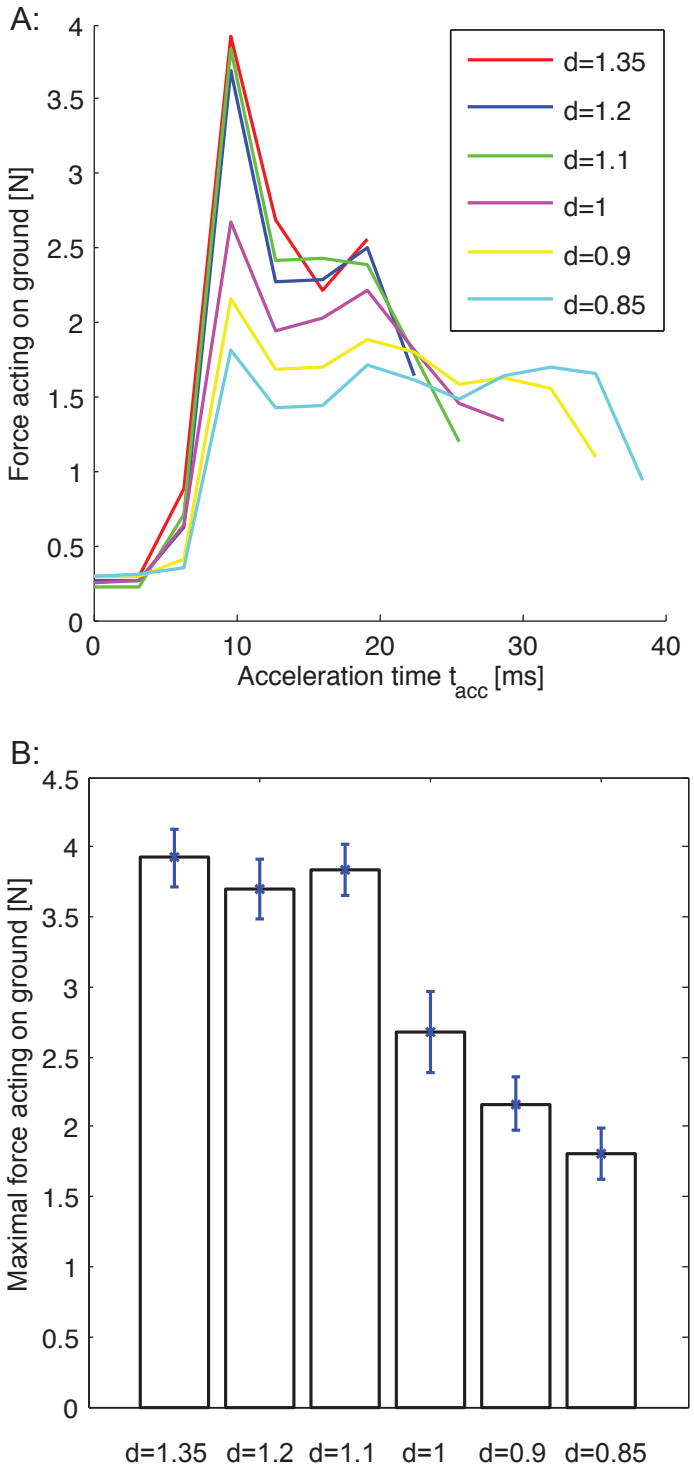

Figure 2.15: Ground force measurements (three runs for every heel length (d)) A: Ground force profile for different heel lengths (d) (mean of three runs), B: Maximal value of the ground force profiles with standard deviation

similar mass.

The second principle is to employ a four bar leg mechanism to change the take-off angle and ground force profile. However, changing those parameters can only be done manually and not by the robot itself during operation. Extensions of this robot could include small actuators that allow changing of those parameters during operation prior to take-off.

Using a 10mAh battery allows the robot to perform a jump every 3s with a theoretical endurance of 108 jumps. The use of larger batteries is possible and would extend the time of operation. For example, a 90mAh LiPo battery weighs 3g and provides 9 times the energy of the 10mAh battery. Due to its heavier weight, it would decrease the jumping height by 40%. Using a larger battery may be the better choice, in case that energy endurance is more important than the obstacle height that the jumper can overcome.

3 Landing

This chapter addresses the challenges of the landing phase which are (i) protection on landing and (ii) uprighting to jump again. After a weighted evaluation of different solutions to these challenges, we present the EPFL jumper v2. It is a spherical system with a mass of 9.8g and a diameter of 12cm that is able to jump, land safely without damaging the jumping mechanism, upright itself and jump again. In order to do this autonomously, it incorporates sensors and a control unit[1].

Note: This chapter is based on the publication (Kovac et al. [80])

[1]See accompanying video at http://lis.epfl.ch/microglider/EPFLjumperV2.mp4

Figure 3.1: EPFL jumper v2, able to jump, land safely, upright and jump again. The cage has a diameter of 12cm (picture: Alain Herzog, EPFL)

3.1 Introduction

The two main challenges during the landing phase are to protect the robot on landing and allow it to upright in order to jump again. This chapter presents the EPFL jumper v2 (figure 3.1) which represents a robotic implementation of solutions to those two challenges. It incorporates a carbon cage structure which deforms elastically on landing to reduce the impact forces. Using on board sensors and control, it can detect its orientation and charging state on ground, enabling it to prepare for the next jump.

In the following, we outline the conceptual design of the solutions and their implementation in CAD and on a prototype. We then give an overview of its electronics and control and characterize the performance of the working and autonomous EPFL jumper v2.

3.2 Design

As a basis for the jumping robot presented in this chapter we take the EPFL jumper v1 as jumping mechanism and extend it with a cage and basic autonomy. We separate the functionality of the EPFL jumper v2 according to the challenges

in two function which we define as (i) protecting the jumping mechanism on landing and (ii) allowing it to upright after landing in order to jump again. In this section we provide the underlying design choices that we take to address those two functions.

3.2.1 Protection on landing

Protection on landing can be realized by either encapsulating the robot in an elastic protecting structure or by reducing the velocity before impact. The latter can be achieved with aerodynamical appendages such as wings and will be discussed in more detail in chapter 5.

The purpose of a protecting structure is to elastically deform on impact and decelerate the jumping mechanism over a longer distance, which leads to lower peak forces (equation 1.9). Since one of the main challenges during the take-off phase is to keep the air friction of the jumping robot as low as possible, the surface area of the cage must be kept at a minimum. At the same time, the cage has to be mechanically solid in order to absorb the impact forces on landing. Therefore, we choose to implement a skeletal cage structure consisting of carbon composite, a flexible and light weight material with high tensile strength.

3.2.2 Uprighting

Based on using such a skeletal cage structure, we define the qualitative design requirements for the uprighting function. The solution should (i) be light weight, (ii) have a simple construction, (iii) high mechanical robustness on landing when impacting on ground and (iv) low power consumption in performing the uprighting movement. As a first step in our development process we considered four different designs regarding the shape of the uprighting mechanism and its integration with the existing jumping robot (figure 3.2).

In solution A, a cage consisting of an upper part (a) and a lower part (b) is attached to (a) the body and (b) the tip of the foot of the jumping robot. As the jumping robot charges for the next jump, it contracts the legs and naturally the center of gravity of the entire structure is moved towards the lower part, which leads to a passive uprighting movement. In order to be able to compact the cage as the robot charges for the next jump, the rods from the lower part slide along

the rods of the upper part, which inevitable produces kinetic friction and calls for an increase of complexity to ensure its structural robustness.

Solution B consists of a spherical cage which is attached to the body and the feet of the jumping robot. Right after landing, the robot will rest in its stable position which is upside down. As soon as the jumping robot charges for the next jump, the cage is squeezed to an ellipsoid and the center of gravity moves to the lower part of the structure. One potential drawback of this solution is that if the uprighting movement is obstructed, there is a certain risk that the robot may end up in its second stable position, which is upside down. In addition, this solution has a higher associated energy cost due to the squeezing of the structure.

The third possibility that we considered, solution C, consists of a stable spherical cage that is attached to the feet of the jumping robot. When charging for the next jump, the body slides down a rail (c) and shifts the center of gravity of the entire structure to the lower part of the sphere which leads to the desired uprighting movement. Since there is no deformation performed on the cage, this solution is structurally simpler, more energy efficient, and the load on the components is lower than in the first two solutions, which increases its mechanical robustness.

The fourth and final solution D, is similar to solution C, only that the cage is attached to the body and not to the feet of the robot. The shortcoming of this solution however is that the legs are outside the cage on landing which exposes them to potential damage.

In order to compare these four possible solutions for the design of the uprighting mechanism, we perform a weighted comparative evaluation [147] (see the evaluation matrix in table 3.1) and decide on implementing solution C due to its structural simplicity, robustness and the additional benefit of being able to roll passively on ground after impact which could allow it to propagate further on ground using the kinetic energy on impact.

3.2.3 Mechanical and electronic design

We implemented the chosen solution in SolidWorks (figure 3.3), a CAD program and assemble the cage using commercially available carbon rods and connecting

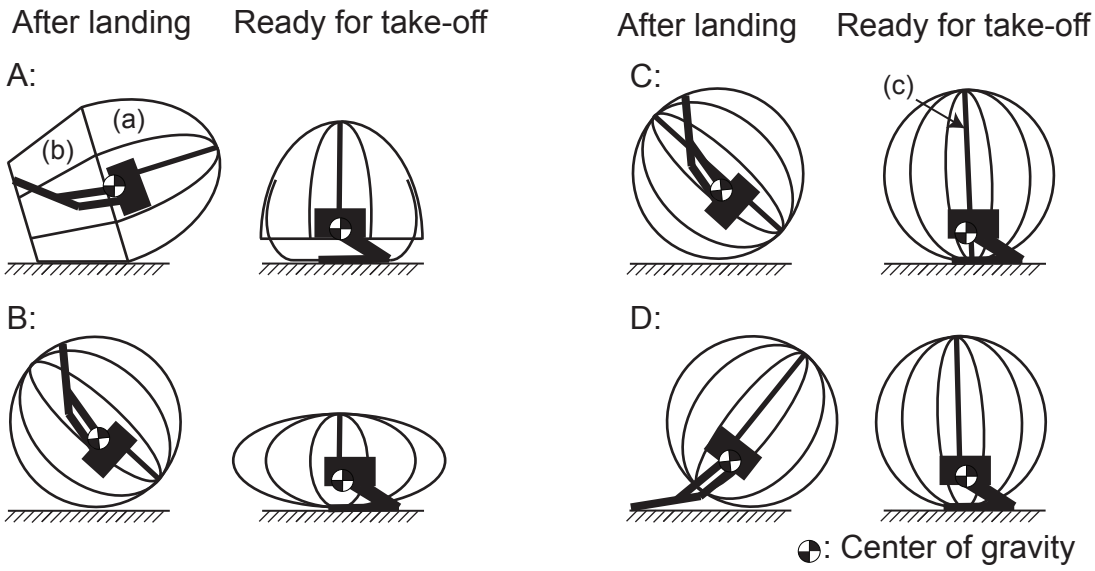

Figure 3.2: Four possible solutions for the mechanical design of the uprighting mechanism. (a) upper part of the cage and (b) lower part of the cage in solution A. (c) rail for solution C

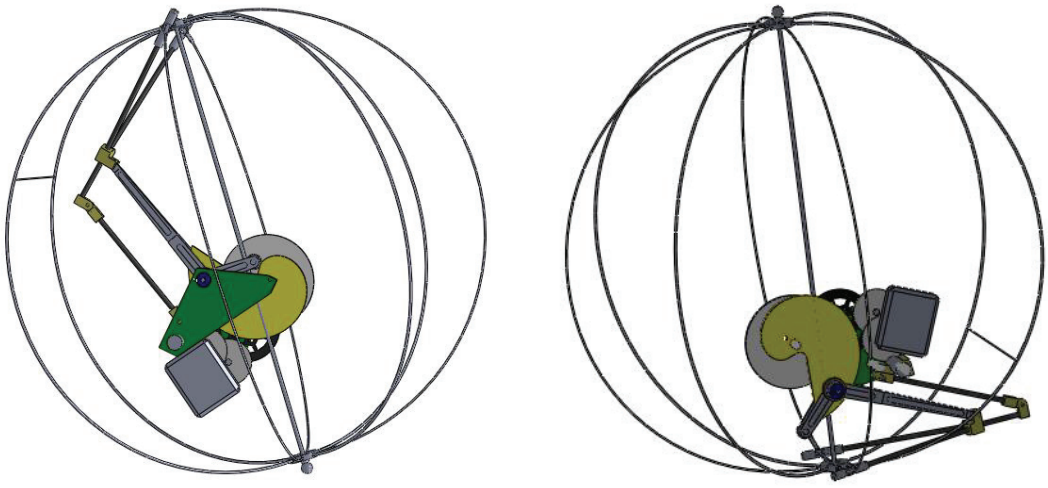

Figure 3.3: Chosen solution C in CAD

Table 3.1: Weighted evaluation of the four different conceptual designs for the uprighting mechanism

Criteria	Weight	(A)	(B)	**(C)**	(D)
Weight	0.4	2	4	**3**	4
Simplicity	0.1	1	3	**5**	3
Robustness on landing	0.2	2	3	**5**	3
Energy consumption	0.3	3	1	**5**	5
Total	1	2.2	2.8	**4.2**	4

(1: Very unfavorable - 5: Very favorable)

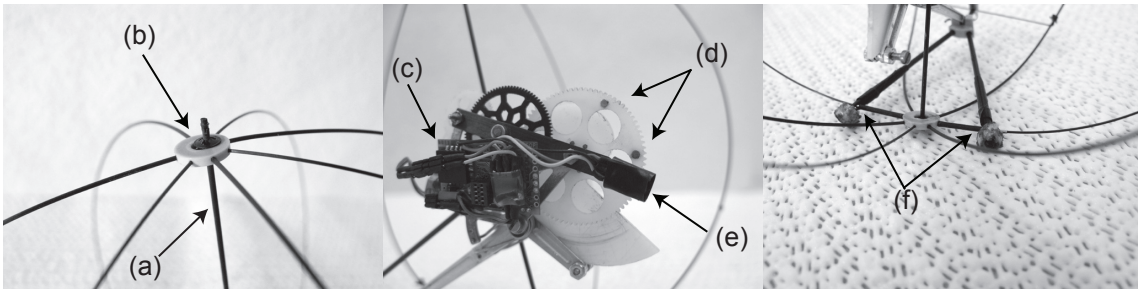

Figure 3.4: Mechanical design details and integration with the jumping system. (a) rail, (b) connection piece, (c) printed circuit board and electronics, (d) two magnets on the last gear stage, (e) hall effect sensor, (f) integration of the cage with the feet.

parts that are produced using a 3D printer [65] out of ABSplus, a light-weight and relatively strong thermoplastic material. The design details of our robot are illustrated in figure 3.4. The structure of the cage consists of the 1mm carbon rail (a) and 0.7mm carbon rods that are held together by the connection piece (b). The printed circuit board (c) is populated with a Microchip Pic18LF4620 microcontroller, a Freescale MMA7260 three-axis accelerometer and an H-bridge motor driver, and is powered using a Full River 10mAh Lithium Polymer battery. The detection of the charging state is done using a hall effect sensor (e) and two small magnets (d) that are integrated on the last gear stage. The uprighting mechanism is fixed on the jumping robot at the feet (f). During the acceleration phase before take-off, the body of the robot slides along the rail and the tips of the feet stick out of the cage to ensure contact with the ground.

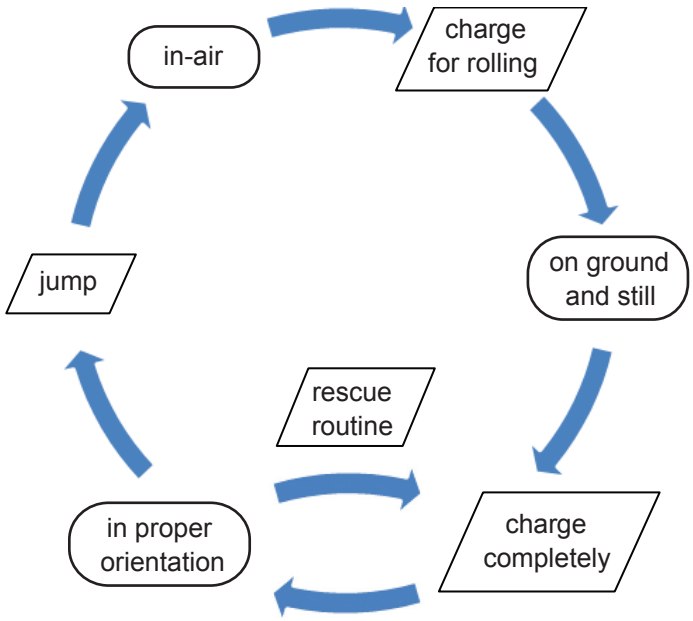

Figure 3.5: Overview of the control strategy, represented as flowchart.

3.2.4 Control strategy

The control strategy of our robot is illustrated in figure 3.5. Using the electronics mentioned above, the robot is able to detect its orientation and charging state. As soon as it is upright, it will jump autonomously. The in-air position is defined as the overall acceleration being less than $0.7 m/s^2$. Once in-air, it charges only partially to keep the center of gravity of the entire robot close to the middle of the cage and to facilitate subsequent rolling. After landing and settling down (acceleration values constant over a period of 500ms), it charges itself completely in order to shift its center of gravity to the bottom part of the cage, thus uprights itself and jumps again. If the orientation is still not upright after charging and just before the jump, it uses a so called 'rescue routine' (rr) to try again to upright itself. The rr consists of a discharging and re-charging cycle. If this rr is performed three times consecutively and the position is still not upright, the robot kicks by releasing a jump in order to free itself from potential stuck situations and starts again with charging completely (see the characterization of the rr in section 3.3.4).

Table 3.2: Weight budget of the EPFL jumper v2

Part	Mass [g]
Total mass of the jumping mechanism	6.87
Carbon cage	0.85
Carbon rail	0.14
Electronics	1.31
LiPo Battery 10mAh	0.63
Total mass of the complete prototype	**9.80**

3.3 Results

3.3.1 Uprighting and charging

The prototype as described above has a diameter of 12cm and weighs 9.8g all together, including battery and electronics (weight budget in table 3.2). A complete uprighting and take-off sequence is illustrated in figure 3.6. The durations, velocities and following trajectories are measured optically, using a high-speed camera system at 500 frames per second and adequate motion analysis software [67]. The charging cycle takes 3s whereby the uprighting movement happens in 0.7s in case the robot is not obstructed. Once jumping, the take-off velocity of 3.52m/s is reached in 17ms.

3.3.2 Jumping performance

The trajectory of the robot jumping out of a box of 50cm depth is shown in figure 3.7. At a take-off angle of 75° it reaches a jump height of 76cm, with a horizontal velocity at the top of the trajectory of 0.93m/s. The comparison of the system with and without uprighting mechanism can be seen in figure 3.8, both at the fourth spring setting with a stored spring energy of 118mJ. The jumping height of the system without uprighting mechanism is 103.3cm at a take-off velocity of 3.92m/s. The height loss due to the addition of the uprighting ability is 27.3cm which corresponds to 26.4% compared to the system without the uprighting mechanism. This height loss is due to the mass increase of 2.8g and the fact that

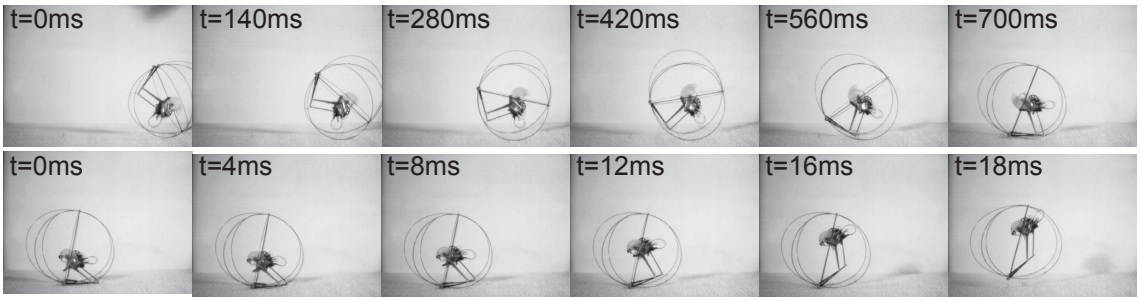

Figure 3.6: 1^{st} row: The uprighting movement takes 700ms. 2^{nd} row: The take-off velocity of 3.52m/s is reached in 17ms

the cage experiences oscillations right after take-off (see accompanying movie). These oscillations are lost energy that cannot be converted into jumping height, as described by Alexander et al. for jumping systems with 'heavy feet' [3]. The jumping performance could thus be further improved by reducing the weight of the components and increasing the rigidity of the carbon cage structure.

3.3.3 Protection on landing

In this subsection we aim at characterizing how much the forces acting on the robot are reduced on impact with the ground due to the protecting carbon cage. We launch the EPFL jumper v2 27 times from a height of 50cm in random orientation and film it at 1000 frames per second using a high speed camera. Based on these movies we measure optically the elastic deformation on impact with the ground as illustrated in figure 3.9. D_1 is the diameter before touching the ground, D_2 the minimal diameter when squeezed due to the impact and ΔD is the difference between D_1 and D_2. We measure the mean deformation to be 14.04mm (SD=7.9). As introduced in chapter 1, we can express the mean impact force as $F_{impact} = (mv_{impact}^2)/(2\Delta D)$, which leads to a average impact force for the 27 trials of $F_{impactave} = 2.78N$. For comparison, we can estimate the impact force acting on the robot in the case that it has no elastic cage for protection. The robot weighs without cage 8.81g which leads to a kinetic energy of $E_{kin} = mgh = 43.2mJ$ when touching the ground. Assuming an elastic deformation of the robot structure of 1mm, we calculate the average force on impact to be 43.2N, which is 15.5 times higher than the force acting on the mechanism when using a cage.

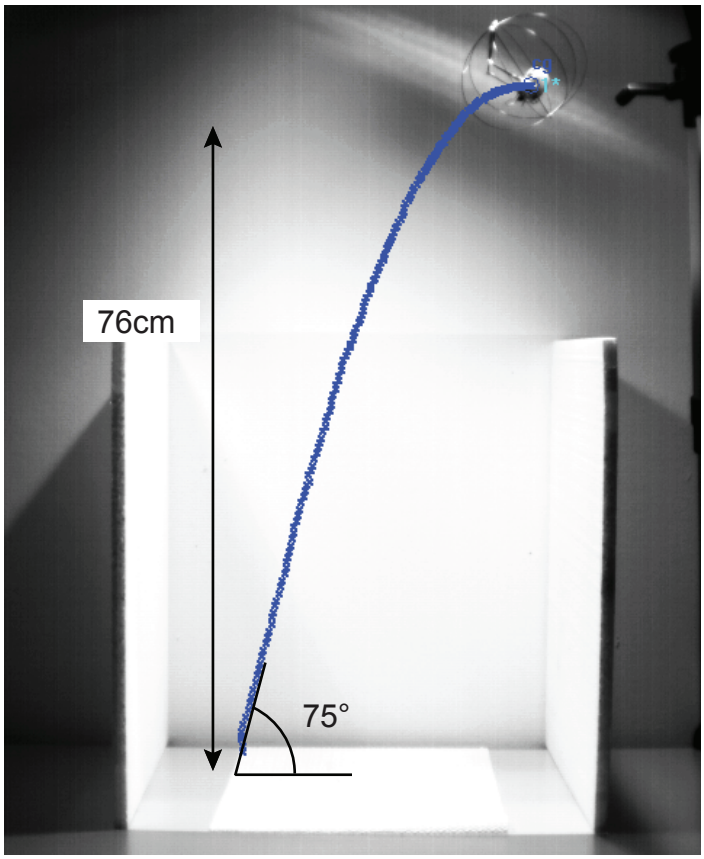

Figure 3.7: Jumping trajectory of our robot, jumping out of a box of 50cm depth. The jumping height is 76cm at a take-off angle of 75°

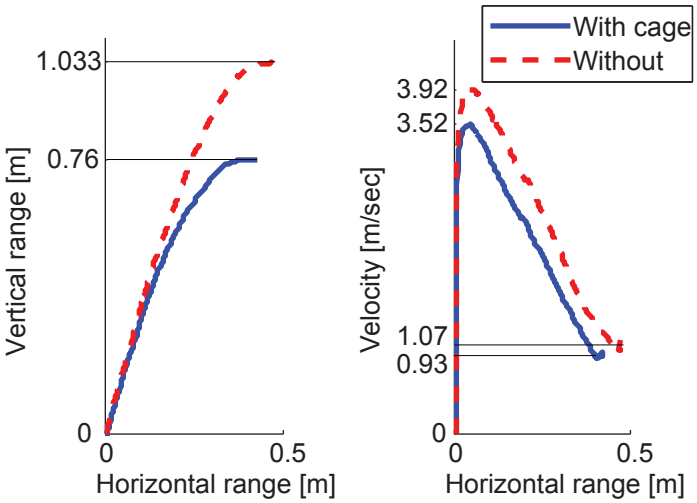

Figure 3.8: Comparison of the trajectories and velocity profiles of the jumping robot with the uprighting cage and without. At a take-off angle of 75°, the caged system is able to jump to a height of 76cm, whereas the cage-less system reaches a height of 103.3cm. The velocity profiles are qualitatively similar, the take-off velocities are 3.92m/s and 3.52m/s respectively

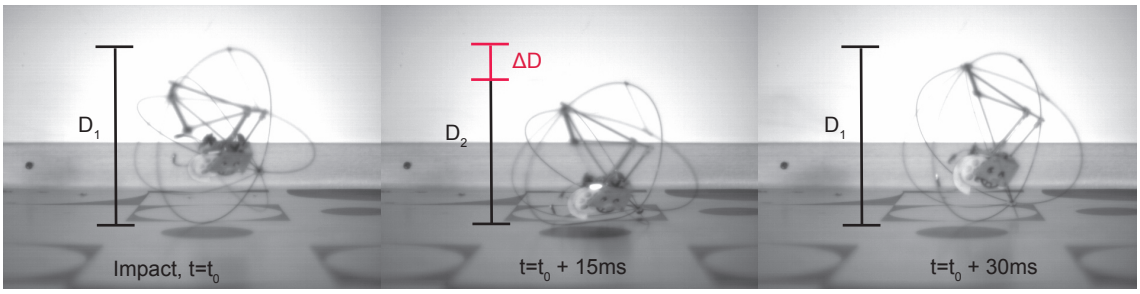

Figure 3.9: Elastic deformation of the cage on impact with the ground. The diameter before impact D_1 is squeezed due to the impact energy by ΔD to a minimal diameter D_2

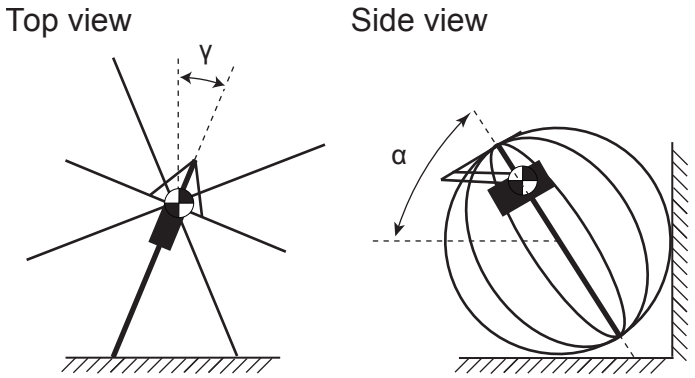

Figure 3.10: We put the robot in 35 different positions facing a vertical wall and measure the time the robot needs to get away from the wall and perform a regular jump at a take-off angle of 75°.

3.3.4 Rescue routine

There are different situations to challenge the uprighting movement by testing the robot in obstructed situations. One scenario where this is the case is when the robot is stuck in a corner of the ground and a vertical wall (figure 3.10). As an attempt to systematically characterize its ability to free itself from such stuck situations, we place the robot in five different pitch angles ($\alpha = 0°, 45°, 90°, 135°, 180°$) and for every one of them in seven yaw angles ($\gamma = 0°, 55°, 112.5°, 157.5°, 202.5°, 247.5°, 305°$) facing the wall. We perform one jump for every of the 35 combinations of pitch and jaw and observe the behavior (table 3.3). To characterize which position is the most difficult for the robot to free itself from, we measure the time in this set of 35 jumps that the robot needs until it performs a regular jump at a take-off angle of 75°(figure 3.11). The data shows that it successfully uses the rr and manages to get out of the situation in every case, whereby the most difficult position is when it is stuck upside down, facing the wall on its back ($\gamma = 0°$ and $\alpha = 180°$).

3.4 Conclusion

The main principles that have been presented in this chapter are (i) the use of an elastic protecting cage which deforms on landing and (ii) the use of the center of gravity shifting to upright. The EPFL jumper v2 incorporates successfully these principles with the additional capability of autonomously freeing itself

Table 3.3: Use of the 'rescue routine' (rr) by the robot to free itself facing a vertical wall at the pitch angle α and the yaw angle γ 0: no need for rr, Nrr: execution of the rr N times, k: kick.

	$\gamma = 0°$	$\gamma = 55°$	$\gamma = 112.5°$	$\gamma = 157.5°$	$\gamma = 202.5°$	$\gamma = 247.5°$	$\gamma = 305°$
$\alpha = 0°$	0	0	0	0	0	0	0
$\alpha = 45°$	1rr	2rr	1rr	3rr+k	3rr+k	3rr+k	1rr
$\alpha = 90°$	3rr+k	1rr	1rr	1rr	1rr	1rr	1rr
$\alpha = 135°$	3rr+k	3rr	0	0	0	0	1rr
$\alpha = 180°$	3rr+k+3rr+k	3rr+k+3rr+k	3rr+k+1rr	1rr	3rr+k	1rr	3rr+k

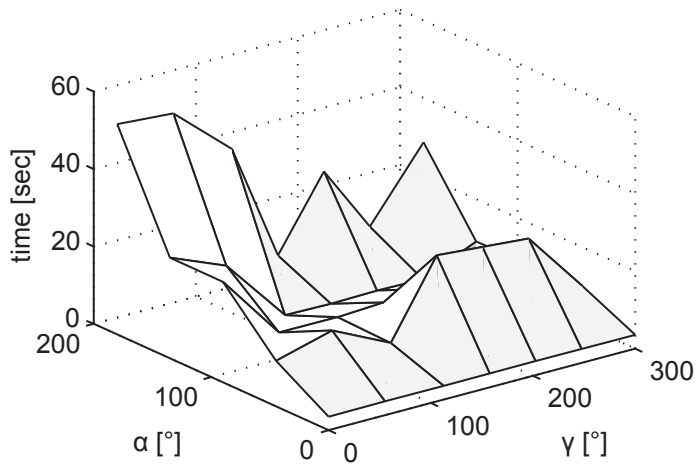

Figure 3.11: Time the robot needs to get away from the wall (α pitch and γ yaw angle) and perform a regular jump at a take-off angle of 75°

from stuck situations. The jumping height of the current configuration is 76cm at a take-off angle of 75°, which is 27.3cm lower compared to the same robot without the spherical uprighting mechanism. The main limitations of the EPFL jumper v2 is that it is not able to steer its jumps, which is elaborated in the next chapter.

4 Preparation for take-off

This chapter focusses on the preparation for take-off phase and it presents and evaluates different principles of steering with onboard energy and control. We introduce the EPFL jumper v3, a 14.3g jumping robot which incorporates solutions for take-off, landing and preparation for take-off phases. It that can perform repetitive steered jumps with a height of up to 62cm at a take-off angle of 75°. As a demonstration of the achieved design goals and its locomotion ability, we show it repetitively moving over an obstacle course where it has to consecutively jump two stairs of 45cm height each and go through a window. Its low weight and the adjustability of the jumping height, jumping distance take-off angle and ground force profile make it a suitable robotic platform for applications such as environmental monitoring or space exploration[1].

Note: This chapter is based on the publication (Kovac et al. [83])

[1]See accompanying video at http://lis.epfl.ch/microglider/EPFLjumperV3.mp4

Figure 4.1: EPFL jumper v3 weighting 14.3g. The cage has a height of 18cm and allows the robot to upright itself after landing, steer and jump again

4.1 Introduction

The main challenge during the preparation phase is the ability to perform steered jumps while having on board energy and control. In this chapter, we describe the development and characterization of our EPFL jumper v3 (figure 4.1) which incorporates solutions to these challenges. It is a caged jumping system of 14.3g which is able to jump, upright passively on landing, reorient to steer and jump again.

In order to design this robot, we first discuss and evaluate different possibilities for uprighting and steering and decide on a solution to meet our main design requirements. Further, we describe the design and fabrication details of the working robotic prototype. As a description of the jumping performance of our robot we characterize and discuss the "cost" of the ability to upright and steer. We also explain and elaborate how the jumping height and the jumping distance can be altered by changing the configuration of the robot. Finally, we demonstrate the remote controlled prototype moving successfully and repetitively over an obstacle course.

4.2 Design

For the mechanical development of the EPFL jumper v3, we apply the engineering design process as described in [147]. The sequential steps in this design process are (i) the conceptual design of the principles needed to fulfill the predefined functions, (ii) their comparison using a weighted comparative evaluation method, (iii) their implementation in CAD and finally (iv) their fabrication and assembly.

In this section we present and explain the principles of uprighting and steering. The EPFL jumper v2 as described in the previous chapter is capable of uprighting on landing to jump again. For the robot presented in this chapter we reconsider the uprighting mechanism design because it has to match the way steering is achieved. We therefore reassess and reevaluate different uprighting principles based on our design requirements. As jumping mechanism for the robot presented in this chapter we use the EPFL jumper v1 which has been described in detail in chapter 2.

As explained in the introduction, to allow the robot to jump high, the weight of the entire system should be kept as low as possible. We therefore choose the first design requirement to be a minimization of the robot's mass. The second design requirement is to keep the structure as simple as possible to ease manufacturing and assembly. The third requirement is to build the mechanism as robustly as possible to minimize the risk of mechanical failure. The fourth and final requirement is to minimize energy consumption for performing the different functions, as this would reflect in a need for bigger and heavier batteries which would again decrease the jumping height. Based on these four design requirements, we decide which principles to implement in our robot.

4.2.1 Uprighting mechanism

We consider three categories of principles on how to achieve the uprighting movement (figure 4.2) and compare them using a weighted comparative evaluation (evaluation matrix in table 4.1). The first principle (A) consists of using arms or levers that are moved actively after landing to upright the structure. This principle offers the advantage to accomplish the uprighting movement on smooth surfaces as well as on rough terrain where the uprighting movement

Table 4.1: Weighted evaluation of the three working principles for the uprighting mechanism (figure 4.2)

Criteria	Weight	(A)	(B)	**(C)**
Light weight	0.4	4	3	**4**
Simplicity	0.1	1	3	**5**
Robustness	0.2	2	3	**4**
Energy consumption	0.3	1	2	**5**
Total	1	2.4	2.7	**4.4**

(1: Very unfavorable - 5: Very favorable)

may be obstructed. Compared to the other solutions, it is thus very effective. Its drawback however is that it requires additional actuators and a certain amount of energy to lift the entire structure and perform the movement. Additional actuators and hinges increase the complexity of the system and potentially decrease its mechanical robustness by making the entire system more error prone.

The second principle (figure 4.2.B) consists of moving a mass that is internal to the structure in order to create a roll momentum and upright the system as it is implemented in our EPFL jumper v2. It is a fairly simple, effective and robust solution, but it has the shortcoming that the robot after impact with the ground first settles in an upside down position and only then, an actuator shifts the weight at a certain energy cost. It carries the risk that the robot can be stuck in case that the terrain is not smooth enough and the rolling moment due to the weight shift is not sufficient to overcome the obstruction.

The third and final principle on the uprighting mechanism (figure 4.2.C) is a completely passive mechanism where the center of gravity is located in the lower part of the structure and creates a roll momentum to upright the robot. Compared to the second solution it is more effective because on landing and bouncing on the ground it already has the strong tendency to settle in an upright position. Since it does not need actuators and moving parts, it is a very simple, robust and energetically cheap solution. We therefore choose this principle to achieve the uprighting for our robot.

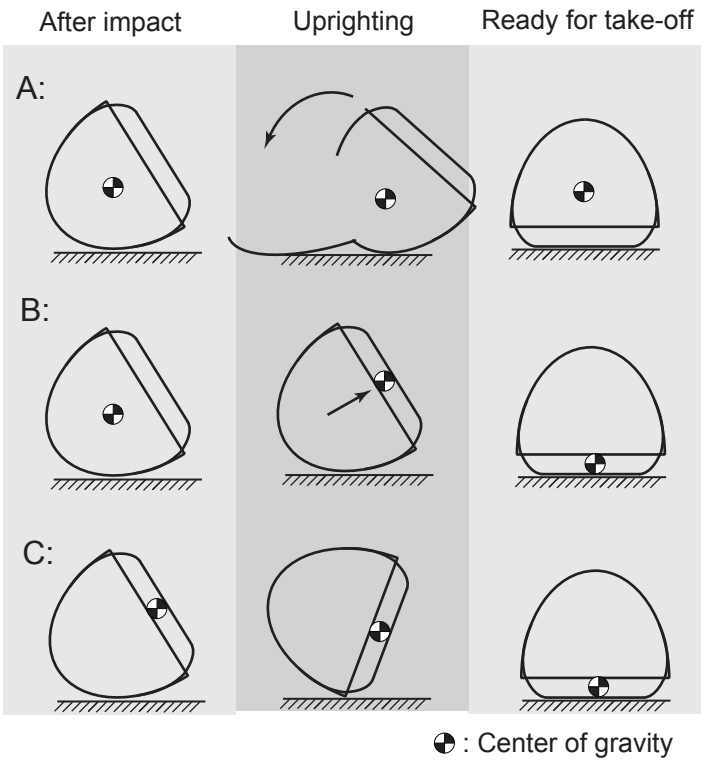

Figure 4.2: Three working principles for uprighting. (A) Arms or levers are moved actively after landing, (B) the center of gravity is actively shifted after landing to upright, (C) the position of the center of gravity leads to a passive uprighting movement

4.2.2 Steering mechanism

We consider four principles for the steering mechanism and compare them using the same weighted comparative evaluation as above (evaluation matrix in table 4.2). The first principle (figure 4.3.A) uses wheels to turn the robot on spot. It is a simple solution, but not very effective in cases where the terrain is not smooth because even small obstacles may prevent it from turning. In addition, it requires structures external to the robot that are exposed to potential damage on landing.

The principle (B) consists of shifting the center of gravity and consequently changing the direction of the jump. The advantage of this solution is that the actuation is inside the structure and therefore it is less prone to damage and more robust compared to the principle (A). The energy consumption is relatively low as only a fraction of the robot weight has to be moved and not the entire structure. The main drawback however, is that it is less effective compared to other principles where the entire robot is oriented prior to jumping because the shifting of the center of gravity can only change the lateral take-off angle. Another potential drawback is that shifting the position of the center of gravity affects the mass distribution of the structure and therefore also changes the in air behavior of the robot. This either leads to uncontrolled tumbling in air which decreases the jumping performance or it calls for a control strategy which then again increases the complexity of the system.

In the principle (C), the entire system turns on a foot. Its main drawback is that in order to turn, the foot must be in contact with the ground and the rest of the structure free to turn, which may be unlikely when the ground is uneven.

Principle (D) is similar to the principle (C) only that the foot is lifted and turned inside the structure. This simple way of orienting the robot combines the effectiveness of turning it prior to jumping such as solution (A) and (C) with the robustness to encapsulate the jumping mechanism inside the structure such as in solution (B). We therefore implement the working principle (D) in our jumping robot.

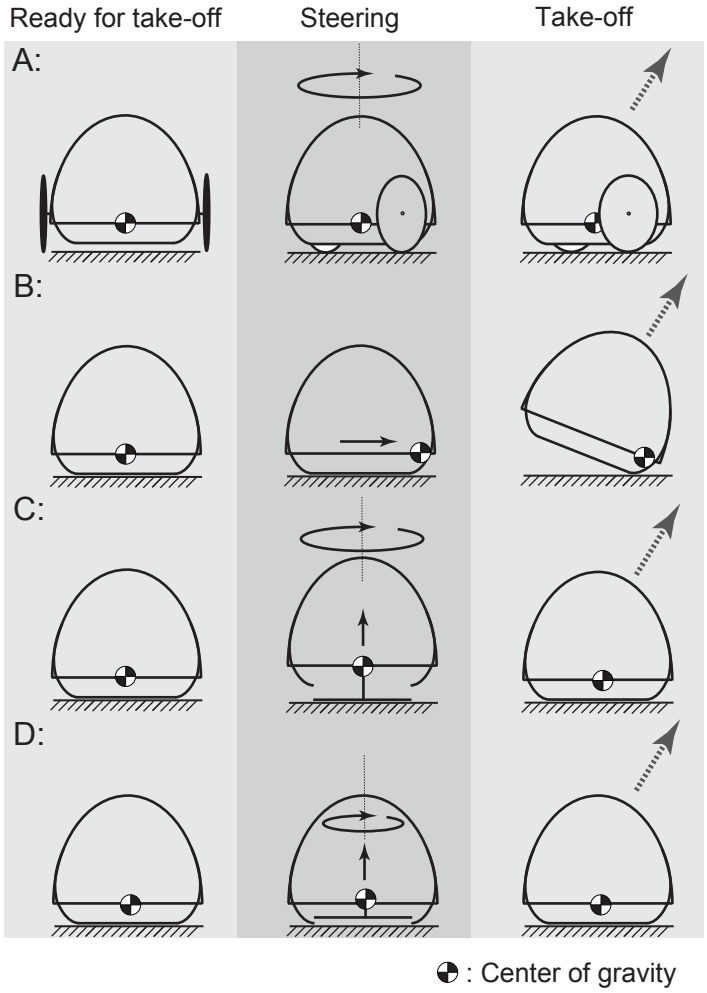

Figure 4.3: Four working principles for steering of the robot. (A) Wheels allow rotation on the spot prior to jumping, (B) center of gravity shifting to change the take-off direction, (C) a foot rotates the robot before jumping, (D) the jumping mechanism is rotated inside of the cage before jumping

Table 4.2: Weighted evaluation of the four different working principles for the steering mechanism (figure 4.3)

Criteria	Weight	(A)	(B)	(C)	**(D)**
Light weight	0.4	3	2	4	**5**
Simplicity	0.1	5	3	2	**2**
Robustness	0.2	2	4	4	**5**
Energy consumption	0.3	3	4	3	**4**
Total	1	3	3.1	3.5	**4.4**

(1: Very unfavorable - 5: Very favorable)

4.3 Implementation

The next step in the development of our jumping robot is to implement the chosen working principles for jumping, uprighting and steering in CAD, integrate the subsystems, fabricate the components and assemble the prototype (figure 4.4). In this section, we describe how we implemented the chosen principles and illustrate the design details of our jumping robot.

4.3.1 Uprighting mechanism

The uprighting mechanism consists of a cage structure designed so that it passively settles into a position suitable for the next jump (figure 4.5). The carbon axis (a) is connected to eight vertical 0.5mm carbon rods (b) and four horizontal 0.7mm carbon rings (c) using rigid joints (d), (e), (f), (g) to hold them together. The jumping mechanism (h) is attached within the cage on the axis using an aluminum fork (i). In order to reinforce the entire structure we added eight wires (k) that hold the axis to the first horizontal carbon ring. The materials used for the cage are commercially available carbon rods connected through rigid joints printed out of ABS plus.

4.3.2 Steering mechanism

The turning of the jumping mechanism inside the cage around the axis is realized using a motor and a double guided axis (figure 4.6). The 1.5mm carbon

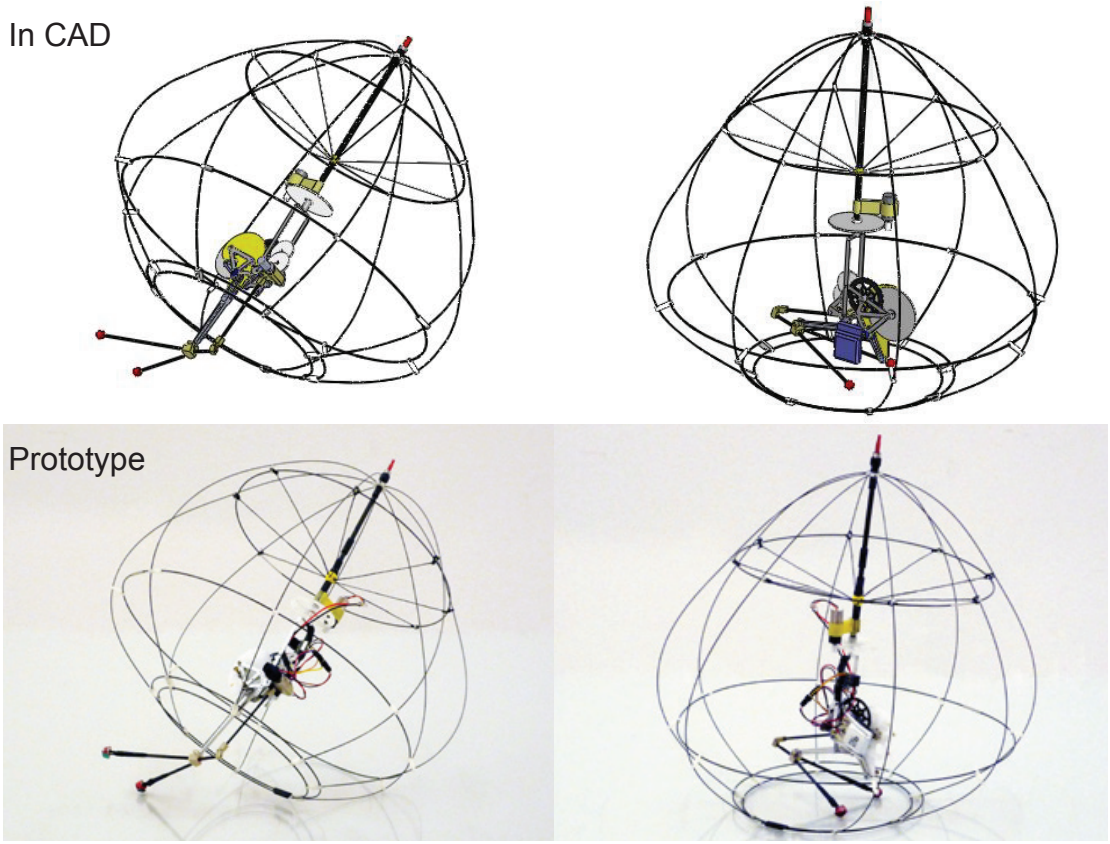

Figure 4.4: Jumping robot CAD design and fabricated prototype. We choose the design principle (figure 4.2.C) for the uprighting and (figure 4.3.D) for the steering of the robot

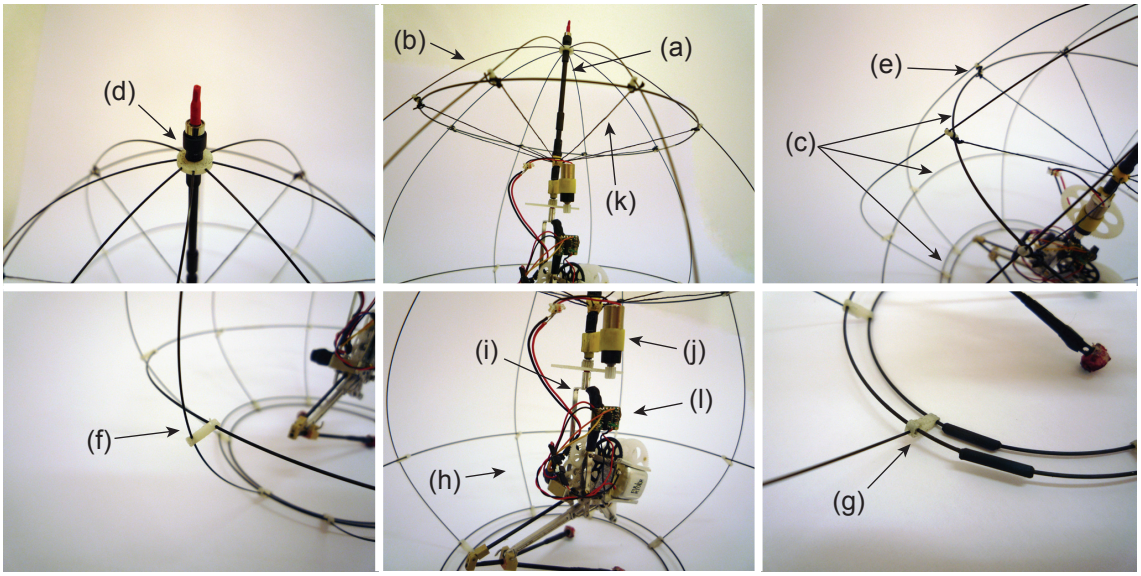

Figure 4.5: Mechanical design details of the EPFL jumper v3. (a) axis of the robot, (b) 0.5mm carbon rods, (c) 0.7mm carbon ring, (d), (e), (f), (g) connection pieces to hold the carbon ring and carbon rods together, (h) jumping mechanism as propulsion unit of the robot, (i) aluminum fork to interface the axis of the robot to the jumping mechanism, (j) 6mm DC pager motor to rotate the jumping mechanism around the axis, (k) wires to reinforce the cage structure, (l) 3-channel remote control

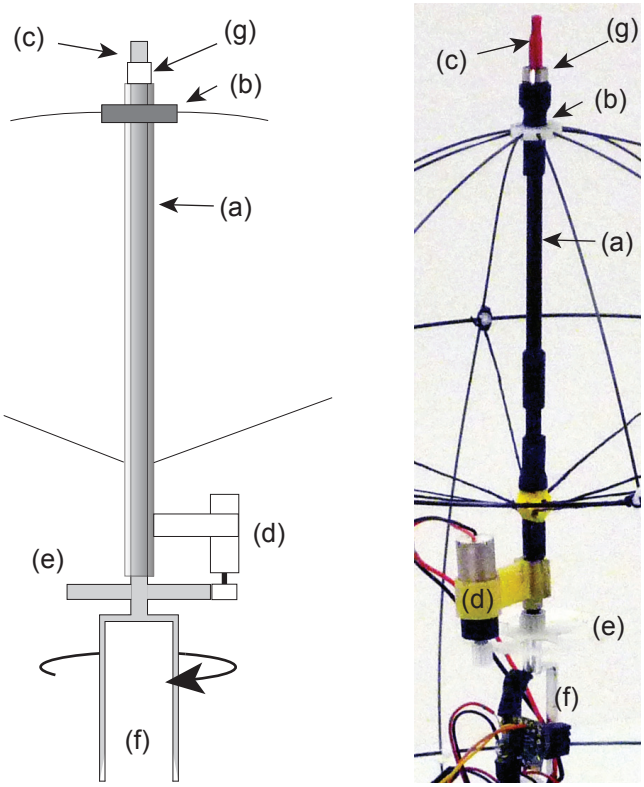

Figure 4.6: Implementation of the steering mechanism. (a) 1.5mm carbon tube, (b) connection piece, (c) 1mm carbon rod, (d) 6mm DC pager motor with inbuilt 1/25 gearbox, (e) module 0.3 12/81 teeth gear, (f) aluminum fork, (g) 1.5mm ball bearing

tube (a) is connected to the cage on the top connection piece (b) and guides a 1mm carbon rod (c) which can rotate freely around its axis. A 6mm DC motor with inbuilt 1/25 gearbox (d) which is fixed to the carbon tube (a) drives a module 0.3 12/81 teeth gear (e) which is attached to the carbon rod (c) and the fork (f) that holds the jumping mechanism. In order to keep the axial position and to reduce friction between the carbon tube (a) and the carbon rod (c), a 1.5mm ball bearing (g) is added as an interface. The transmission ratio from the motor to the axis is 1/225 in order to allow a slow enough rotation of the axis of 35.5 rotations per minute at a motor speed of 8000 rotations per minute.

4.3.3 Integration

After landing and settling, the jumping mechanism charges for the next jump and the cage passively uprights until the only contact with the ground is the

Table 4.3: Weight budget of the EPFL jumper v3

Part	Mass [g]
Total mass jumping mechanism	6.87
Carbon cage and axis	3.79
Motor with transmission	2.24
Remote control	0.70
LiPo Battery and cables	0.73
Total mass prototype	**14.33**

base of the cage (figure 4.7). The duration of the uprighting movement takes 2s. Once upright, the entire jumping mechanism is inside of the cage and can rotate around its vertical axis as illustrated in figure 4.6. The take-off sequence takes 18ms from touching the ground with the feet until the robot leaves the ground with a take-off velocity of 3.47m/s (figure 4.8).

In order to reduce the risk of damaging the legs on landing, the charging of the jumping mechanism starts already during the aerial phase to better protect the legs inside of the cage. As the center of gravity is in the lower part of the structure, the robot settles in a stable upright position and is ready to steer and jump again. The position of the center of gravity is located 5.2cm above the base of the cage when the legs are extended and 5.3cm when the legs are contracted.

The motor to steer and the motor of the jumping mechanism are remotely controlled using a miniature DIDEL 3-channel infra red controller (figure 4.5.l) which has a mass of only 0.7g. The battery used is a FullRiver 10mAh Lithium Polymer battery with a operating voltage of 3.7V which would theoretically allow 108 jumps.

The completely functional remote controlled prototype has a total size of 18cm and a mass of 14.33g including batteries and electronics (weight budget in table 4.3).

4.3.4 Adjustment of the jumping parameters

As described and characterized for the EPFL jumper v1, the jumping height can be adjusted by choosing a different pre-load angle for the torsion springs. The

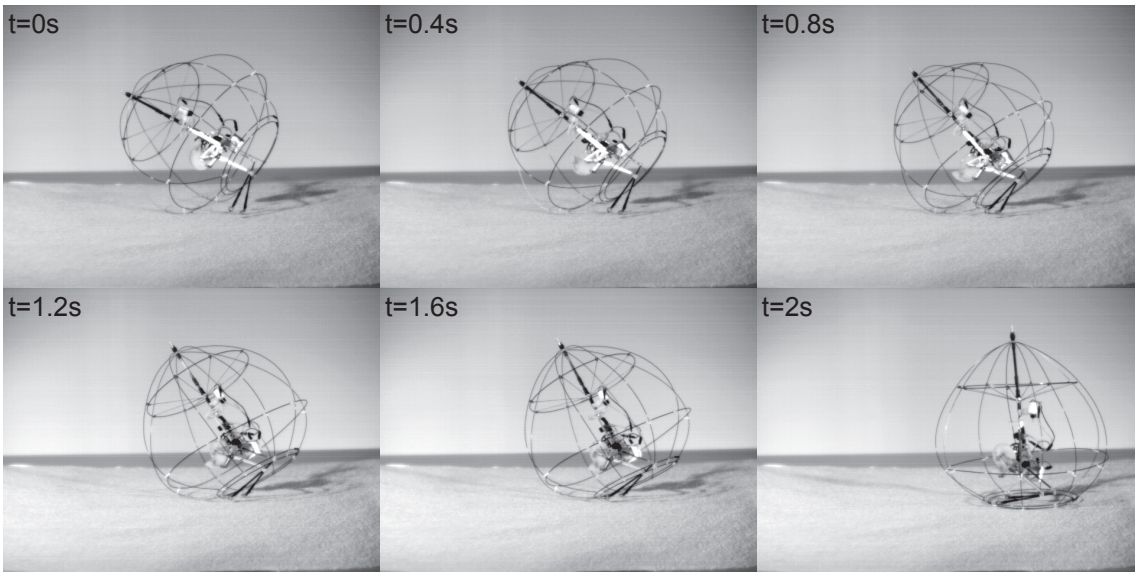

Figure 4.7: Uprighting sequence after landing and charging for the next jump. The center of gravity of the entire structure is in the lower part of the cage so that the robot uprights passively. When the jumping mechanism charges for the next jump, the legs are retracted within the cage in 2s. After this, the jumping mechanism is free to rotate around its vertical axis inside of the cage and jump

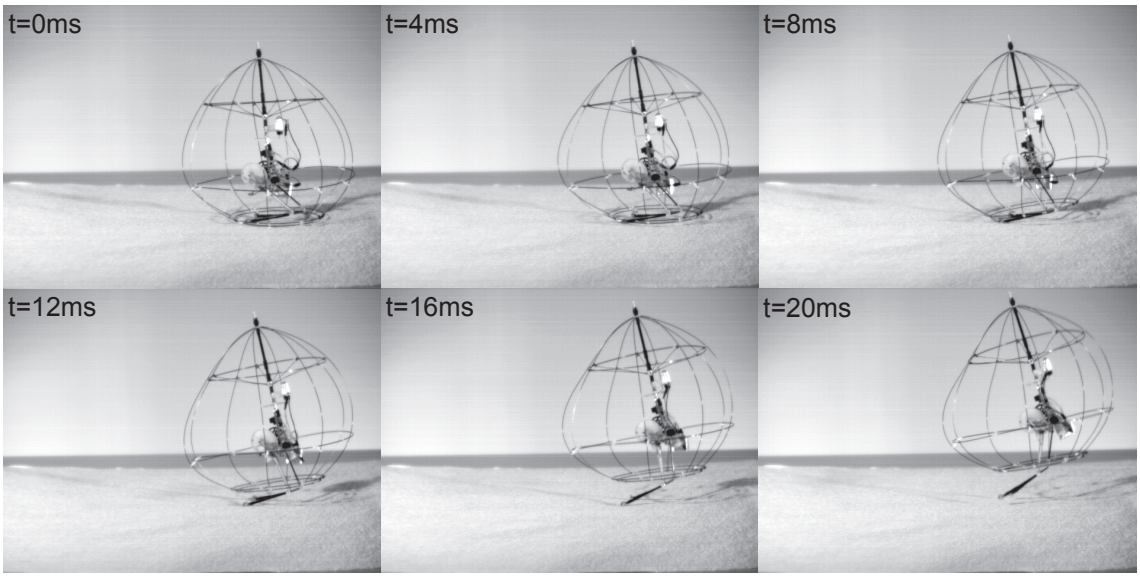

Figure 4.8: Take-off sequence. The take-off velocity of 3.47m/s is reached in 18ms

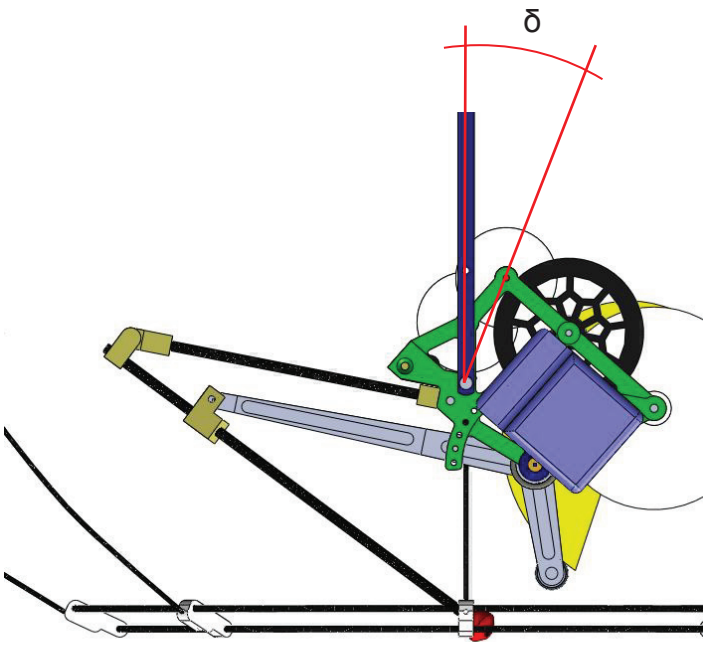

Figure 4.9: Integration of the jumping mechanism with the cage. The jumping distance can be changed by adjusting the angle δ which positions the attitude of the jumping mechanism inside of the cage

take-off angle can be adjusted by changing the foot length (e) (figure 2.4). In addition to this adjustments, the EPFL jumper v3 offers the possibility to change the jumping distance by altering the attitude of the jumping mechanism inside of the cage (angle δ in figure 4.9).

4.4 Results

In order to characterize the performance of the robot, we performed a series of experiments to determine the jumping height, take-off angle and jumping distance, depending on the different settings of the jumping robot. The durations, velocities and trajectories are measured optically, using a high-speed camera at 500 frames per second and ProAnalyst, to track the flight trajectory (see the accompanying movies for a summary of the experiments).

4.4.1 The cost of the cage

The goal of this first set of experiments is to estimate how much the jumping height is reduced due to the addition of the uprighting and steering ability. To do this, we perform jumping experiments for three configurations of the EPFL jumper v3. The first configuration is the complete EPFL jumper v3, including cage with a total mass of 14.33g. The second configuration is the EPFL jumper v3 without cage but the same weight as the caged system. The third configuration is the EPFL jumper v3 without the cage and a total mass of 7.57g.

For every configuration we perform one jump and plot the jumping trajectory in figure 4.10. In the first configuration, the robot jumps a height of 62cm, at a take-off angle of 75°. In the second configuration it jumps a height of 69cm at a take-off angle of 75°. In the third configuration the robot jumps a height of 111cm at a take-off angle of 75°.

4.4.2 Adjustment of the jumping parameters

In this set of experiments we characterize the change of jumping distance for three different settings of the angle δ , i.e. 0°, 6° and 21° (figure 4.9) which positions the attitude of the jumping mechanism inside the cage. For each of these three configurations we perform five jumps and compare the average jumping height, average jumping distance and the average take-off angle (figure 4.11). The average jumping distance for δ=0° is 42.2cm at an average take-off angle of 71.7°. The average jumping distance for the configuration with δ=6° is 24.2cm at an average take-off angle of 78.6°. For the third configuration with δ=21°, the robot jumps an average distance of 17.8cm at an average take-off angle of 81.7°. In order to analyze if the jumping heights, jumping distances and take-off angles are different, we perform a Kruskalwallis test [57]. The jumping distance is significantly different ($df = 14$, $p < 0.01$), the take-off angle as well is significantly different ($df = 14$, $p < 0.05$), and the jumping height is not significantly different (p=0.087) for the three configurations of the robot (figure 4.9, δ=0°, 6°, 21°).

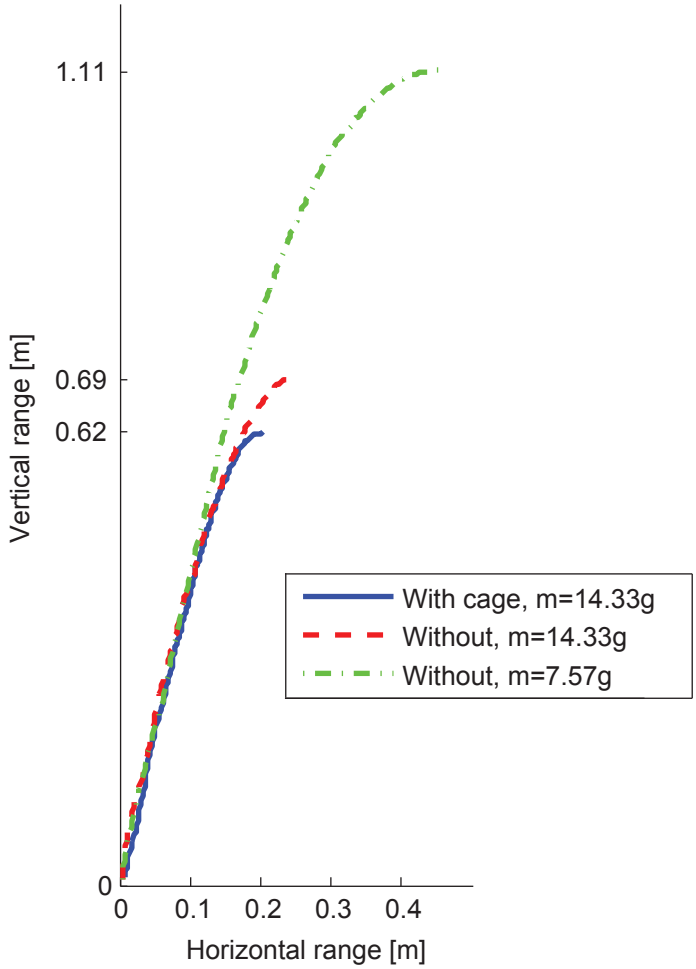

Figure 4.10: Jumping trajectory of the jumping robot for the complete robot prototype with cage, the robot without cage but the same weight as the caged system, and the jumping mechanism only, without cage. With the cage as a fully functional prototype it can jump a height of 62cm and a distance of 46cm at a take-off angle of 75°

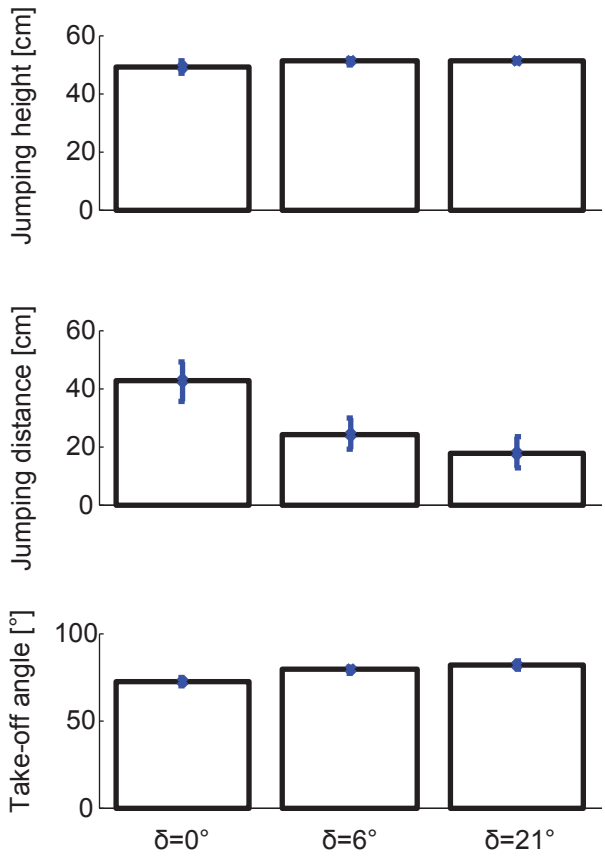

Figure 4.11: Average values and standard errors for the jumping height, the jumping distance and the take-off angle for δ=0°, δ=6°, δ=21° (figure 4.9).

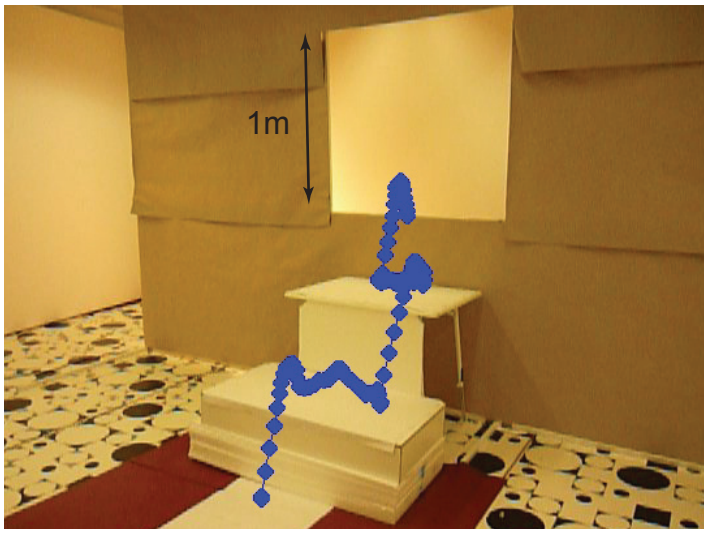

Figure 4.12: Trajectory of the jumping robot successfully climbing two stairs of each 45cm height and jumping into a window. The accompanying video 4 shows the behavior of three subsequent successful passages of this obstacle course.

4.4.3 Locomotion on an obstacle course

As a demonstration to show the ability of our jumping robot prototype to successfully perform steered jumps in cluttered environments, we built an obstacle course in our laboratory which consists of two stairs with a height of 45cm each and a window of 1m $\times$ 1m (figure 4.12). We place the robot on the ground at 10cm distance to the first stair and aim at jumping with several sequential steered jumps upstairs and into the window, all without human intervention on the scene. Depending on the operating skill of the human operator the window can be entered in approximately four jumps (see the accompanying video 4 for three successful passages of this obstacle course). For a better overview of the obstacle course, we depict the trajectory of only one successful run in figure 4.12. This demonstration summarizes the achieved design goals and successful locomotion ability of our jumping robot in cluttered environments.

4.5 Conclusion

The main bioinspired design principles that have been elaborated in this chapter are the use of a caged structure to protect the robot on landing and reorientation on ground to steer the jumps. It allows the EPFL jumper v3 to perform steered

repetitive jumps over obstacles that are more than 3.5 times its size.

Compared to the same robot without cage, the mass increase of 6.76g reduces the jumping height by 38% from 111cm to 69cm. By adding the actual cage structure it is reduced further by 7cm. This additional decrease in jumping height is due to the higher aerodynamical friction during jumping and the fact that the cage experiences oscillations right after take-off, which is lost energy that can not be converted into jumping height. Therefore, for our current robot, the 'cost' of having the ability to upright on landing and being able to steer corresponds to a decrease in jumping height of 44% compared to the jumping robot mechanism without those abilities.

The jumping height of the EPFL jumper v3 could be increased by reducing the weight of the cage, e.g. using a smaller motor to turn the jumping mechanism inside the cage, or by increasing the structural stiffness of the cage to reduce the oscillations after take-off. However, when using carbon rods as the structural material for the cage, it may be very difficult to further increase the stiffness of the cage without adding much additional material.

The results of the experiments for the adjustment of the jumping parameters indicate that the jumping distance and the take-off angle are different for the three settings of δ ($p < 0.01$ for the jumping distance and $p < 0.05$ for the take-off angle). Therefore, changing δ to alter the take-off angle offers an alternative to the variation of the foot length (e).

The main limitation of our current robot is a payload of only a few grams in order to be still able to jump a reasonable height of several times its own size. It is thus rather suited for low weight and low energy sensors and communication devices. For example, the electronics used on the EPFL jumper v2 consisting of a PCB populated with a microcontroller, a three axis accelerometer, a Hall sensor on the cam and an H-bridge motor driver has a weight of only 1.3g. Already this minimal electronic setup would allow the robot to detect its orientation and cam charging state and perform repetitive jumps autonomously. Adding two linear cameras with rate gyros could enable it additionally to avoid obstacles using optical flow at an additional mass of only 1.8g [168].

Depending on the desired task which this jumping robot is supposed to fulfill, other sensors could be added as well. If needed, the robot could be scaled up to carry higher payloads. However, designing the robot to carry higher pay-

loads would require its structure to be more robust as the impact forces on landing increase linearly with the mass of the system. Thus, there may be a trade-off between possible payload of the robot and its own weight. Further research could address scaling issues of this robot in order to optimize trade-offs between payload and weight of the system.

5 Flight

This chapter addresses the challenges of the flight phase and evaluates under which conditions the addition of wings to a jumping robot gives added benefits compared to jumping without wings. We developed a theoretical model which allows to estimate whether the addition of wings to a jumping robot can prolong its jump when jumping with the same take-off energy. The calculation are confirmed by experiments with a winged jumping robot. The results from both the model and the experiments indicate that wings can prolong the jump in case that the robot jumps from an elevated starting position, but not when jumping from ground. Based on this conclusion, we developed the EPFL jumpglider, the first miniature robot capable of jumping and gliding that has been presented so far. It has a mass of 16.5g and is able to perform jumps from elevated positions, perform steered gliding flight, land safely and locomote on ground by repetitive jumping[1].

[1]See accompanying video at http://lis.epfl.ch/microglider/EPFLjumpglider.mp4

5.1 Introduction

The jumping robots that we reviewed in the state of the art section and our EPFL jumpers v1-3 are ballistic jumpers. This means that once they leave the ground, they behave like passive projectiles in air and fly on a parabolic trajectory, assuming the ideal case of no air friction. The addition of aerodynamical appendages such as wings to a ballistic jumping robot can have two benefits compared to jumping without wings. We call this concept of winged jumping 'jumpgliding'. First, the wings can create aerodynamical lift to prolong the jump. Second, they can decrease the airborne velocity which reduces the potentially hazardous kinetic impact energy on landing, which needs to be absorbed by the robot structure. One drawback of having wings is an increase in mass and size of the jumping robot, which potentially reduces the jumping distance.

This chapter evaluates the conditions under which the addition of wings to a jumping robot increases its jumping distance and reduces the impact energy on landing when compared to ballistic jumping. In order to do that, we start by presenting a theoretical model for the energetic cost of locomotion and the impact energy on landing for ballistic jumping and jumpgliding. The model allows to determine whether adding wings could potentially provide a ballistic jumper with the above mentioned two benefits.

We then apply the model to our EPFL jumpers and present a novel winged jumping and gliding robot called 'EPFL jumpglider'. It has a mass of 16.5g and is able to jump from elevated positions and steer during gliding flight. Once on ground, it can progress with small repetitive jumps. The EPFL jumpglider specifically addresses the challenges of the flight phase, which we defined as (i) being compact in shape and having low air friction, (ii) creating aerodynamical lift and (iv) being able to steer in air.

5.2 Jumpgliding versus ballistic jumping

In this section we present a theoretical model that aims at comparing jumpgliding to ballistic jumping. We start by evaluating the horizontal distances traveled per energy unit for both locomotion strategies. Based on projectile physics laws [130], we propose a simplified model for jumpgliding and its comparison to

ballistic jumping.

Similarly to the calculations in chapter 2, the model assumes a ballistic jumper with a mass m_j which is propelled with a jumping energy E. The flight phase is sketched in figure 5.1.A. For the simplified case without air friction, its maximal jumping distance is reached at a take-off angle $\alpha_0 = 45°$ and is given by

$$d_{jmax} = \frac{2E}{m_j g} \tag{5.1}$$

For jumpgliding, we decompose the flight trajectory into three phases as illustrated in figure 5.1.B. The jumpgliding sequence starts with the 'ascending phase' where the jumpglider performs a ballistic jump as in the ballistic case. Once on top of the jumping trajectory it enters the 'transition phase' to the subsequent steady state 'gliding phase'. Jumping in air inevitably creates air friction. For simplicity, we do not try to model the air friction in detail in this chapter, but we account for air friction losses by multiplying the jumping energy E by a friction factor c_f, for both, ballistic jumping and jumpgliding. For example, a friction factor of $c_f = 0.6$ means that 40% of the jumping energy is consumed by air friction during the flight trajectory. In the following, we describe the detailed modeling and assumptions of these three phases.

Ascending phase

We model the ascending phase as ballistic jumping with the take-off energy E and a jumpglider mass m_{jg}. The height reached h_{jg} and distance traveled d_{jgj} is given by

$$d_{jgj} = \frac{c_f E \sin(2\alpha_0)}{m_{jg} g} \tag{5.2}$$

$$h_{jg} = \frac{c_f E \sin(\alpha_0)^2}{m_{jg} g} \tag{5.3}$$

The horizontal velocity on top of the jump, v_{top} can be expressed as [130]

$$v_{top} = \sqrt{\frac{2c_f E}{m_{jg}}} \cdot \cos(\alpha_0) \tag{5.4}$$

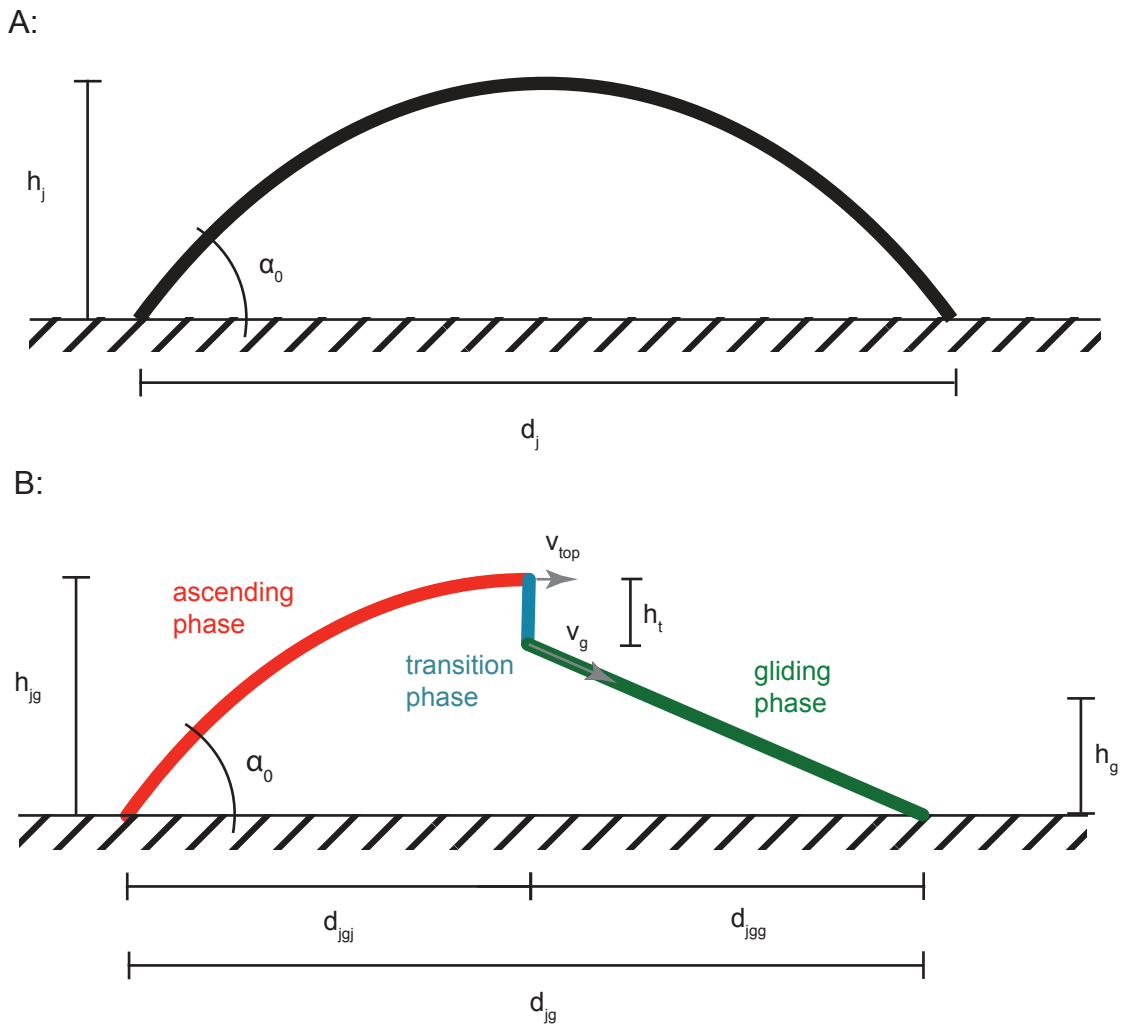

Figure 5.1: Sketch of the flight trajectories when locomoting on ground. A: Ballistic jumping trajectory, B: Jumpgliding trajectory, consisting of an ascending phase, a transition phase and a gliding phase

Transition phase

During the transition phase the jumpglider moves from the ascending phase to the subsequent gliding phase. In reality, this is a dynamic stalling maneuver in which the jumpglider recovers from the top of the jumping trajectory, accelerates to the required gliding velocity in order to then perform a dynamic gliding sequence. For simplicity, we assume that the only component to consider for our model is an acceleration from the top velocity v_{top} to the gliding velocity v_g. We assume that the velocity is minimal on top of the ascending phase, which is naturally the case when no propulsion is applied to the system during the ascending phase. Based on a simple energy balance we can express the required height loss h_t to reach the gliding velocity as

$$h_t = \frac{1}{2g}(v_g^2 - v_{top}^2) = \frac{1}{2g}(v_g^2 - \frac{2E}{m_{jg}} \cdot \cos(\alpha_0)^2) \tag{5.5}$$

Gliding phase

We assume the gliding phase to be steady state stable gliding [77] with the gliding ratio f [142] from the height $h_g = h_{jg} - h_t$. The distance traveled during the gliding phase is given by

$$d_{jgg} = f \cdot (h_{jg} - h_t) \tag{5.6}$$

Summarizing, the distance traveled by jumpgliding can be expressed as

$$d_{jg} = \underbrace{\frac{c_f E \sin(2\alpha_0)}{m_{jg} g}}_{\text{ascending phase}} + \underbrace{\frac{f}{g} \cdot (\frac{c_f E}{m_{jg}} - \frac{v_g^2}{2})}_{\text{gliding phase}} \tag{5.7}$$

The take-off angle at which the distance traveled is maximal, can be found by setting $\frac{\partial d_{jg}}{\partial \alpha_0} = 0$ and solving it for α_0. It follows that d_{jg} is maximal at a take-off angle of 45°. By inserting $\alpha_0 = 45°$ into equation 5.7, the maximal horizontal distance that can be reached with jumpgliding can be expressed as

$$d_{jgmax} = \frac{c_f E}{m_{jg} g}(1 + f) - \frac{f v_g^2}{2g} \tag{5.8}$$

It can be seen that the maximal horizontal distance traveled for jumpgliding

increases when increasing the jumpgin energy E and the gliding ratio f. The jumping distance decreases with increased system mass m_{jg}, increased gliding velocity v_g and a lower air friction factor c_f. Therefore, the design requirements for a jumpglider are low mass, air friction and gliding velocity, while maximizing its gliding ratio and jumping energy. The equations 5.1 and 5.8 allow evaluating under which conditions jumpgliding leads to larger traveled distances compared to ballistic jumping. This condition can be mathematically expressed as

$$d_{jgmax} > d_{jmax} \tag{5.9}$$

$$\frac{c_f E}{m_{jg} g}(1+f) - \frac{f v_g^2}{2g} > \frac{2 c_f E}{m_j g} \tag{5.10}$$

In order to simplify the expression, we introduce a wing mass factor k which indicates the mass increase due to the addition of wings to the jumping robot.

$$k = \frac{m_{jg}}{m_j} \tag{5.11}$$

Solving equation 5.10 for the term E/m_j allows to express the energy density given by the jumping robot as a function of the increase in mass k due to the wings and the parameters of gliding flight v_g and f. It indicates the minimal needed energy density of a jumping robot so that the addition of wings would lead to an energetically cheaper locomotion strategy. It is given by

$$\boxed{\frac{E}{m_j} > \frac{1}{c_f} \cdot \frac{f v_g^2}{2} \cdot \frac{k}{1+f-2k}} \tag{5.12}$$

As a variation of the equations presented above, we consider the case of jumping from an elevated position (figure 5.2), such as jumping from a cliff, down a slope or when descending stairs. For a height of the elevated position of h_o, the horizontal distance that can be covered with ballistic jumping is given by [130]

$$d_j = \frac{v_o \cos(\alpha_0)}{g}(v_0 \sin(\alpha_0) + \sqrt{(v_0 \sin(\alpha_0))^2 + 2 g h_o} \tag{5.13}$$

The maximal horizontal distance that can be covered when jumping ballisti-

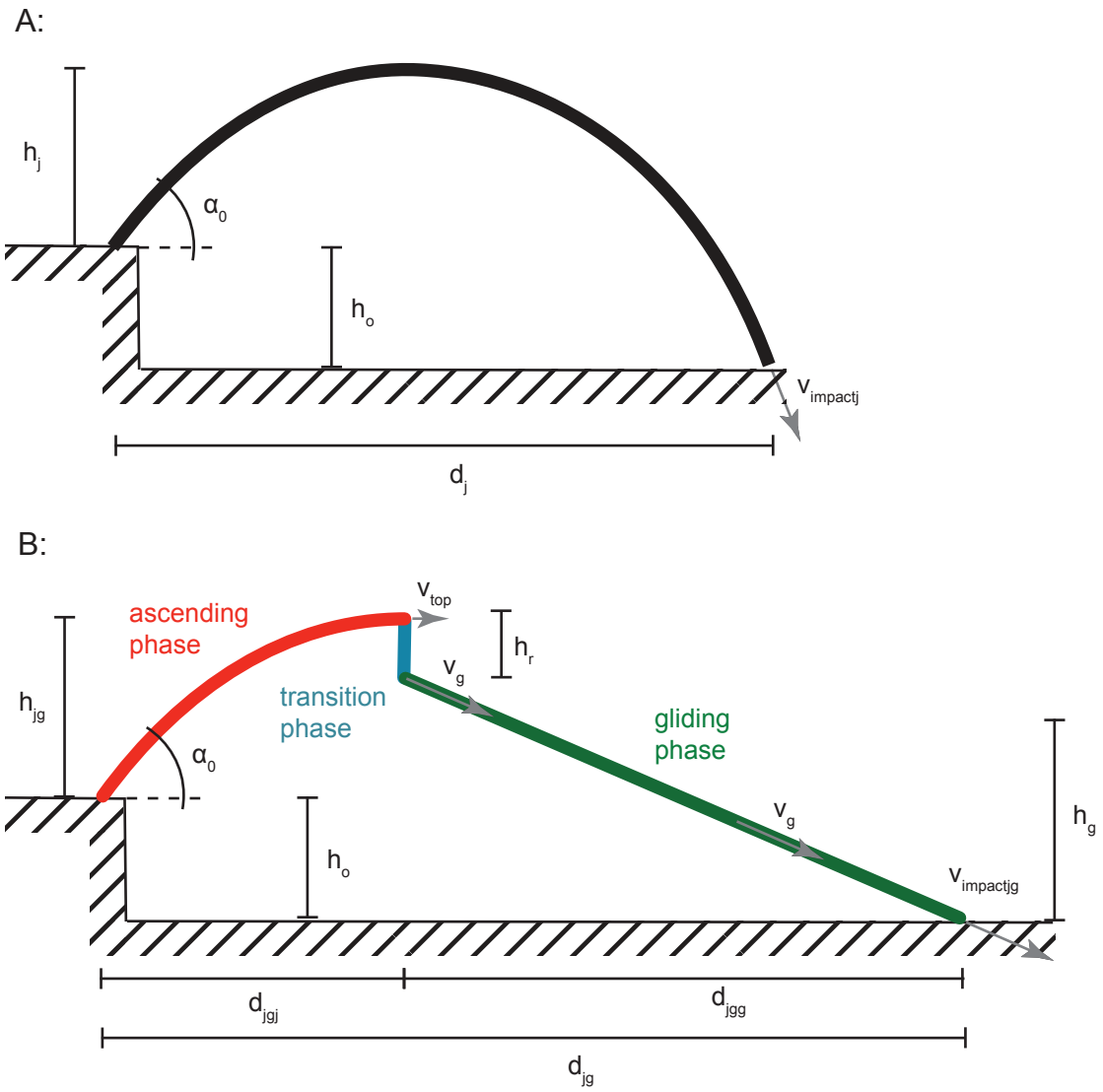

Figure 5.2: Sketch of the flight trajectories when jumping from an elevated starting position. A: Ballistic jumping trajectory, B: Jumpgliding trajectory

cally from an elevated position can be determined by setting $\frac{\partial d_j}{\partial \alpha_0} = 0$ and solving it for the take-off angle α_0. It follows that

$$d_{jmax} = \frac{v_0\sqrt{v_0^2 - 2gh_o}}{g} \tag{5.14}$$

$$= \frac{2}{g}\sqrt{\frac{c_f E}{m_j}(\frac{c_f E}{m_j} - gh_o)} \tag{5.15}$$

For jumpgliding, we extend equation 5.7 with the term $h_o f$ which accounts for the additional horizontal distance covered due to the additional height h_o

$$d_{jg} = \underbrace{\frac{c_f E \sin(2\alpha_0)}{m_{jg} g}}_{\text{ascending phase}} + \underbrace{\frac{f}{g} \cdot (\frac{c_f E}{m_{jg}} - \frac{v_g^2}{2}) + f \cdot h_o}_{\text{gliding phase}} \tag{5.16}$$

$$d_{jgmax} = \frac{c_f E}{m_{jg} g}(1 + f) - f(\frac{v_g^2}{2g} + h_o) \tag{5.17}$$

The condition under which jumpgliding leads to larger distances covered for a given take-off energy can be expressed analogous to equation 5.10. In order to determine in which cases the addition of wings is beneficial, we are interested in the limit height of the elevated position h_o for which this is the case. For a given jumpgliding robot where the parameters E/m_j, k, f, v_g and c_f are given due to its mechanical design, this limit height indicates from which height jumpgliding locomotion leads to larger horizontal distances covered when compared to ballistic jumping.

$$d_{jgmax} > d_{jmax} \tag{5.18}$$

$$\frac{c_f E}{m_{jg} g}(1 + f) - f(\frac{v_g^2}{2g} + h_o) > \frac{2}{g}\sqrt{\frac{c_f E}{m_j}(\frac{c_f E}{m_j} - gh_o)} \tag{5.19}$$

With $m_{jg} = km_j$, $a = E/m_j$ and $b = (1+f)/k$ it follows that

$$\boxed{h_o > \frac{\sqrt{2v_g^2af^2 + 4a^2f^2 - 4ba^2f + 4a^2} - 2a + abfg}{f^2} - \frac{v_g^2}{2g}} \tag{5.20}$$

The second potential benefit that we investigate is under which circumstances jumpgliding leads to less impact energy on landing. The impact energy corresponds to the kinetic energy on impact which is defined as

$$E_{impact} = \frac{1}{2}mv_{impact}^2 \tag{5.21}$$

with m being the robot mass and v_{impact} the velocity on impact. For ballistic jumping, the impact velocity v_j can be expressed with v_{jy} being the vertical impact velocity and v_{jx} the horizontal impact velocity as

$$v_{jy} = \sqrt{2g(h_o + h_j)} \tag{5.22}$$

$$v_{jx} = \sqrt{\frac{2c_fE}{m_j}} \cdot \cos(\alpha_0) \tag{5.23}$$

$$v_j = \sqrt{v_{jx}^2 + v_{jy}^2} = \sqrt{2(gh_o + \frac{c_fE}{m_j})} \tag{5.24}$$

For jumpgliding, the impact velocity corresponds to the gliding velocity v_g. We aim at determining from which height the impact energy on landing is lower for the jumpglider compared to the ballistic jumper. This condition can be expressed as

$$E_{impactj} > E_{impactjg} \tag{5.25}$$

$$\frac{1}{2}m_jv_j^2 > \frac{1}{2}m_{jg}v_g^2 \tag{5.26}$$

with $E_{impactj}$ as the impact energy of the ballistic jumper and $E_{impactjg}$ as the impact energy of the jumpglider. Solved for the elevated position height, we

obtain

$$\boxed{h_o > \frac{1}{2g} k v_g^2 - \frac{c_f E}{g m_j}} \tag{5.27}$$

Equation 5.27 indicates the limit height from which jumpgliding leads to a lower kinetic energy on impact compared to ballistic jumping.

In conclusion, the theoretical model can be used to predict under which circumstances adding wings to a ballistic jumper can increase the jumping distance and decrease the impact energy on landing. For an existing jumping robot it allows to estimate the minimal gliding ratio that needs to be reached in order that adding wings could have benefits compared to ballistic jumping without wings.

5.3 Evaluation of adding wings to jumping robots

In this section, we aim at applying the model to our EPFL jumpers in order to evaluate whether the addition of wings can prolong its jumps on ground and from elevated positions. The same elaboration can be applied analogously to other jumping robots in order to estimate the benefits of jumping with wings.

In order to define the design requirements for the wings that shall be added to our jumpers, we use the model to estimate the minimal needed gliding ratio that has to be reached so that a jumpgliding strategy would be beneficial. As modeled in chapter 2, the EPFL jumper v1 has a target mass of 10g and a take-off energy of 82mJ which leads to an energy density of 8.2J/kg. This is the highest energy density of all miniature jumping robots that have been presented to date. Therefore, the EPFL jumper v1 is taken as platform to estimate the benefits of adding wings. For such a jumping robot with wings, we first estimate the values for the friction factor, the gliding velocity and the wing mass factor. Based on these values, we then discuss the results from the model.

We start by assuming a value for the friction factor. Bennet-Clark [11] measured the jumping height of insects in air and in vacuum with the goal to estimate how much of their jumping energy is lost due to the air friction. He concludes that locusts jump a height of only between 51% and 68% in air compared to a jump in vacuum. This means that these insects loose between 32% and 49% of their jumping energy due to air friction. For the example in this

section we therefore assume that the average loss of the jumping energy is 40%, which corresponds to a friction factor of $c_f = 0.6$.

The gliding velocity can be estimated based on experiments with gliding robots and animals of similar size as the jumpglider. The gliding velocities of miniature gliders that have been presented range from 1.5m/s in [77] up to 5m/s in [154]. Flying squirrels jumpglide at a velocity of 2.5m/s [44], and flying lizards glide at a velocity of around 6.3m/s [99]. Based on these values of existing systems, we assume an average value of $v_g = 2.5$m/s for the steady state gliding velocity of our jumpglider.

The added mass due to the wings can as well be estimated based on examples of existing miniature flying robots. The airframe and wings of the perching glider presented in [82] has a mass of 1.4g, the foldable wings of the glider in [79] weigh 4.5g, and the airframe and wings of the AirBurr in [76] have a total mass of around 12g. We assume that it is possible to construct the wings for the jumpglider at a mass of 5g, which corresponds to a wing mass factor or $k = 1.5$.

Based on a friction factor of 0.6, a gliding velocity of 2.5m/s and a wing mass factor of 1.5, we illustrate and discuss the implications of these assumptions on the inequalities 5.12, 5.20 and 5.27.

Figure 5.3 shows the limit lines of the inequality 5.12 and for variations of the wing mass factor and the gliding velocity. It can be seen that for an energy density of 8.2J/kg and a gliding velocity of 2.5m/s it is very difficult to reach the area where adding wings prolongs the jump. For example, with a wing friction factor of 1.5, it would be necessary to build wings with a gliding ratio of more than 42.3 in order for jumpgliding to travel further than ballistic jumping. For comparison, gliding squirrels have a gliding ratio of around 1-3 [70], small gliders reach a gliding ratio of between 3 [43] and 5.6 [77] and fast flying Micro Aerial Vehicles can have gliding ratios of up to around 8 [51]. Based on these gliding ratios of existing gliders in nature and robotics, we consider it to be unfeasible to reach a gliding ratio of more than 42.3 with a winged version of our EPFL jumper v1. In a more realistic scenario with a gliding ratio of 3 such as for gliding squirrels, our jumping robot would need an energy density of at least 23.4J/kg (+169%) to jump further with wings on ground when compared to ballistic jumping.

Figure 5.4 illustrates the limit lines of the inequality 5.20. The elevated posi-

tion height where jumpgliding leads to further traveled distances increases for higher energy densities of the robot. Therefore, the limit height from which having wings prolongs the jumps decreases for robots with less jumping performance and heavier wings. For a winged EPFL jumper v1 and an assumed gliding ratio of 3, the limit height would be 33cm.

In order to evaluate the reduction of impact energy on landing, we illustrate the inequality 5.27 in figure 5.5. The graph indicates that the impact energy is reduced for jumpgliding compared to ballistic jumping for a wide range of parameter combinations. For our example, the impact energy is reduced in all cases, when jumping on ground and from elevated positions.

It can be concluded based on the case of the EPFL jumper v1 a jumpgliding locomotion strategy reduces the impact energy on landing. It is the energetically cheaper locomotion strategy compared to ballistic jumping when the jump starts from elevated positions, but not when moving on ground. In the following sections we follow a synthetic approach and present an implemented version of a jumping robot with wings. It allows an experiment based evaluation of the benefits of jumpgliding as opposed to ballistic jumping for our EPFL jumper v1.

5.4 Implementation of a jumpglider

In order to practically explore the benefits and limitations of jumpgliding from elevated positions in miniature robotics compared to ballistic jumping, we developed the 'EPFL jumpglider' (figure 5.6). To the best of our knowledge, it is the first physical miniature jumping and gliding system that has been presented to date. It has a wingspan of 50cm and a maximal chord length of 10cm. The wings have a surface area of $0.039m^2$ and a wing loading of $4.15N/m^2$. As wing material we use Durobatics™, a Polysterene foam which is widely used in the hobbyist community to build light weight wings for remote controlled airplanes. The EPFL jumpglider consists of the EPFL jumper v1 as propulsion unit and a CNC cut Polyimide frame to hold the wings. We initiate the jumps and control the steering by way of a 3-channel infra red remote control and power it using a 20mAh LiPo battery located on top of the wing. For steering, we add a tail with rudder, taken from a commercially available MicroCeline airplane. Due to the wings, the robot keeps an upright position after landing for the next take-

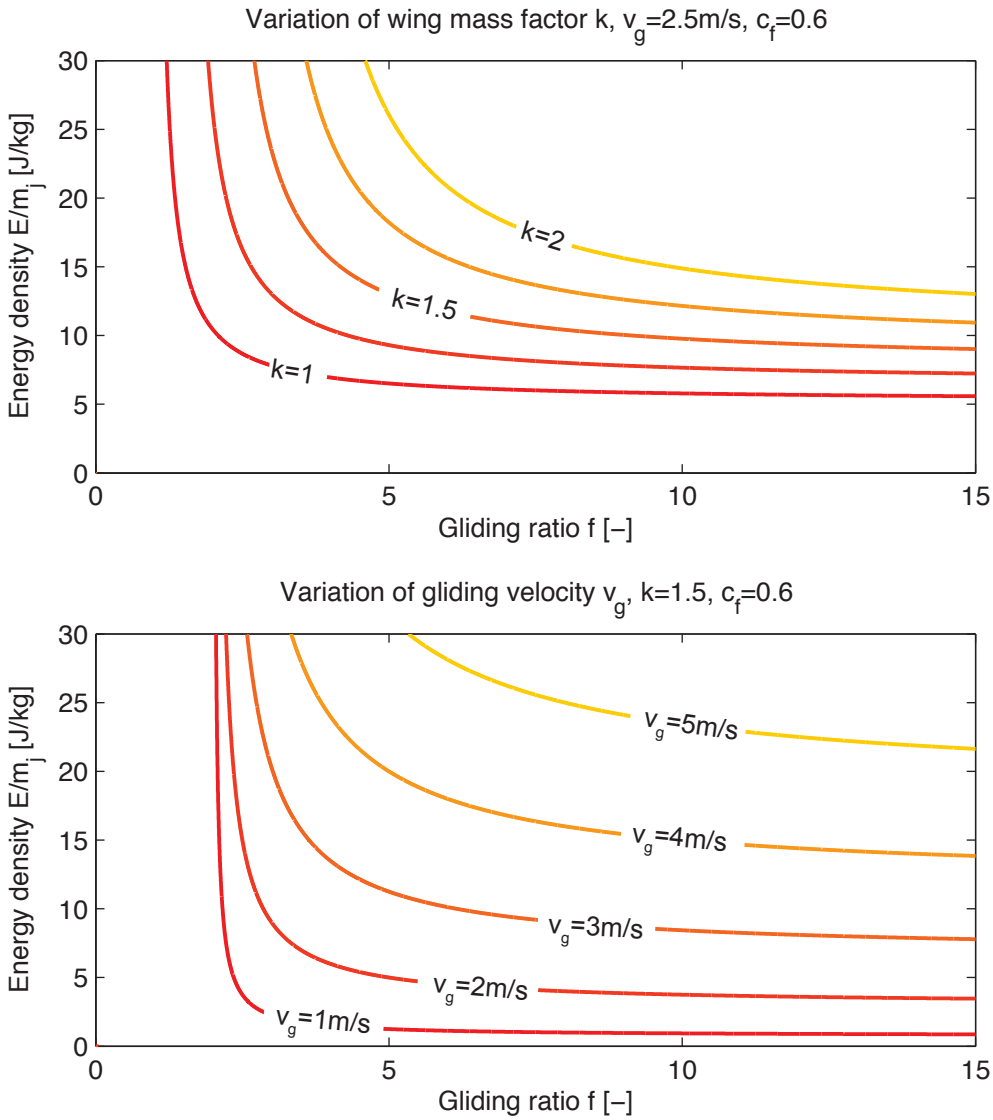

Figure 5.3: Energy density of the robot for which jumpgliding leads to larger distances traveled compared to ballistic jumping (limit lines of the inequality 5.12)

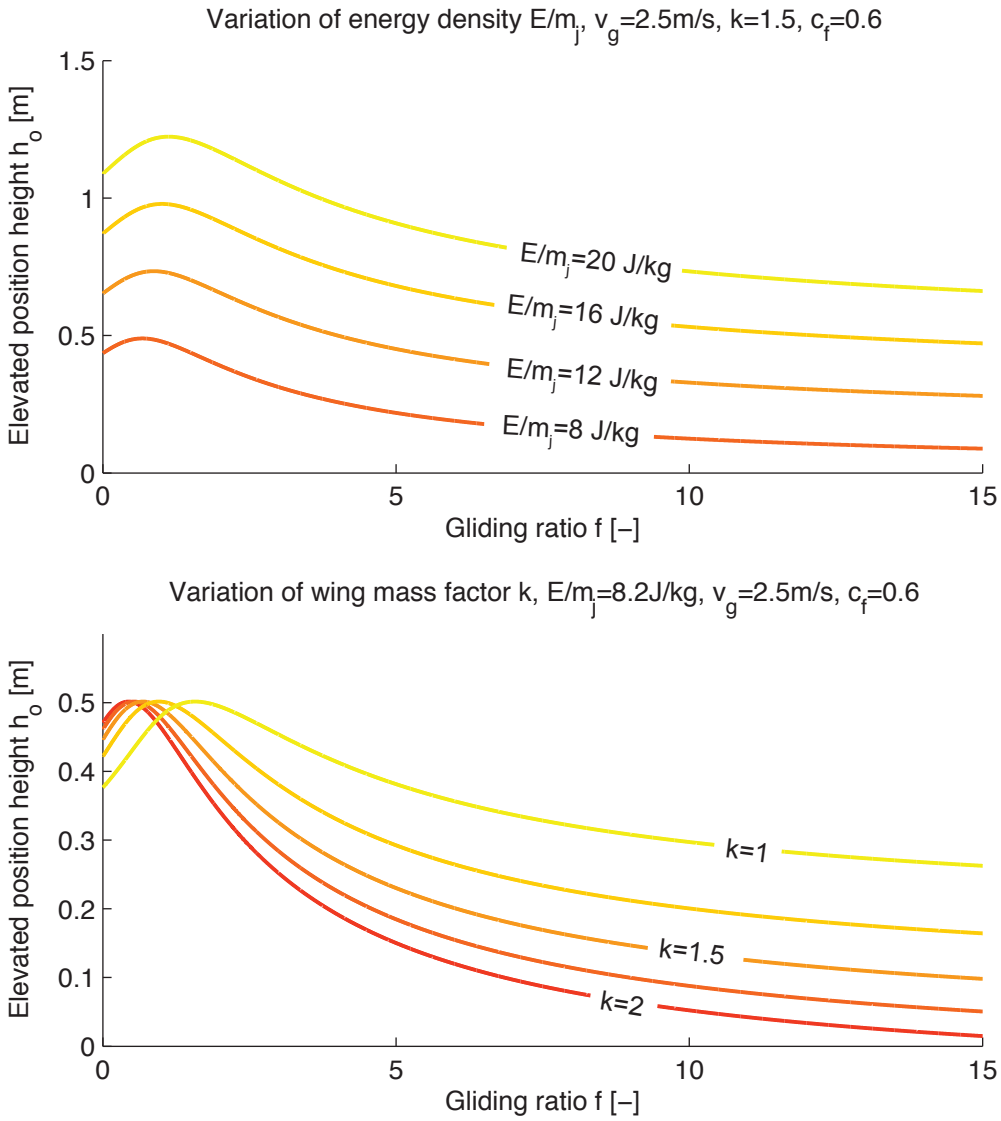

Figure 5.4: Elevated position height from which jumpgliding leads to larger distances covered compared to ballistic jumping (limit lines of the inequatlity 5.20)

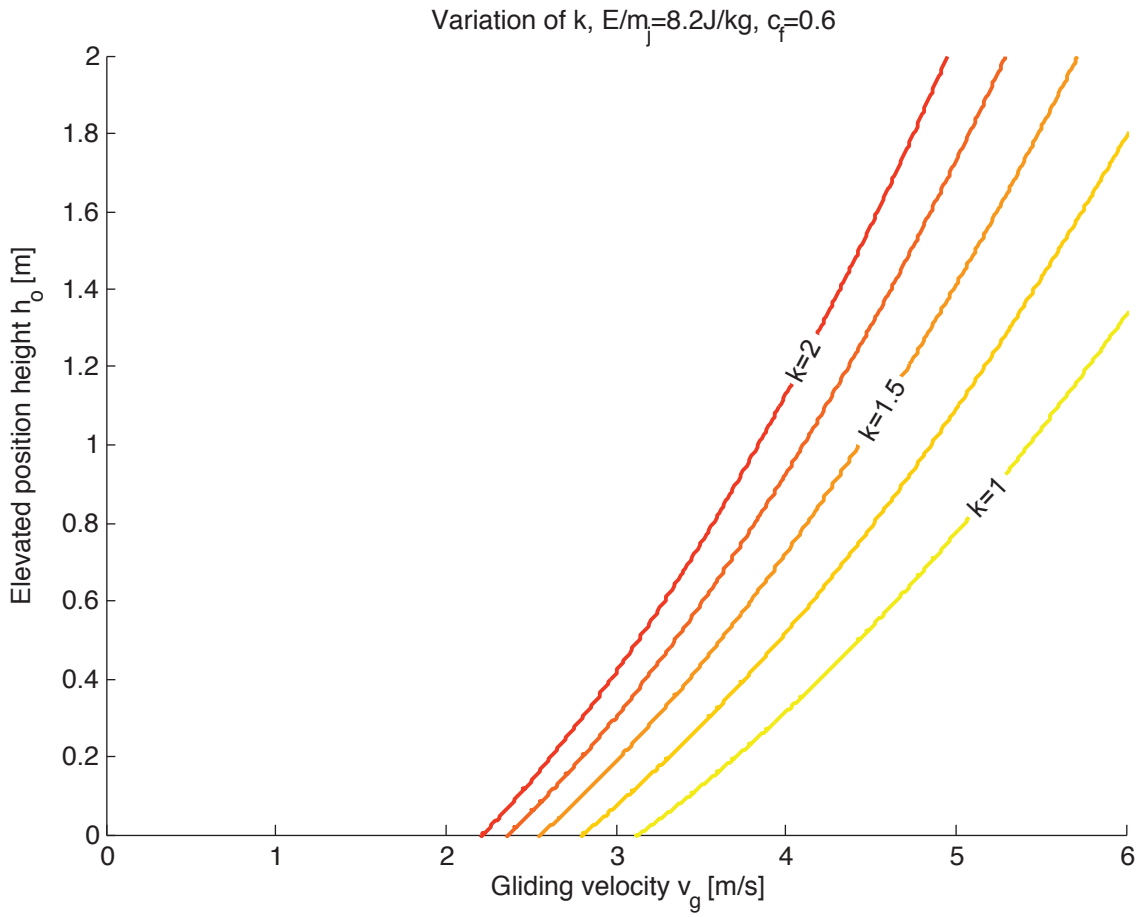

Figure 5.5: Elevated position height where jumpgliding reduces the impact energy on landing compared to ballistic jumping down from an elevated position with height h_o (limit lines of the inequality 5.27)

off. This enables the robot to perform repetitive jumps without needing a cage or an uprighting mechanism. The weight budget is summarized in table 5.1. The wings contribute an additional mass of 8.72g (+121%) to the ballistic EPFL jumper v1, which corresponds to a wing mass factor of 1.89.

5.4.1 Jumpgliding performance

This subsection provides an experimental comparison of jumpgliding and ballistic jumping from elevated positions (see the accompanying movie material for a summary of the jumpgliding performance). The experimental setup consists of an elevated start position, located 2m above the ground. We performed ten consecutive jumps with the jumpglider and the ballistic jumper, both at a take-off angle of 45°and filmed the flight trajectories at 30 frames per second. Based on these movies we track the trajectories (figure 5.7.A) using ProAnalyst, a feature tracking software and calculate the flight velocity (figure 5.7.B). The results show that the flight velocity of jumpgliding increases during the transition phase when descending from the top of its trajectory and converges towards its steady state gliding velocity. On the contrary, the flight velocity of ballistic jumping increases monotonically until impact. Figure 5.8 shows the measured average impact velocity v_{impact}, average horizontal distance traveled d and average impact energy E_{impact} for both, the jumpglider and the ballistic jumper. It can be seen that the velocity on impact is reduced by 53% when jumpgliding, resulting in a reduced impact energy of 54%. Further, we measure that the horizontal distance traveled of jumpgliding is increased by 123% compared to ballistic jumping. These results clearly show that jumpgliding from an elevated starting position offers an increased jumping distance and reduced impact energy when compared to ballistic jumping.

The second set of experiments aims at illustrating the locomotion capabilities of the EPFL jumpglider when jumping from an elevated starting position and propagating on ground. The EPFL jumpglider jumps from a height of 2.53m, glides and lands safely on a table, where it progresses by jumping (figure 5.9). A closeup view of these jumps on the table can be see in figure 5.10. With every jump it progresses an average measured distance of 30.2cm with a jumping height of 12cm. It can perform such a jump every 3s, which leads to an average

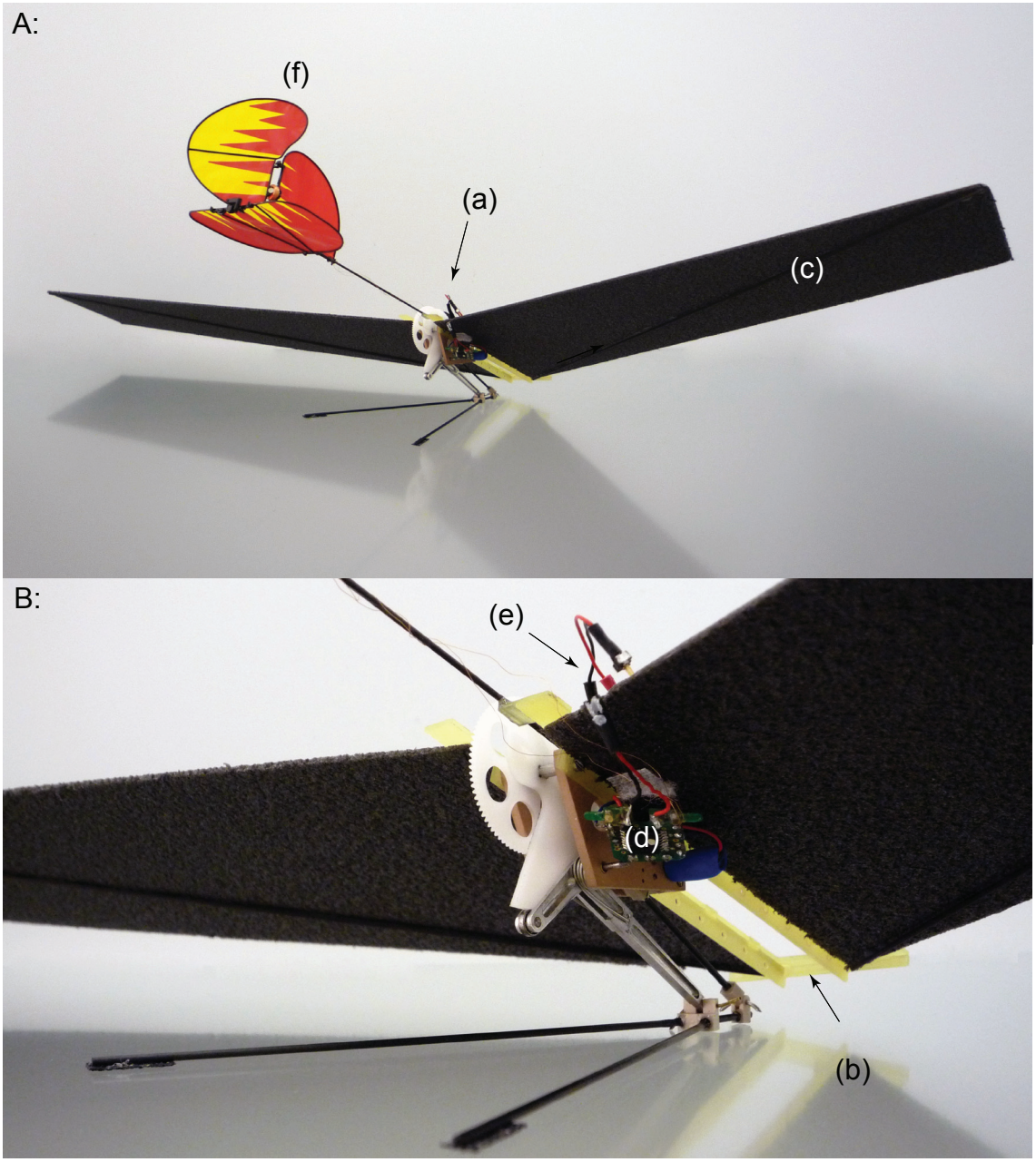

Figure 5.6: EPFL jumpglider. 16.5g jumpgliding robot that can jump, perform steered gliding flight and move on ground with small jumps. (a) EPFL jumper v1, (b) CNC cut Polyimide frame, (c) wings, (d) 3-channel infra red remote control (e) 20mAh LiPo battery (located on top of the wing), (f) tail with rudder

Table 5.1: Weight budget of the EPFLjumpglider

Part	Mass [g]
EPFL jumper v1	6.03
20mAh battery	0.94
Remote control receiver	0.81
Wings	4.5
Polyimide frame	2.59
Tail	1.63
Total	**16.5**

forward velocity of 0.1m/s.

The third set of experiments demonstrates the steering capabilities of the EPFL jumpglider during gliding flight. The jumpglider is hand launched from a height of around 2m and is filmed at 30 frames per second (figure 5.11). It is launched three times for every side and the steering is initiated manually with a remote control. The tracked trajectories show that the implemented EPFL jumpglider is capable of steering in air in order to perform goal directed gliding flight.

5.4.2 Discussion

Based on the experiments illustrated in figure 5.8 we measured the average gliding ratio to be $f = 2.1$ for jumpgliding at an average gliding velocity of $v_g = 2.26$m/s. The jumpglider has a mass of 16.5g, which is 8.72g more than the ballistic jumper. In order to compare the experimental data to our model, we plot the horizontal distance traveled for ballistic jumping and jumpgliding in figure 5.12. It can be seen that overall, the model fits the measured values, although the jumpgliding model predicts a linear gliding slope, which differs from the slightly curved trajectory from the measurements. We argue that the waviness of the measured jumpgliding trajectory has two possible reasons. First, the jumpglider may not have been perfectly balanced for stable gliding flight, which naturally leads to oscillations in pitch during gliding [142]. Second, the oscillations may be introduced because of the velocity variation during the transition phase. The jumpglider accelerates from the velocity v_{top} to the steady state

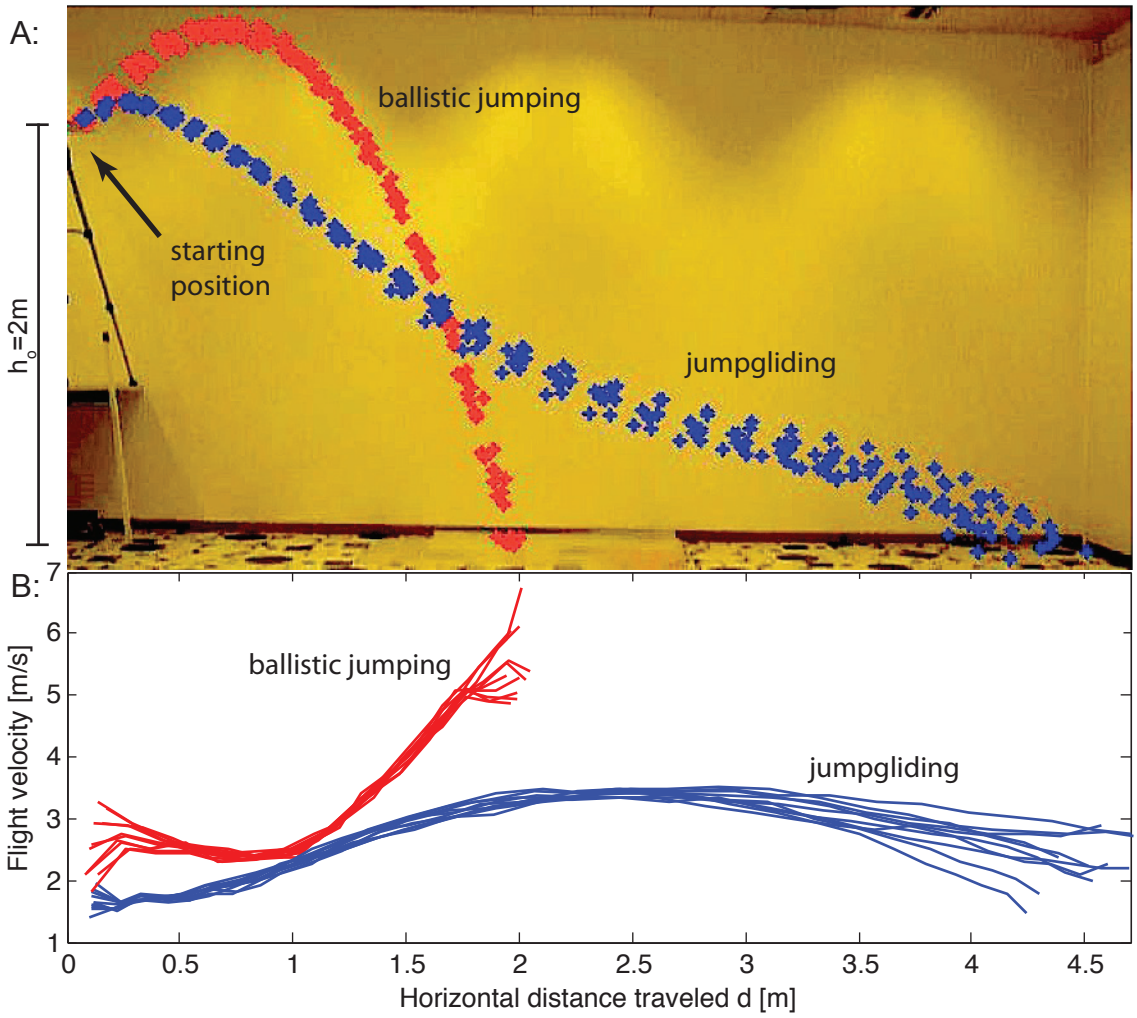

Figure 5.7: A: Tracked trajectories of jumpgliding and ballistic jumping from an elevated starting position of two meters height (10 consecutive trials each). B: Flight velocity profiles of the tracked trajectories

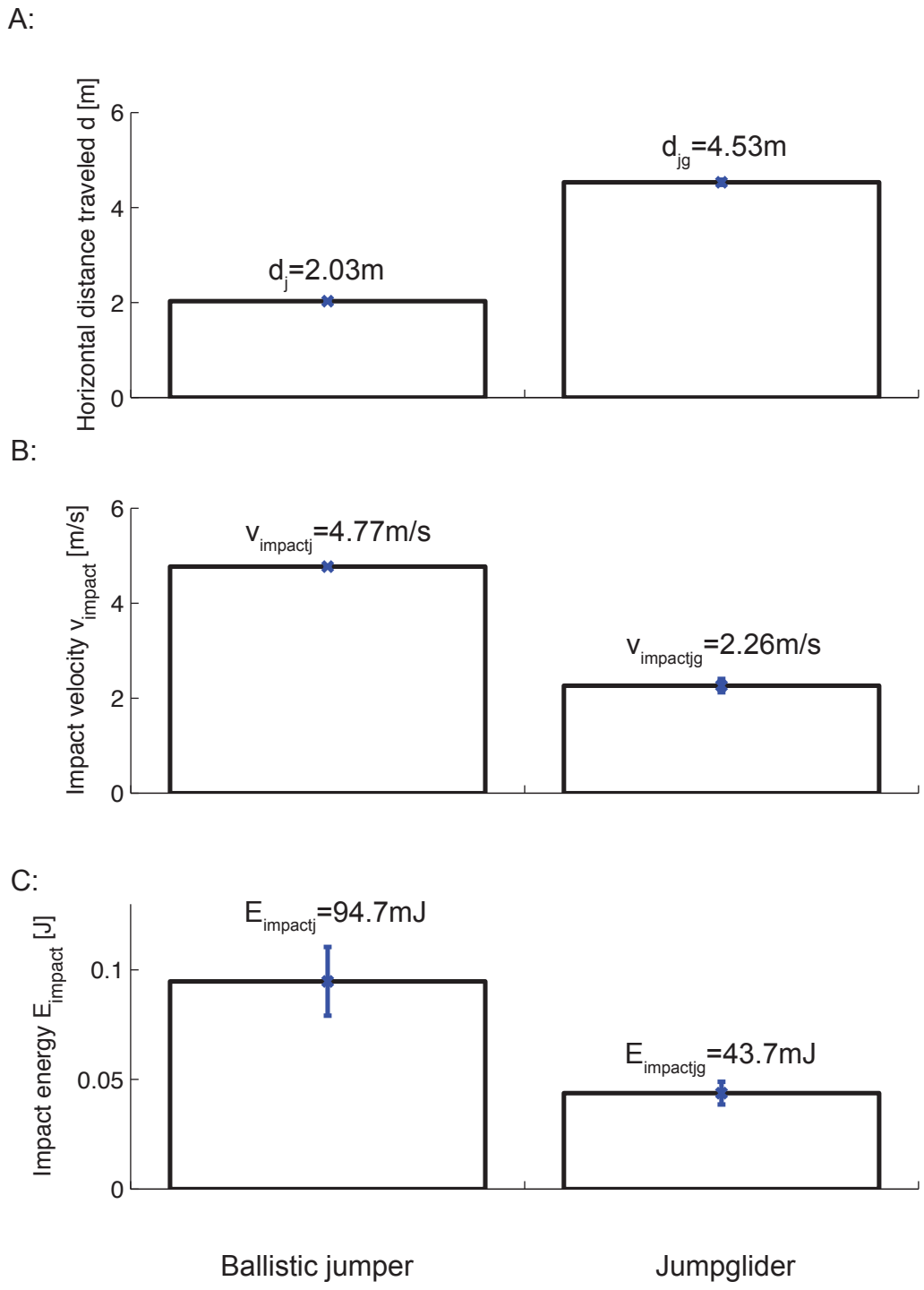

Figure 5.8: Measured parameters based on the tracked trajectories with the jumpglider and the ballistic jumper (figure 5.7), when jumping from an elevated starting position of two meters height (10 consecutive trials each). A: Mean distance traveled d for ballistic jumping and jumpgliding, B: Mean impact velocity, C: Mean impact energy. The bars indicate the standard errors for the 10 trials

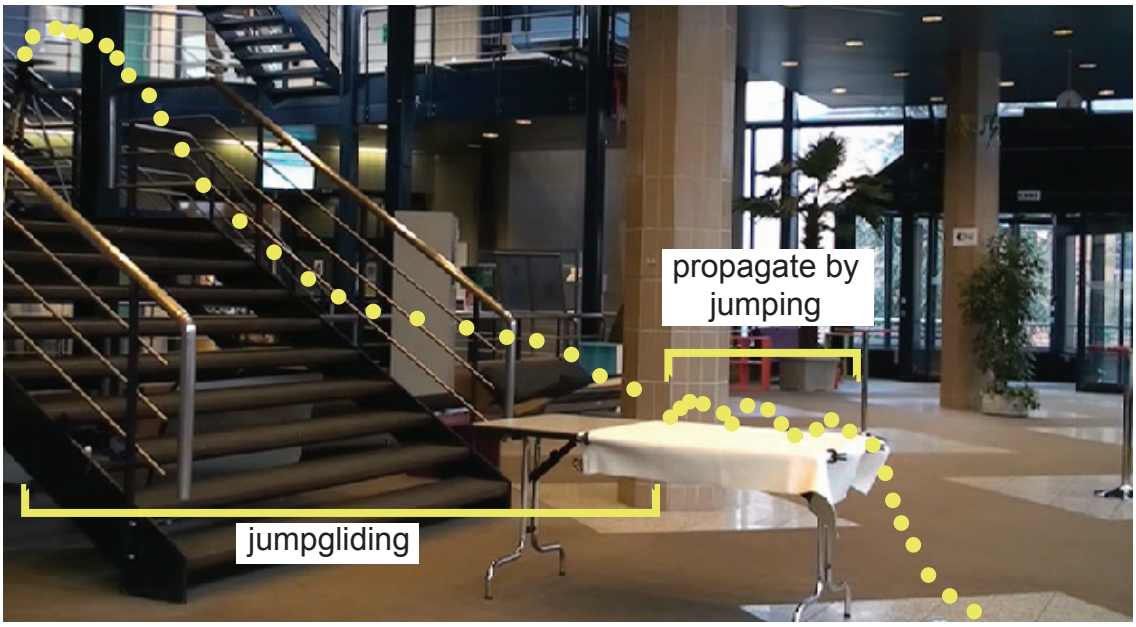

Figure 5.9: Illustration of the locomotion capabilities of the EPFL jumpglider. It jumps from an elevated position of 2.53m height, lands safely on a table and performs three sequential jumps to progress on level terrain. Finally, it jump off the table to glide down to the floor

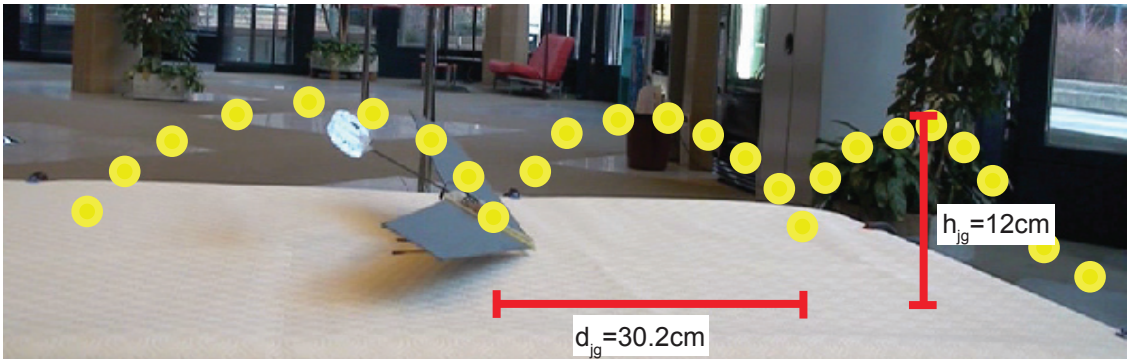

Figure 5.10: Jumpglider locomoting on level terrain. Each jump allows the jumpglider to progress a distance of 30.2cm

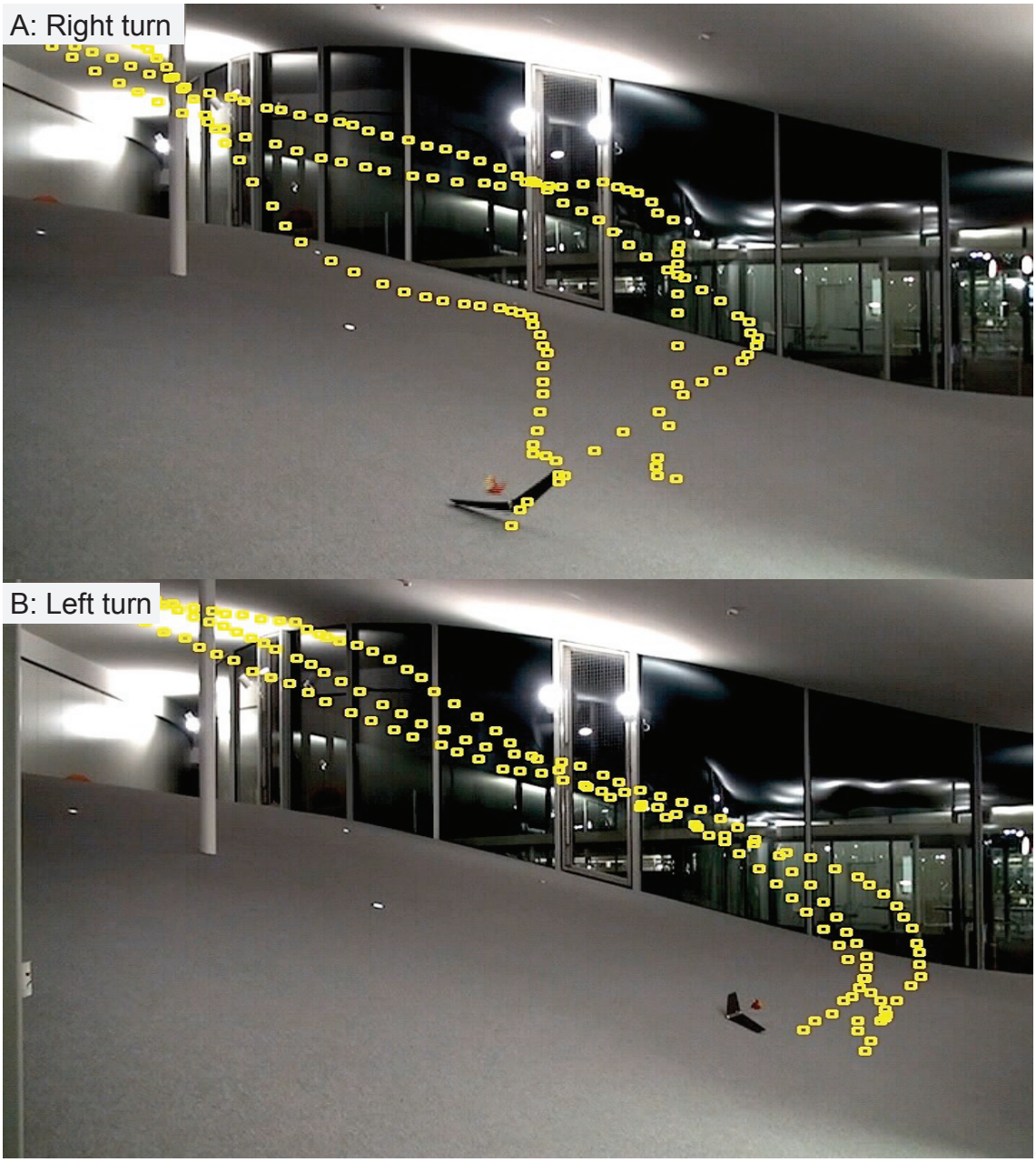

Figure 5.11: Tracked flight trajectories of the EPFL jumpglider illustrating its steering capabilities. The jumpglider is hand launched from a height of around 2m (three launches each) A: Right turn, B. Left turn

gliding velocity v_g, leading to variations in lift and attitude and therefore to oscillations of the flight trajectory due to the dynamics of the glider. In our model we assumed that this transition phase is instantaneous, which is a simplification. The oscillations observed in the experiments could be decreased by improving the pitch stability of the glider. This could be done by for example increasing the sweep angle of the wings or by adding a longer tail [142].

In order to estimate the accuracy of the theoretical model, we summarize and compare the measured and calculated values for jumping on ground (h_o =0m) and from an elevated position (h_o =2m) in table 5.2. We conclude that the prediction of the model is more accurate when jumping from an elevated position as opposed to jumping on ground. Nevertheless, the model and the experiments are in very good agreement for indicating which locomotion strategy leads to larger distances covered: The measurements indicate that on ground the ballistic jumper travels 63.2% further than the jumpglider. Our model predicts a difference of 69.8%. From an elevated position of 2m we measure an increase of 123% with jumpgliding whereby the model predicts an increase of 92%.

The limit height h_{limit} above which jumpgliding leads to larger distances covered is $h_{limitmod}$ =65.4cm from the model. To measure the limit height from the trajectories in the experiments, we interpolated the tracked points with a polynom of fourth order for the jumpgliding trajectory and a polynom of second order for the ballistic jumper. The average limit height from the experiments is $h_{limitexp}$ =82.2cm, which is 25.7% more than predicted by the model.

5.5 Conclusion

We conclude that the model and the experiments are in general agreement with each other when comparing the horizontal distance traveled for jumpgliding and ballistic jumping as two alternative locomotion strategies. Both, the model and the experiments clearly indicate that adding wings to our EPFL jumper v1 does not prolong the jump when locomoting on level terrain. However, when jumping from an elevated position, jumpgliding leads to increased horizontal distances traveled when compared to ballistic jumping.

In this chapter we successfully developed and implemented the EPFL jumpglider with similar abilities as the ballistic EPFL jumper v3. The ballistic jumper as

Table 5.2: Comparison of measured horizontal distances traveled (ten trials each) with the prediction from the model

	Ballistic jumper		**Jumpglider**	
	experiments	model	experiments	model
$h_o = 0m$	1.36m (SD=0.03)	1.29m (-5.1%)	0.50m (SD=0.05)	0.39m (-28.2%)
$h_o = 2m$	2.03m (SD=0.03)	2.37m (+16.7%)	4.52m (SD=0.17)	4.55m (+0.6%)

presented in chapter 4 has a mass of 14.3g and features jumping, safe landing, uprighting and is able to perform steered jumps. Our jumpglider has a similar mass of 16.5g and is also able to perform repetitive jumps, land safely and steer. The main advantage of the jumpglider is that it can reduce the impact energy on landing and increase the distance traveled when jumping from elevated positions or in an environment where it encounters declivities or edges. When moving on level ground, the ballistic jumper is clearly the better solution because it can overcome much larger obstacles and travel at a lower energetic cost.

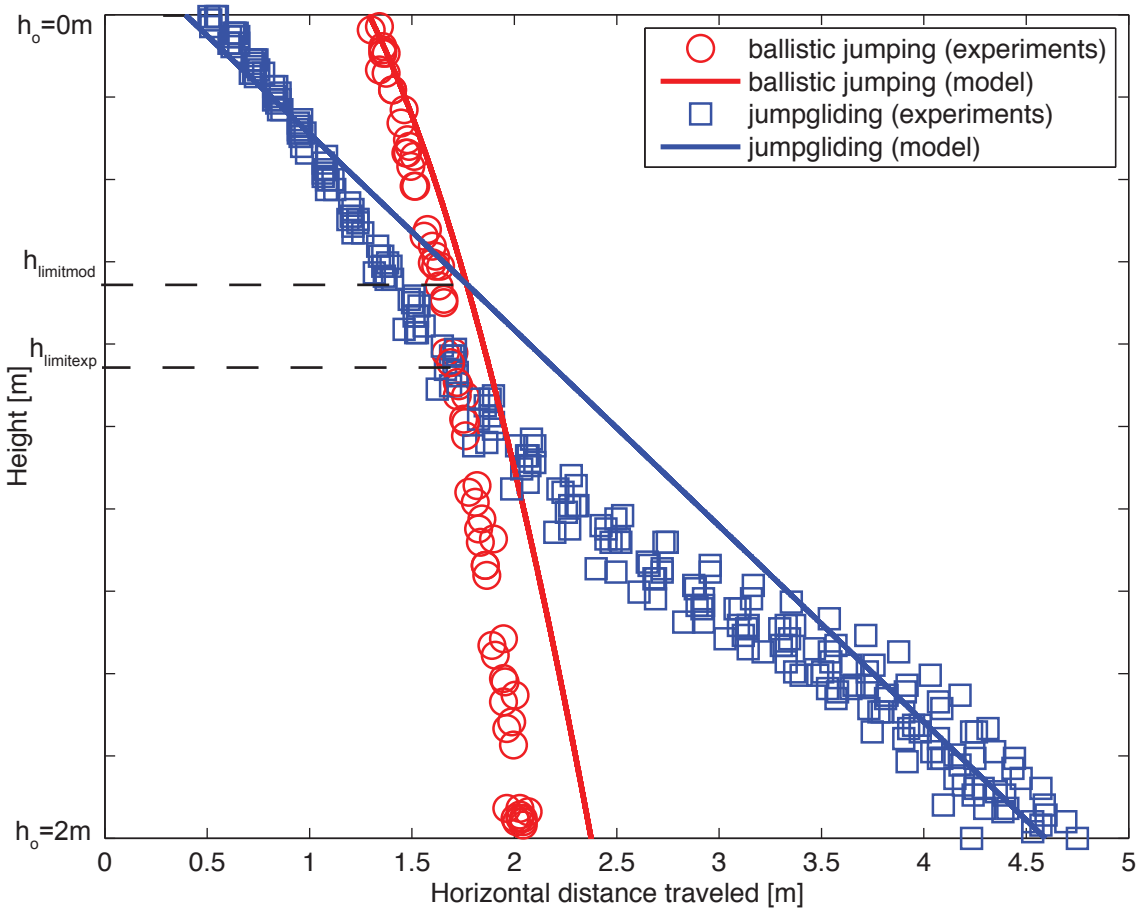

Figure 5.12: Comparison of the measured horizontal distance traveled to the calculated distances based on our theoretical model for ballistic jumping and jumpgliding

6 Concluding remarks

In this thesis we showed that jumping allows miniature robots to overcome much bigger obstacles than any other mode of ground locomotion. Compared to the state of the art of existing miniature jumping robots, our presented prototypes are able to jump one order of magnitude higher for their size and weight (appendix A). This high jumping performance has been achieved by using bioinspired mechanical design principles to address the challenges of jumping locomotion. This chapter provides a summary of our main conclusions and highlights what we consider to be important in the mechanical design of miniature jumping robots. At the end of the chapter, we finish with an outlook of possible extensions to our robots and future directions.

The jumping strategy of slowly charging an elastic element and releasing it to initiate the jump is essential for high performance jumping in miniature robots. Compared to direct actuation, this strategy allows using low power actuators and keeping the robot light weight while providing a high power jump. The prototypes presented in this thesis reach a jumping height of up to more than 27 times their size while carrying their energy supply and controls on board. With current technology, we consider this as not feasible with direct actuation on a miniature robot with a similar mass.

The addition of wings to prolong the jump is worthwhile when jumping from an elevated position, but not when jumping on ground. We developed a theoretical model which allows an estimation whether the addition of wings to a jumping robot can prolong its jump when jumping with the same take-off energy. The calculation was confirmed by experiments with a winged jumping robot. The results from both the model and the experiments indicate that wings

can prolong the jump in case that the robot jumps from a elevated starting position or has a power density above a certain threshold. For our EPFL jumpers, the height above which it reaches further with wings is 82cm. On ground its power density should be increased by a factor of around three so that jumping with wings would lead to further distances traveled per energy unit.

Protection of the robot on landing is essential in order to decrease the risk of mechanical failure. This thesis describes two ways to ensure safe landing for miniature jumping robots. First, by implementing an elastic cage which deforms on impact to protect the robot and second, by using wings that decrease the velocity on impact. We show that both wings and a cage can be used in order to protect the robot on landing. The main advantages of using wings is that the airborne velocity during the jump converges towards a constant gliding velocity when jumping from an elevated starting position. Therefore, the risk of mechanical failure can be kept low even when jumping from higher heights. The main advantage of a cage is that it can be constructed at a very low mass and that it poses less aerodynamical friction than wings, allowing the robot to move at a lower energetic cost on ground.

A possible further characterization of the jumping robots presented in this thesis could be aimed at measuring the energetic cost of transport for moving over different terrains. This would allow a comparison to other jumping robots and other modes of locomotion. Over very rough terrain with many large obstacles, the combination of jumping with propelled flight may be energetically cheaper than single mode jumping. On very smooth terrain with few obstacles, wheeled locomotion with occasional jumps may be the more adapted solution. Future work could abstract terrains found in nature and evaluate systematically different locomotion modes with regard to energetic cost of transport.

Future work could address extending the jumpers and the jumpglider with additional capabilities and combining it with other modes of locomotion. We explored five extensions that could be integrated on the robots in future. First, we propose foldable wings for the jumpglider that can be useful to enter narrow spaces when propagating on ground (appendix B and [81]). Second, we explored the possibility of autonomous gliding flight in miniature robotics and steering using Shape Memory Alloy (SMA) actuators (appendix C and [77]). Third, we developed a perching mechanism that could be added on the jumpglider and

would allow it to land on vertical surfaces of trees and buildings (appendix D and [82]). Fourth, we developed a gecko adhesive based climbing mechanism that can be added to the EPFL jumper v1, allowing it to climb over obstacles in case that they are to large to be cleared by jumping (tech report [128]). Finally, we explored the feasibility of solar powered energy harvesting method for miniature robotics and showed that it is possible to have a complete charging circuit using flexible solar cells and batteries at a weight of less than 3g (tech report [49]). A possible completely integrated system could climb up walls, jump from the top, glide down or attach to walls and climb up again. On ground it could propagate with small jumps and be powered using solar cells. Based on the prototypes presented so far, such a robot could be realized at a weight of around 25g-30g. One of the main challenges in its design is the optimal positioning of the gravity center allowing balanced gliding flight.

Future work could address as well scaling of jumping robots. The robots presented in this thesis are mechanically constructed in a way that they can be scaled up easily. This would allow them to carry more payload, such as larger batteries to prolong endurance. As described in chapter one for scaling in jumping animals, a drawback for scaled up systems is that they need proportionally stronger protecting structures for a damage free landing. However, an advantage may be that the mechanical fabrication and assembly could be easier compared to smaller robots. For example, the jumping robots presented in this thesis have mechanical features down to the sub-millimeter scale which require relatively high precision machining and assembly of these components (e.g. gearbox, leg, cam). A potentially interesting scientific question could be whether scaling laws found in jumping animals are analogous to the change in jumping performance for scaled up jumping robots.

This thesis mainly focussed on hardware development to enable miniature robots with locomotion capabilities and basic autonomy. Future work could include a larger emphasis on control and sensing which would allow applications of our proposed robots to perform environmental monitoring as a single unit or in swarms. The robots presented in this thesis are not able to carry heavy sensors such as laser range finders or high resolution cameras. Nevertheless, they could, with a payload of several grams, be equipped with minimal sensing capabilities. A sensory set consisting of two light sensors, a temperature sensor,

a humidity sensors, a microphone, a DSPic micro controller and a 2.4GHz radio module can be realized at a mass of only 3.5g using off the shelf components (tech reports [114, 149]). For applications such as forest fire monitoring, a swarm of jumping robots equipped with these sensors could move towards heat sources in the forrest, detect emerging fires and alarm fire guards autonomously.

A Comparison to other robots

This appendix compares the EPFL jumpers v1-3 to existing miniature jumping robots and jumping animals. The jumping performance of the robots presented in this thesis is several times higher in absolute jumping height, jumping height per size and one order of magnitude higher with regard to jumping height per size and weight compared to similar robots.

In this appendix we provide a comparison of our jumping robots to other existing systems. As introduced in chapter 1, we classify the robots according to their locomotion capabilities. Class one robots are able of performing standing jumps. Class two robots can perform standing jumps with onboard energy and control. Class three robots have on board energy and control and can upright on landing to perform repetitive jumps. The final class four, describes robots that can perform steered repetitive jumps with on board energy and control.

Table A.1 has been introduces in chapter 1 and is extended with the EPFL jumpers v1-3. It describes how the different challenges of jumping locomotion have been addressed by the different robots.

The EPFL jumper v1 belongs to the class two. Compared to the Grillo robot it has the additional capability of varying its take-off angle and ground force profile. This allows it to jump on slippery surfaces and be adaptive to different terrains.

The EPFL jumper v2 is part of class three. Compared to Microbot and the Michigan jumper, it is able to change its take-off angle and ground force profile. For protection on landing, it uses a cage, similar to the plastic shell used for Microbot. However, the cage in the EPFL jumper v2 is a skeletal structure, which offers less air friction during the jump compared to a shell as used by Microbot.

The EPFL jumper v3 belongs to the class four. Its main difference to existing designs is that it is capable of changing its take-off angle and ground force profile, which is different from Jollbot, Scout or Mini-Whegs. The steering of the EPFL jumper v3 is realized by rotating the jumping mechanism inside of the cage, which is different from other robots. Scout and Mini-Whegs use wheels to orient the robot body prior to jump. The main disadvantage of using wheels to steer is that they are exposed to damage on landing and can get stuck on obstacles in rough terrain, which would prevent the body orientation.

The main jumping performance metric that we introduced in chapter 1 is the jumping height per unit of size and weight. It indicates the obstacle height or terrain rugosity that the robot can overcome for its size and weight and it is therefore a measure for the energy density of the robot. We compare the jumping performance of the existing robots to our EPFL jumpers in table A.2 and figure A.1.A.

The EPFL jumper v1 is a 7g jumping robot that can perform standing jumps

of more than 27 times its own size. Compared to existing jumping robots from the same class and with the same locomotion capabilities it jumps 16.1 times higher for its mass and size.

The EPFL jumper v2 has a weight of 9.8g and outperforms the best competing robot from the same class by a factor of 9.2 with regard to jumping height per mass and size. In addition, the EPFL jumper v2 incorporates basic autonomy which is different to other similar robots. A control unit and addition of sensors allow it to free itself from stuck situations where it is facing a vertical wall by moving its center of gravity. After successful completion of this rescue maneuver, it can then autonomously start the next jump.

The EPFL jumper v3 has a weight of 14.3g and is capable of taking off, uprighting after landing, steering and taking off again. Compared to the record in other similar robots, it jumps 21.1 times higher for its mass and size. Although it has a superior ability of jumping over obstacles, wheeled designs such as Mini-Whegs or Scout are able to move much faster over flat terrain when there are not obstacles to overcome.

Table A.3 and figure A.1.B compare the jumping performance of the EPFL jumpers v1-3 to jumping animals with similar size and weight. It can be seen that the EPFL jumpers perform in the same order of magnitude as desert locusts or frogs regarding jumping height for their size and weight.

Table A.1: Summary of the solutions found in existing robots and the EPFL jumpers to address the challenges of jumping locomotion (continued on the next page)

	TAKE-OFF			LANDING		PREPARATION FOR TAKE-OFF	
Name	High power actuation	Hariable take-off angle	Variable ground force profile	Protection	Uprighting	Steering	On board energy
Class 1: Able to perform standing jumps							
Closed elastica jumper Yamada et al. [157]	Using power amplification based on energy storage in an elastic buckling mechanism	Not addressed	Not addressed	Not addressed	Not addressed	Not addressed	Not addressed
Voice coil jumper [163]	Direct actuation based on voice coil	Not addressed	Not addressed	Not addressed	Not addressed	Not addressed	Not addressed
Spherical crawling/rolling robot [138]	Using SMA wires to charge elastic ribbons which are released to jump	Not addressed	Not addressed	Yes, using elastic ribbons as outer shell	Yes, when charging by changing its shape	Not addressed, but crawling ability allows it to propagate in a wanted direction	Not addressed
Class 2: Able to perform standing jumps with on board energy							
Grillo [127]	Using an electric motor to charge a spring which releases a piston to jump	Not addressed	Not addressed	Not addressed	Not addressed	Not addressed	Yes, using on-board batteries
EPFL jumping robot v1 [78]	Using an electric motor to charge a torsion spring which releases a four-bar mechanism to jump	Yes, by changing the geometry of the four-bar mechanism	Yes, by changing the geometry of the four-bar mechanism	Not addressed	Not addressed	Not addressed	Yes, using on-board batteries

	TAKE-OFF			LANDING		PREPARATION FOR TAKE-OFF	
Name	High power actuation	Variable take-off angle	Variable ground force profile	Protection	Uprighting	Steering	On board energy
Class 3: Able to perform repetitive standing jumps with on board energy							
Microbot [39]	Dielectric Elastomer Actuators (DEA) are used to charge a bistable snapping mechanism which is released to jump	Not addressed	Not addressed	Yes, using a plastic shell around the mechanism	Yes, passively through center of gravity position	Not addressed	Yes, using a miniature fuel cell
Michigan jumper [165]	Using an electric motor to charge a linear spring which is released to jump	Not addressed	Not addressed	Not addressed	Yes, passively through center of gravity position	Not addressed	Yes, using on-board batteries
EPFL jumping robot v2 [80]	Using an electric motor to charge a torsion spring which releases a four-bar mechanism to jump	Yes, by changing the geometry of the four-bar mechanism	Yes, by changing the geometry of the four-bar mechanism	Yes, using a carbon cage around the jumping mechanism	Yes, by shifting its center of gravity when charging for take-off	Not addressed	Yes, using on-board batteries
Class 4: Able to perform repetitive steered standing jumps with on board energy							
Jollbot [5]	Using an electric motor to charge linear springs which are released to jump	Not addressed	Not addressed	Yes, using an elastic cage	Yes, by shifting the center of gravity position	Yes, by leaning prior to jumping. Additional ability of rolling by rotating a mass around its axis	Yes, using on-board batteries
Scout [137]	Using an electric motor to charge an elastic ribbons coiled around its body which is released to jump	Not addressed	Not addressed	Not addressed	Yes, passively through center of gravity position	Not addressed, but wheels allow it to propagate in a wanted direction	Yes, using on-board batteries
Mini-Whegs [87]	Using an electric motor to charge a linear spring which releases a four-bar mechanism to jump	Not addressed, but possible by changing the geometry of the four-bar mechanism	Not addressed, but possible by changing the geometry of the four-bar mechanism	Not addressed	Not addressed, but can run on its back and change its orientation by running into a wall	Not addressed, but wheels allow it to propagate in a wanted direction	Yes, using on-board batteries
EPFL jumping robot v3 [83]	Using an electric motor to charge a torsion spring which releases a four-bar mechanism to jump	Yes, by changing the geometry of the four-bar mechanism	Yes, by changing the geometry of the four-bar mechanism	Yes, using a carbon cage around the jumping mechanism	Yes, passively through center of gravity position	Yes, can rotate inside of the cage to change the take-off direction	Yes, using on-board batteries

Table A.2: Performance of existing miniature jumping robots

Name	mass [g]	size [cm]	jump height [cm]	jump distance [cm]	jump height per mass[a] [cm/g]	jump height per size[a] [-]	jump height per mass and size[a] [cm/(10^2·cm·g)]
Class 1: Able to perform standing jumps							
Closed elastica jumper [157]	30*	30.5	20	70	1.18*	1.16	3.86
Voice coil jumper [163]	42*	3	5	0	0.12*	1.67	3.97
Spherical crawling/rolling robot [138]	5*	9	20	5	4.02*	2.23	44.62
Class 2: Able to perform standing jumps with on board energy							
Grillo [127]	8	5	5	20[b]	1.25	2	25
EPFL jumping robot v1 [78]	7	5	138	79	20.12	28.17	402.36
Class 3: Able to perform repetitive standing jumps with on board energy							
Microbot [39]	11	46	38	0	3.45	0.83	7.51
Michigan jumper [165]	42	11	15	11	0.37	1.4	3.36
EPFL jumping robot v2 [80]	9.8	12	76	81	8.31	6.79	69.21
Class 4: Able to perform repetitive steered standing jumps with on board energy							
Jollbot [5]	465	29.4	18.4	0	0.04	0.63	0.13
Scout [137]	200	11	30	20	0.15	2.8	1.4
Mini-Whegs [101]	190	10.4	22	22	0.12	2.25	1.18
EPFL jumping robot v3 [83]	14.3	18	62	46	4.49	3.56	24.92

* Weight without batteries or control unit

[a] Jumping height at 90°, calculated using equation 1.1-1.3

[b] Value N/A, here calculated (equation 1.1-1.3), assuming a take-off angle of 45°

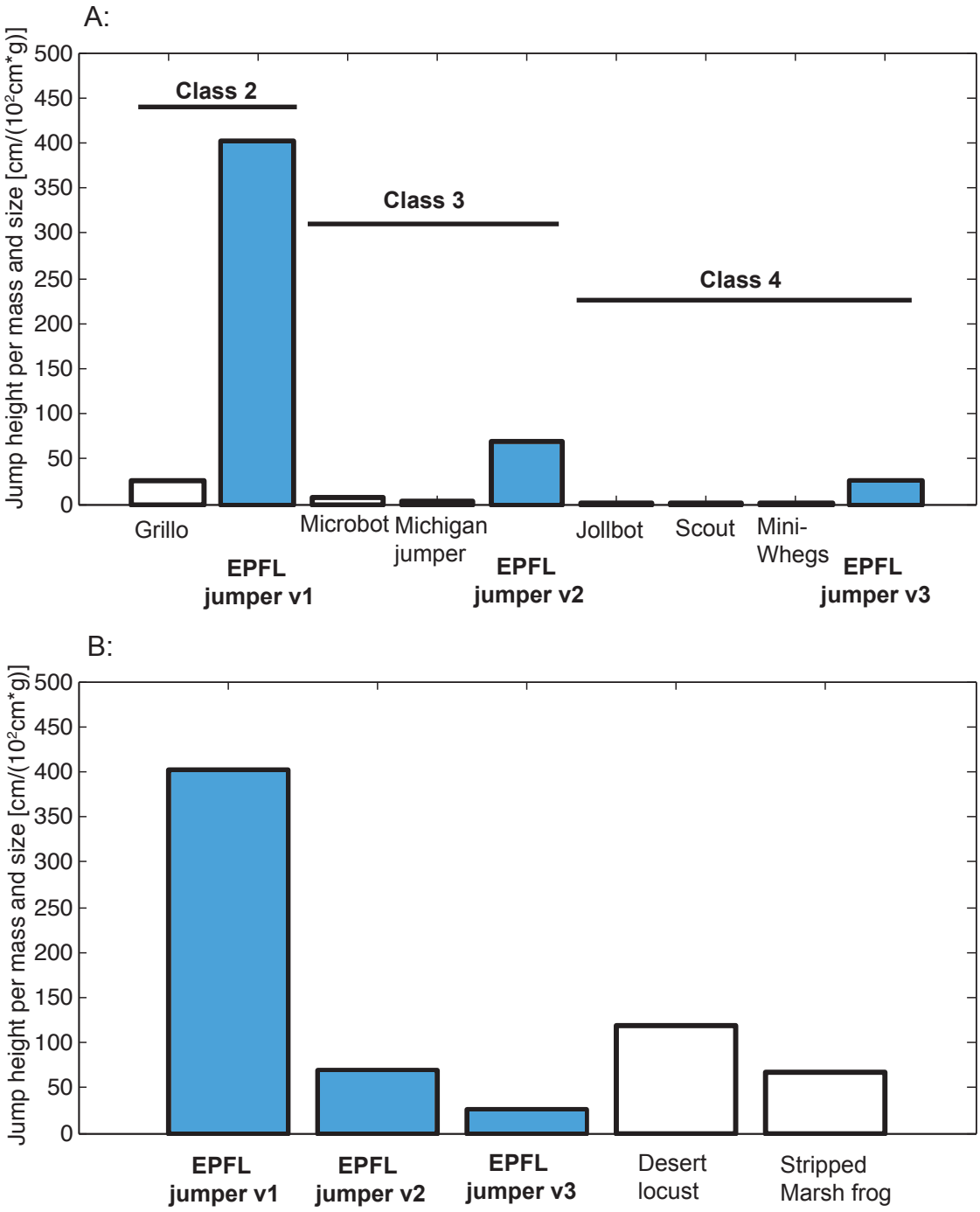

Figure A.1: Comparison of jumping performance with regard to the jumping height per mass and size. A: Comparison between the state of the art in robotics and our EPFL jumpers. B: Comparison to jumping animals

Table A.3: Comparison of the jumping performance of jumping animals to the EPFL jumpers v1-3

Name	mass [g]	size [cm]	jump height [cm]	jump distance [cm]	jump height per mass[a] [cm/g]	jump height per size[a] [-]	jump height per mass and size[a] [cm/(cm·g)]
Desert locust [11]	3.5	6	12[b]	50	7.14	4.17	119.15
Stripped march frogs [153]	10	6	20[b]	80	4	6.67	66.67
EPFL jumping robot v1 [78]	7	5	138	79	20.12	28.17	402.36
EPFL jumping robot v2 [80]	9.8	12	76	81	8.31	6.79	69.21
EPFL jumping robot v3 [83]	14.3	18	62	46	4.49	3.56	24.92

[a] Jumping height at 90°, calculated using equation 1.1-1.3

[b] Value N/A, here calculated (equation 1.1-1.3), assuming a take-off angle of 45°

B Wingfolding

In this appendix we consider different mechanical designs of foldable wings that could be used for the EPFL jumpglider. Based on an exploration of different folding principles found in nature, we propose three wing folding designs and compare them qualitatively. Finally, we implement a locust inspired solution on the EPFL jumpglider and compare its performance to ballistic jumping and jumpgliding with rigid open wings.

Note: This chapter is based on the publication (Kovac et al. [81])

.

Most birds, bats and flying insects are able to fold their wings with the goal to protect the often fragile structures when moving on ground and to be able to enter narrow spaces [55]. For the EPFL jumpglider we explored different wing folding designs with the goal to reduce its size when moving on ground and to reduce the air friction during the ascending phase of jumpgliding. To do so, we do not limit the search for inspiration to only flying animals. Nature offers many foldable and deployable structures for different applications. For example, leaves unfold from a very compact package to the complete deployed leaf with very high structural stability [93, 113]. Other ways of unfolding can be found in soft animals, such as anemones and various worms [144, 148]. Many insects use Origami-like mechanisms to fold their wings, such as the hind wings of *Dermaptera* [55, 56]. Most birds and bats fold their wings using an underlying skeleton folding structure, which is covered with skin. Many flies, butterflies and other insects with rigid wings simply fold the wings backwards similar to a japanese foldable fan. Figure B.1 shows some examples of folding structures found in nature.

In robotics, wing folding designs have been proposed which allow flying systems to move on ground and through narrow openings such as the hybrid locomotion platform MMALV [18]. Other projects aim at developing morphing wings to steer MAVs in air [9].

For the EPFL jumpglider, we considered three designs which we will shortly outline in this appendix. Further details and a more detailed description of their working principles can be found in the tech reports [59, 81, 90, 126, 131].

As a first design, we considered a bat inspired solution [126] (figure B.2). It consists of carbon rods (a) and hinges (b) with embedded torsion springs that keep the wings (c) open. When the jumping mechanism charges for the next jump, it rolls a thread (d) and releases it on command using a SMA based click mechanism (e) located under the wings.

The second wing folding design that we considered [90] is illustrated in the CAD design in figure B.3. The working principle is that when the jumpglider jumps, the air friction keeps the wings closed. As soon as it reaches the top of the jumping trajectory and starts to descend, the air enters under the wings and opens them which then allows the jumpglider to glide. Once on ground, it charges for the next jump and closes the wings by means of a thread (a) which

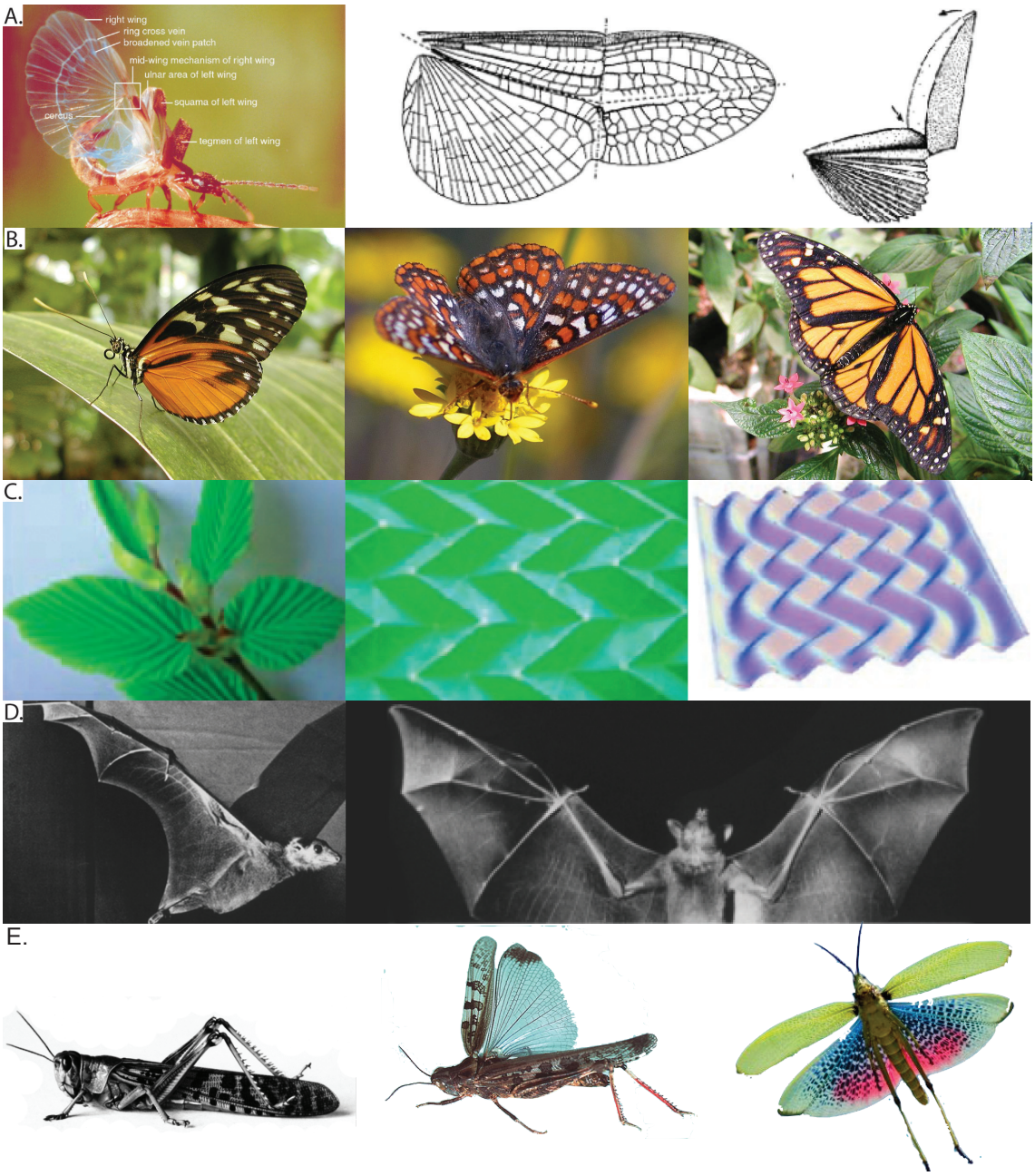

Figure B.1: A selection of folding structures in nature. A: Hind wings of *Dermaptera* [55, 56]; B: Wing folding of butterflies [68]; C: Folding leafs [24, 93]; D: Wing folding in bats [106]; E: Wing folding in desert locusts [155]

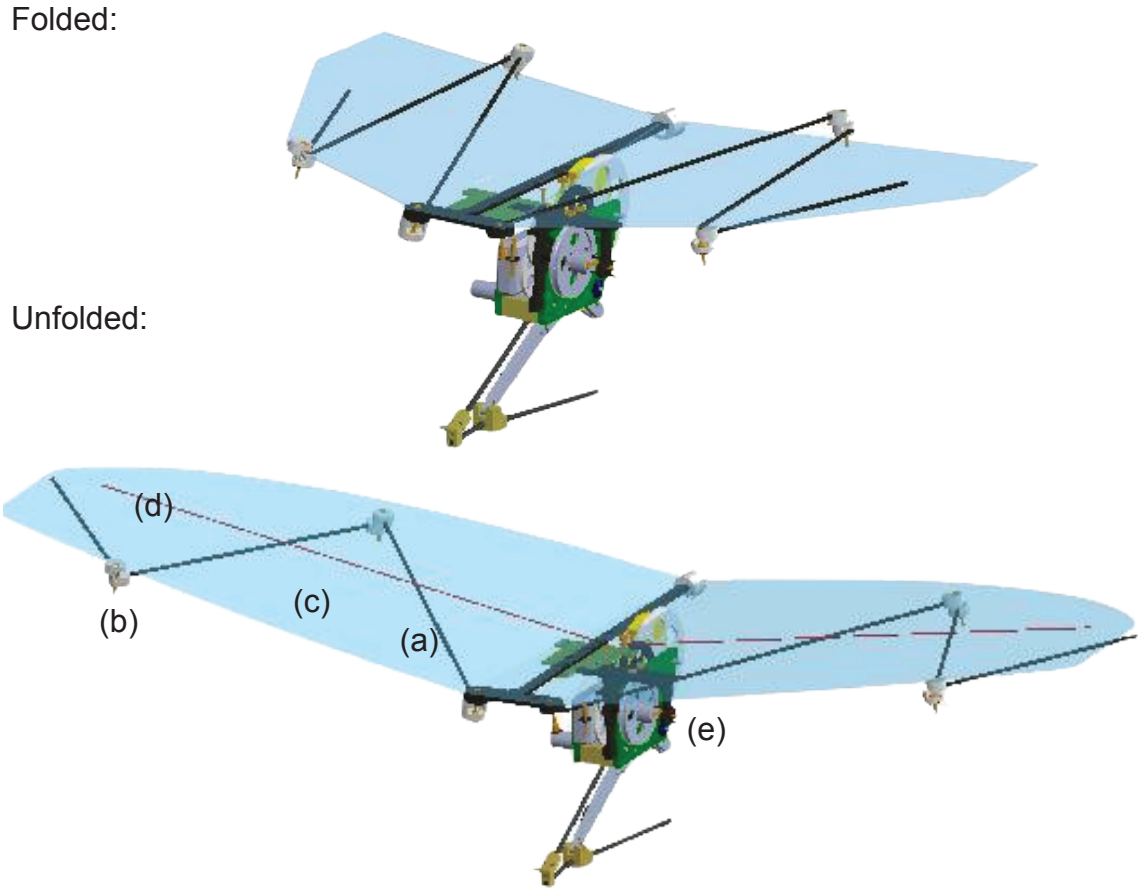

Figure B.2: Design 1: Bat inspired folding mechanism consisting of carbon rods (a) and hinges (b) with embedded torsion springs that keep the wings (c) open. When the jumping mechanism charges for the next jump, it rolls a thread (d) and releases it on command using a SMA based click mechanism (e) located under the wings

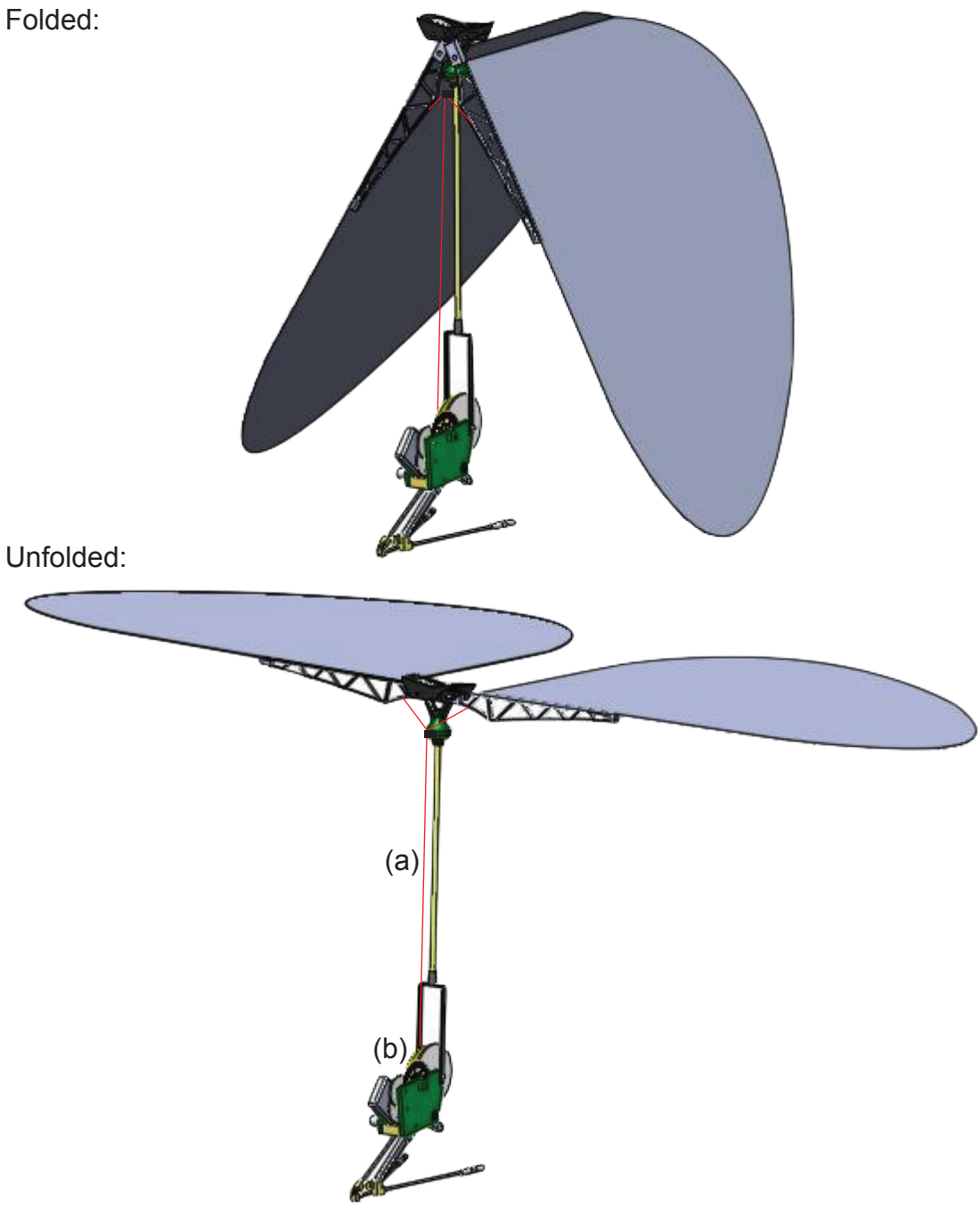

Figure B.3: Design 2: Passive wing folding mechanism. The wings are closed by means of a thread (a) which is attached to the cam (b). On top of the jumping trajectory, the air friction opens the wings and allows the jumpglider to glide

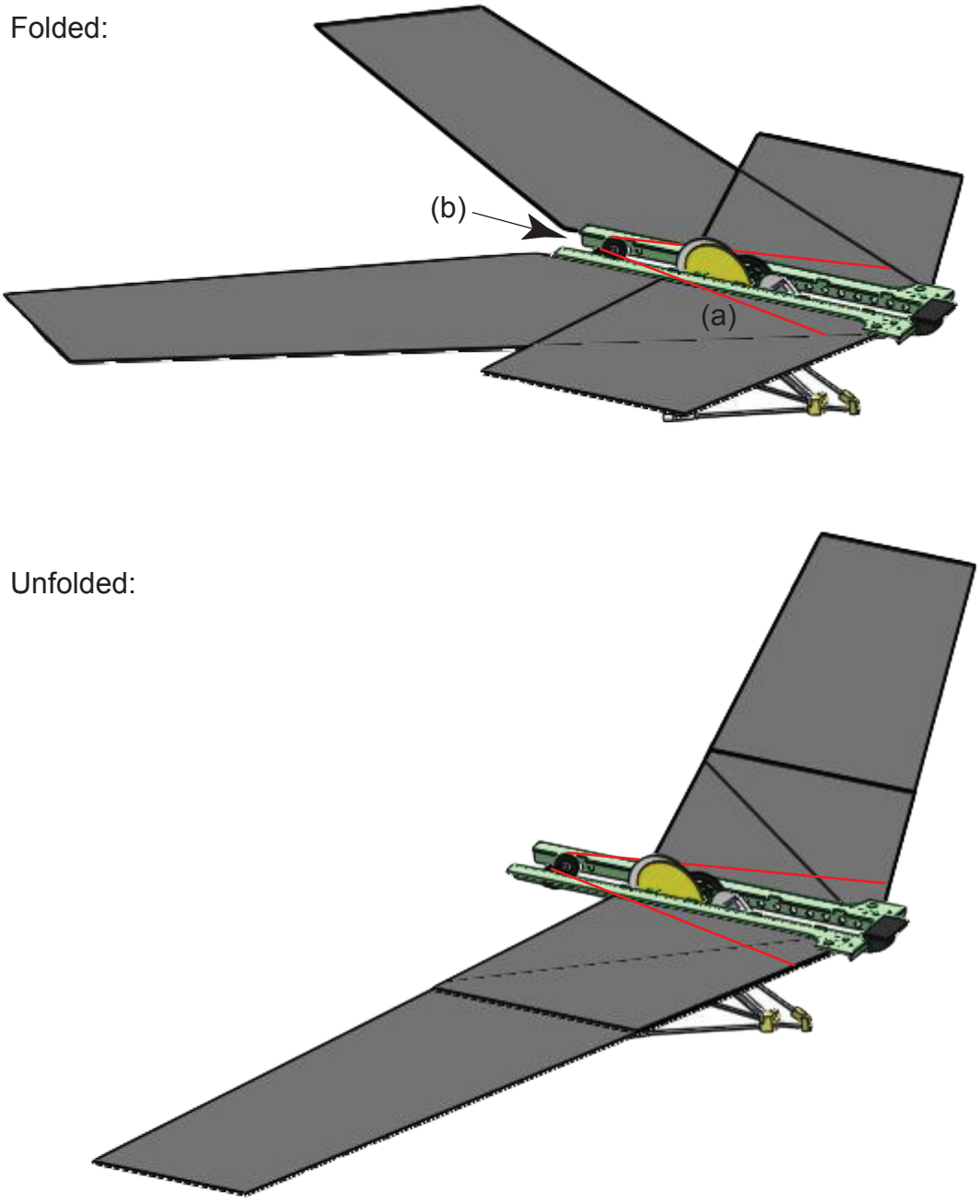

Figure B.4: Design 3: Locust inspired folding mechanism. A spring keeps the wings open while two threads (a) which is attached to the wing root and the legs via two pulleys (b) folds the wings when the jumper charges for the next jump. As soon as it takes off, the wing start to open allowing the jumpglider to perform gliding flight with open wings

Table B.1: Qualitative comparison for the three different wing folding designs

Design requirement	Design 1	Design 2	Design 3
Weight	-	+	++
Compactness when folded	+	- -	-
Rigidity when open	-	++	+
Mechanical complexity	-	++	+
Robustness	- -	++	+

is attached to the cam (b) of the jumping mechanism.

The third design [59, 131] is based on the wings being folded backwards, similar to many insects, such as locusts or fleas (figure B.4). A spring provides the force to keep the wings open. When charging for the next jump, two threads (a) which are attached to the wing root and the legs fold the wings by way of two pulleys (b). As soon as ithe robot takes off, the wings start to open allowing the jumpglider to perform gliding flight with open wings.

These three designs are compared qualitatively in table B.1. The main design requirements in the development of these three designs were (i) to keep the structural weight as low as possible, (ii) be as compact as possible when folded, (iii) rigid when open, (iv) mechanically simple and (v) robust to mechanical damage.

Based on the experience with these designs and initial experiments, we consider the design solution three as the most promising one for miniature jumpgliders. Its main advantage compared to the other designs is that it is mechanically robust, simple to implement and light weight.

We implemented the design three with our EPFL jumping robot v1 leading to a 20.3g jumpglider that can fold its wings (figure B.5). It opens its wings 160ms after take-off and allows the robot to perform gliding phase (figure B.6). Compared to the jumpglider with rigid open wings of the same size as presented in chapter 5, this system can fold its wings which allows it to move through more narrow openings such as half open doors, under tables or cluttered outdoor terrain. However, due to the foldable wing and additional weight, the gliding behavior is not as good as the solution with rigid wings.

In order to characterize the jumpgliding performance of the EPFL jumpglider

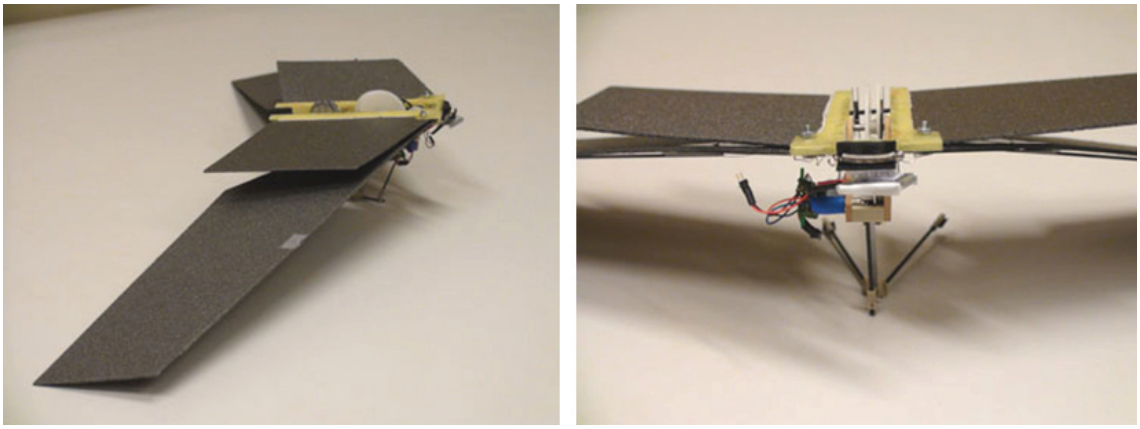

Figure B.5: Jumpglider with foldable wings using the locust inspired folding mechanism (design 3)

with foldable wings, we use the same setup as in chapter 5 (figure 5.7.A) and perform ten jumps (figure B.7 and B.8). It can be seen that although the impact velocity is lower compared to the ballistic jumper, the impact energy is increased by 14.2% which is due to its higher weight (+161%).

The distance traveled is less than a ballistic jumper at 45°(-19.7%). However, this may be due to the almost vertical dive of the jumpglider with foldable wings at the beginning of the gliding trajectory (figure B.7). If the height of the elevated position would be larger, the distance traveled would be much more favorable in this comparison.

Based on these experiments, we conlude that it is possible to jumpglide with foldable wings. However, both the jumping and the gliding performance are decreased due to the additional weight compared to a jumpglider with rigid wings. For situations where small size is of very high importance, foldable wings may be an interesting option.

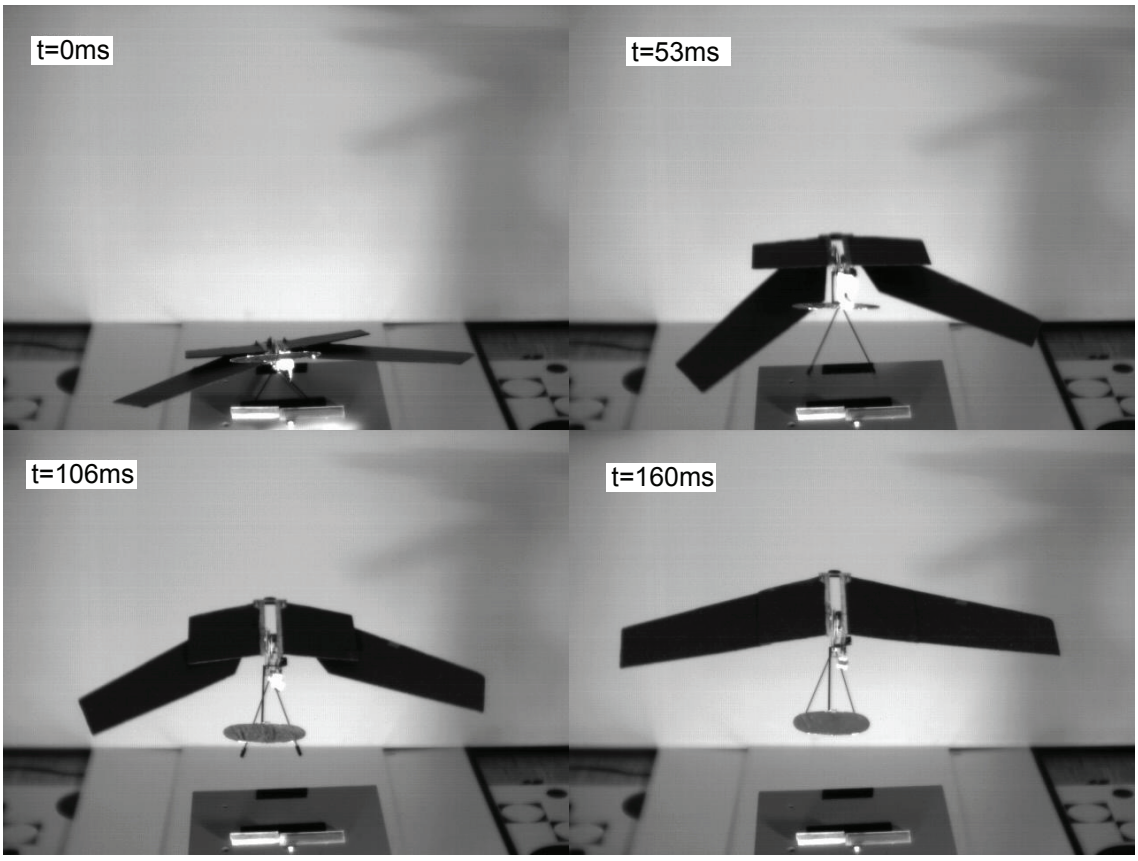

Figure B.6: Unfolding sequence of the locust inspired wing folding implementation. After take-off, it takes 160ms to completely unfold the wings

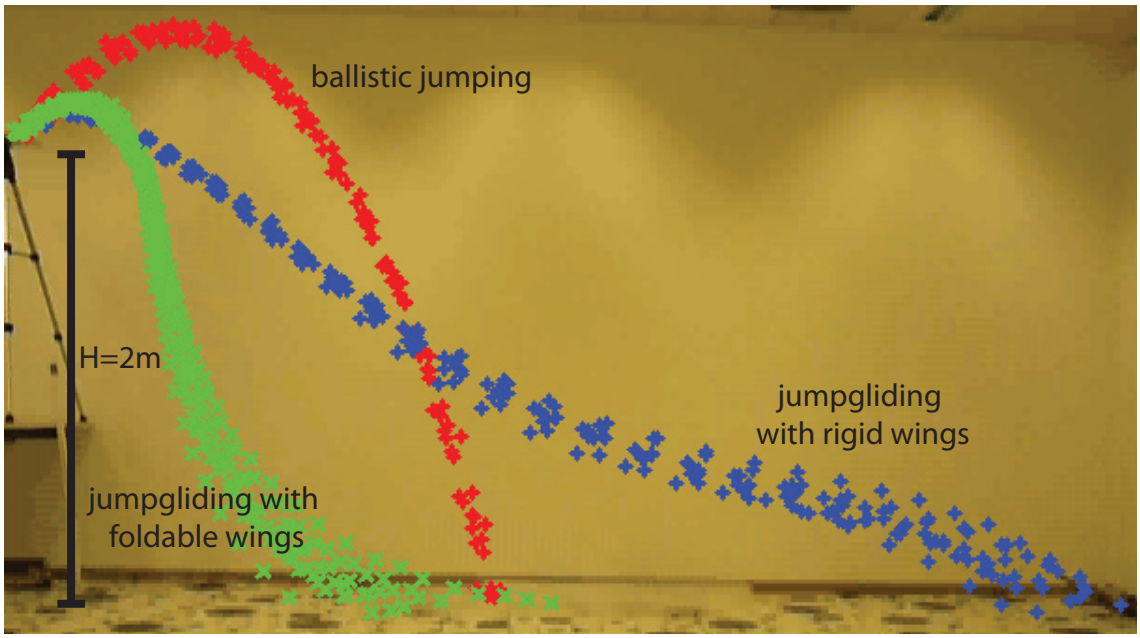

Figure B.7: Flight trajectories, 10 trials for ballistic jumping, jumpgliding with rigid wings and jumpgliding with foldable wings

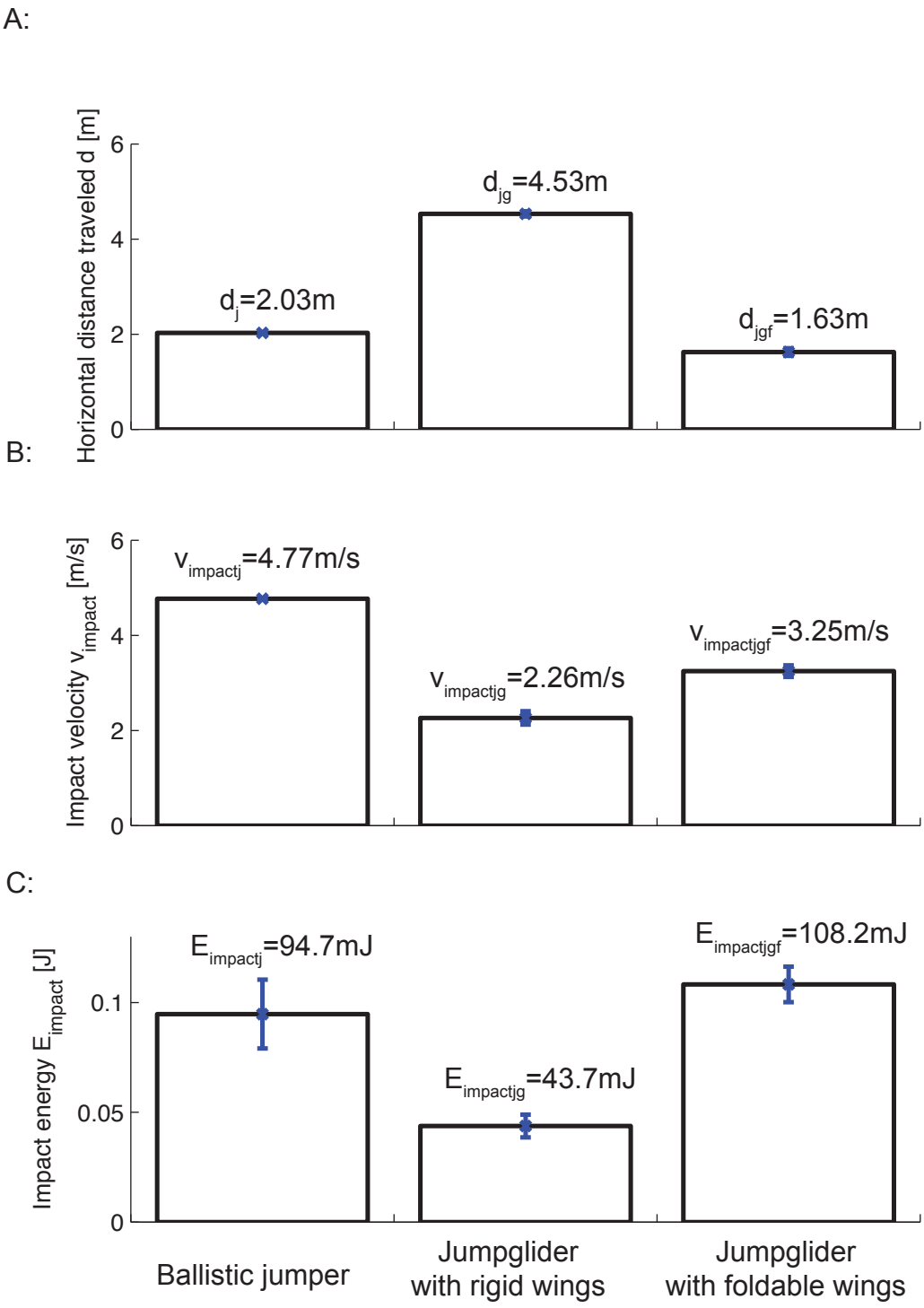

Figure B.8: Measured parameters from the experiments as shown in figure B.7. A: Distance traveled d from 2m height for ballistic jumping, jumpgliding with rigid wings and jumpgliding with foldable wings, B: Impact velocity, C: Impact energy. The bars indicate the standard error for the 10 runs

C Autonomous gliding and SMA actuated tail

In order to explore the potential of autonomous gliding flight in the domain of miniature robotics, we developed a 22cm airplane, called 'EPFL microglider', weighing a mere 1.5g and flying at around 1.5m/s. It is equipped with sensors and electronics to achieve phototaxis, which can be seen as a minimal level of control autonomy. A novel 0.2g Shape Memory Alloy (SMA) actuator for steering control has been specifically designed and integrated to keep the overall weight as low as possible. In order to characterize autonomous operation of this robot, we developed an experimental setup consisting of a launching device and a light source positioned 1m below and 4m away with varying angles with respect to the launching direction. Statistical analysis of 36 autonomous flights demonstrates its flight and phototaxis efficiency[1].

Note: This chapter is based on the publication (Kovac et al. [77])

[1]See accompanying video at http://lis.epfl.ch/microglider/EPFLmicroglider.mp4

C.1 Introduction

In this appendix, we explore the possibility of using low weight actuators and autonomous gliding flight for miniature robots, such as the EPFL jumpglider. We present the development and characterization of an ultra light microglider (figure C.1) which acts as the testing platform for the newly developed steering actuator and the autonomous control.

To date, different attempts have been made to build small scale flying robots using rotors [84], fixed wings [168] or flapping wings [46], but none of these systems have been designed for unpowered flight. A remarkable 2.2g microglider using a four-bar piezo actuator to steer has recently been presented [154]. Although this realization is a master piece of micromechatronics, no characterization of autonomous gliding has been provided so far. In addition, this glider flies at a velocity of more than 5m/s and requires a 8m turning radius to perform a 180 degree turn [43].

In order to obtain efficient gliding distances with small scale systems, special care has to be taken to achieve very low weight. This is because the lift to drag ratio is known to naturally decrease with size, due to increasing viscous and boundary layer effects [102, 104]. To achieve low weight and low power consumption, while maintaining an acceptable level of complexity allowing for fast prototyping, we opted for a relatively new kind of steering system. We developed a 0.2g Shape Memory Alloy (SMA) actuator that is harmoniously integrated into the structure of the microglider and allows for direct control of the rudder.

Two tiny photoreceptors and a simple control strategy were used to provide our 1.5g robot with a minimal level of autonomy. The microglider was fully tested and characterized for its gliding and phototaxis capabilities.

In the following sections we first present the construction principles of the microglider along with the design of the SMA actuator and the embedded electronics. We then describe the control mechanism enabling the phototaxis behavior. Finally, we report on the characterization procedure and flight results.

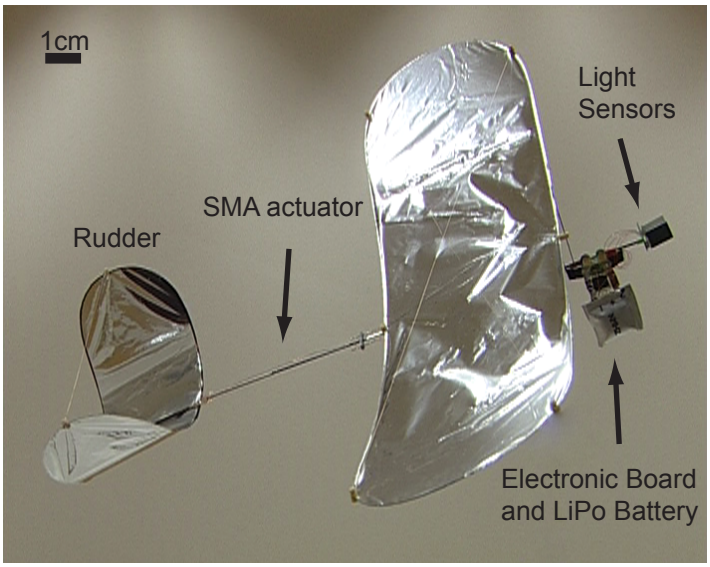

Figure C.1: 1.5g SMA-actuated EPFL microglider capable of autonomous phototaxis, wingspan 24cm, length 22cm, flying at around 1.5m/s

C.2 Design

Our design strategy is aimed at low weight and simplicity, for fast prototyping. Therefore, the same airframe architecture (figure C.2) used in our previous research activities in indoor flying robots [166, 167] has been chosen, but with particular effort to further reduce the weight and energy consumption. The construction principle is to use a structural frame of high strength for stability and to cover the aerodynamical surfaces with light and smooth materials for minimal aerodynamical friction. Carbon fiber material with a fiber volume fraction of 65% and a specific density of $1.55 g/cm^3$ has been chosen for the fuselage and the frame of wing, elevator and rudder.

The fuselage presents the major contribution to the weight of the airframe (Table C.1). Therefore, a 0.7mm carbon tube (figure C.2, Fuselage Profile) has been used to provide strength while minimizing the mass.

The frame of wings and rudder has been constructed out of 0.3mm round profile carbon rods to allow for homogeneous flexing and formation of the 3-dimensional wing structure. The material for the actual wing surface is biaxially-oriented polyethylene terephthalate (boPET) polyester film (trade name "Mylar foil") because of its high tensile strength and dimensional stability. Its weight of $6 g/m^2$ allows for covering the elevator and main wing with a mass of only

Table C.1: Weight budget of the EPFL microglider

Part	Mass (g)
Electronic Board	0.33
Battery 10mAh	0.55
Fuselage	0.18
Front wing	0.1
Rudder	0.03
Light sensors	0.1
SMA actuator	0.2
Cables and soldering	0.02
Total mass	**1.51**

0.09g. In addition, a camber support (figure C.2.f) made of 0.12mm thick carbon bars has been added in order to maintain structural stability of the main wing. The resulting weight of the airframe including wings is only 0.31g.

Actuation

Miniature airplanes flying at low velocities are strongly constrained by weight and power consumption. Different actuation systems could potentially be employed for actuating the control surfaces, such as magnetic coils, piezo actuators or SMA. Table C.2 compares three examples of different actuator types used on airplanes of less than 10g. The mass and power consumption can easily be quantified. However, other important figures of merit like commercial availability, mechanical complexity and force output are rather qualitative.

Magnetic coils have the advantage of relatively uncomplicated manual assembly and can easily be obtained commercially, but deliver comparably lower forces and are difficult to control precisely in position. Piezo materials have very low power consumption, deliver high forces and repetition rates, but with very limited displacement. They usually require complex micromechanical design for its amplification [46] and adequate costly equipment and expertise to fabricate the actuators. In addition, the very low weight of the actuator itself is diluted with weight expensive drive electronics to achieve the high voltage that is re-

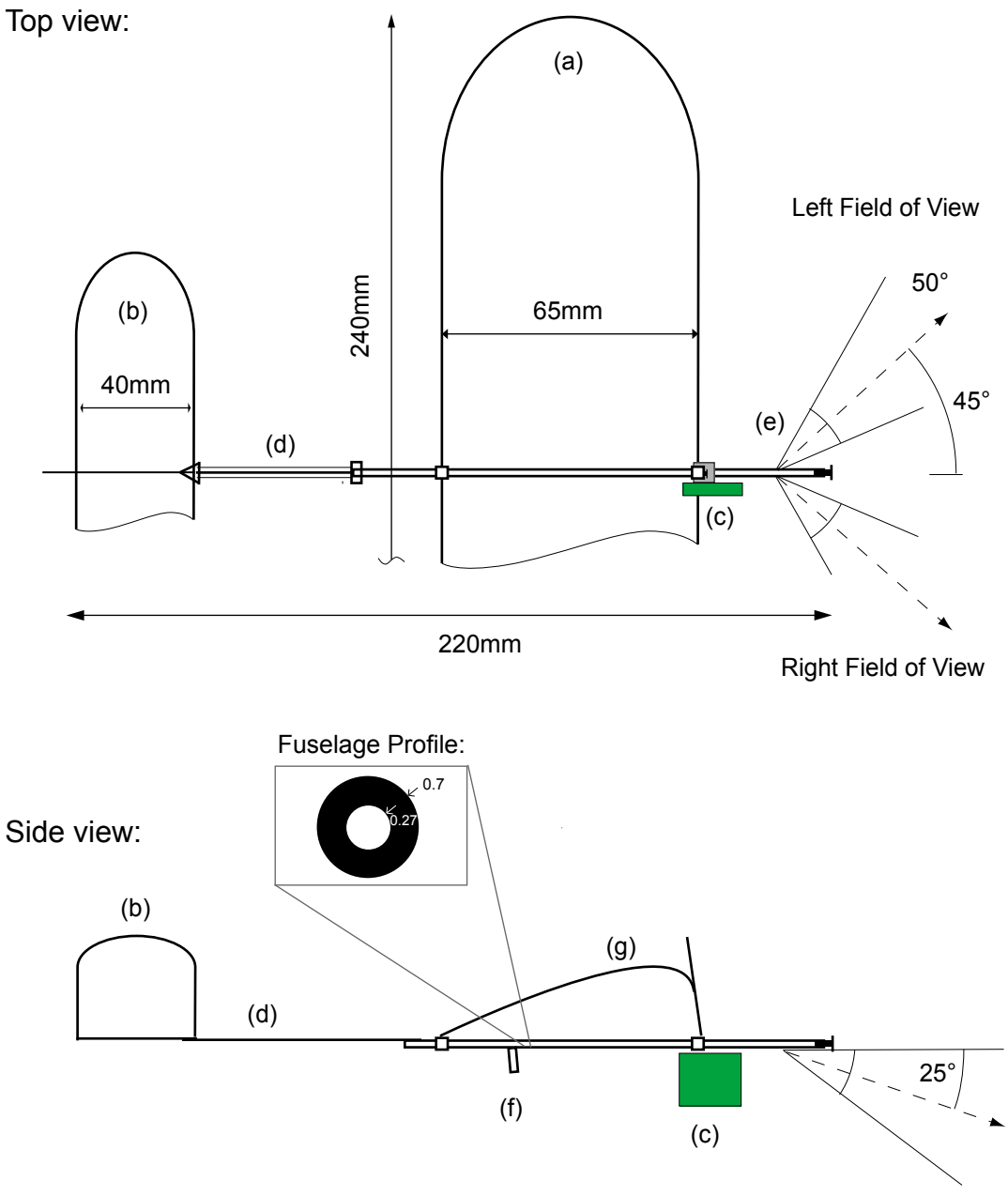

Figure C.2: Construction plan of the EPFL microglider. (a) main wing, (b) rudder, (c) electronic board and battery, (d) SMA actuator, (e) light sensors, (f) catcher for launching, glued to the bottom side of the fuselage, (g) camber support

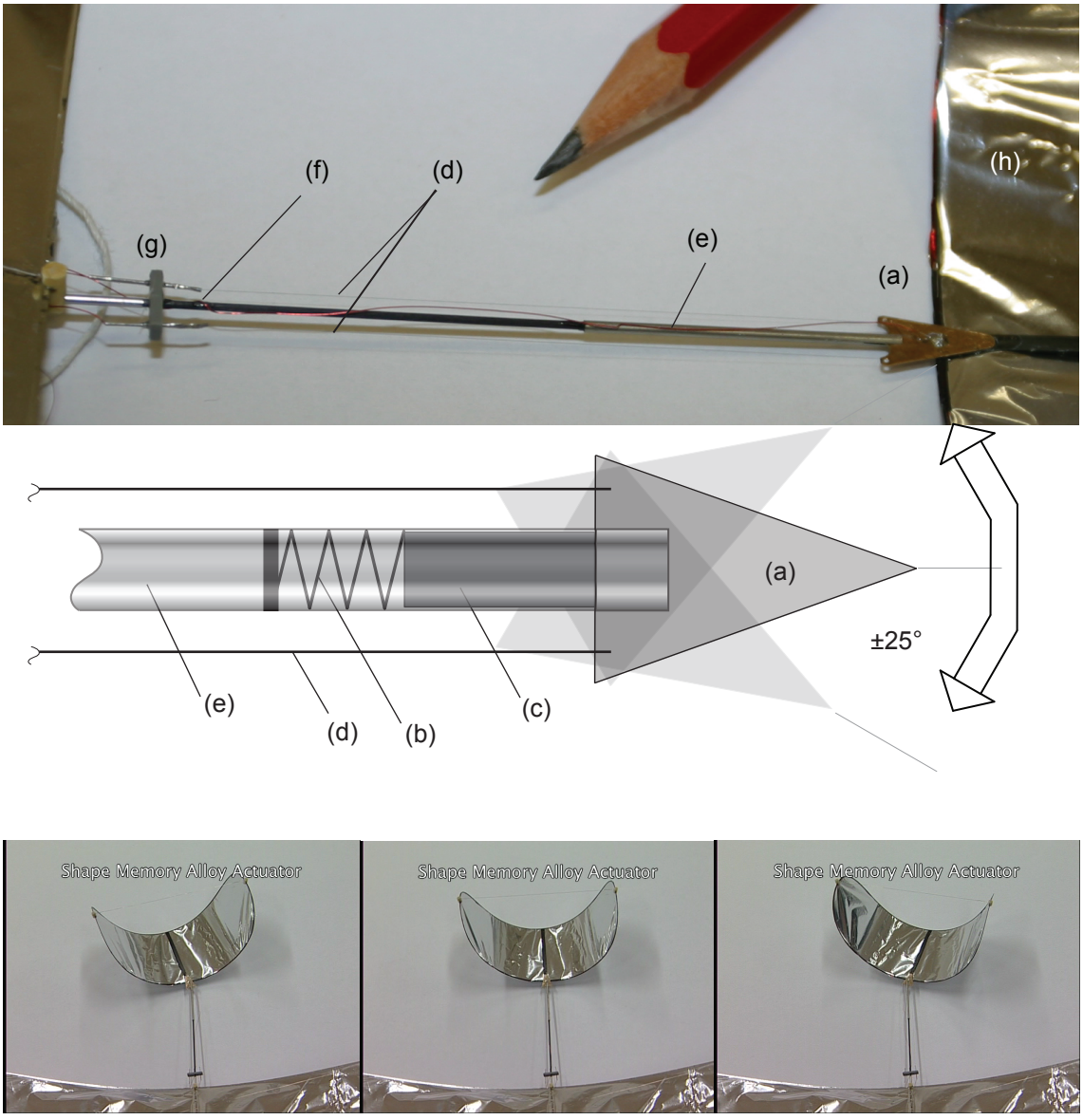

Figure C.3: 0.2g SMA actuator, (a) horn, (b) spring, (c) piston, (d) SMA wire, (e) steel tube, (f) carbon fuselage, (g) frame with electrical interface to Electronic Board, (h) rudder

Table C.2: Actuator comparison for miniature airplanes

Actuator type	Mass (g)	Drive Electronics (g)	Power (mW)	Commercial availability	Mechanical complexity	Force output
Magnetic coils [168]	0.15	0.02	180	+++	++	–
Piezo [154]	0.05	0.2	7	+	–	+++
SMA [75]	0.12	0.01	171	+	+	++

(+++: Very favorable, ---: Very unfavorable)

quired (200V in [154] leads to a weight of about 0.2g for the DC-DC converter, its peripheral components and additional board material). SMA wires offer comparably large displacements of around 5% of their length [33], very high power density and are used alternatively to conventional magnetic coils in hobbyist remote control airplanes [75]. The drive electronics is minimal and consists of one 0.01g transistor. However, potential disadvantages of SMA are a higher power consumption, lower repetition rate and more delicate dynamic control compared to, e.g., magnetic coils, due to hysteresis effects. For our application of rudder control, Nickel Titanium Alloy (Nitinol) wire, also known as "Artificial Muscles" [33], has been used due to its very high strength to weight ratio, precise control, simplicity and the very low power consumption (less than 160mW, depending on the duty cycle).

The working principle of SMA wire is that it exploits the crystallographic structure change of martensite to austenite (thermoelastic martensitic transformation) when heated above the transition temperature. This phase change produces a force that can be used for actuation. We used "Alloy M Flexinol™" wire [66] with a transition temperature of 70°C and 25μm diameter for maximal performance and low power consumption.

The actuator that we developed (figure C.3) consists of (a) a Copper-Beryllium horn, (e) a 0.7mm steel tube, (g) a frame with electrical interface and (d) two SMA wires attached to the frame and the horn. The stability of the actuator is given by the carbon fuselage (f). The wires are activated with a Pulse Width Modulation (PWM) signal as described below, which leads to a contraction of

up to 3.5mm with a maximal force of 0.069N ($\widehat{=}$7g) at the attachment point of the horn. This leads to a deflection of the horn and the rudder which is glued on the horn. The point of rotation is the attachment point of the other SMA wire. Depending on the PWM duty cycle, a torque of up to 0.27mNm can be obtained. The counterpart of this movement is the custom made brass spring (b) with a spring constant of 45.8N/m which ensures back alignment of the rudder to the neutral position at zero PWM duty cycle.

Perception

Autonomous navigation requires a sensory system. Many different solutions are commercially available, but complex sensors such as Inertial Measurement Units (IMU) or GPS are far too heavy or energy consuming to be used on such a microglider. We decided therefore to equip the microglider with one photodetector on each side in order to demonstrate minimalist autonomous operation similar to the phototactic vehicles proposed by Braitenberg [20]. To this end, TAOS TSL237T High Sensitivity Light Sensors were chosen for their low weight of only 0.05g, low cost and sensitivity in the visual spectrum.

Embedded Electronics

A new 0.33g Electronic Board (EB) (figure C.1) has been specifically designed for our microglider. This low weight EB incorporates a 14pin 8-Bit CMOS Microchip™ PIC16F676 microcontroller with a 20MHz oscillator. It supports low voltage (3V) power supply and possesses built-in analog to digital converters allowing different types of interfaces with the sensors and actuators. The EB also includes one Single Chip (SC70) MOSFET transistors to drive the SMA actuator.

Control

The microglider is intended to fly towards a light source. Depending on the difference between the two light sensors, it determines if the light source is on the left or right side of the microglider and the corresponding SMA wire is activated (figure C.4) by a PWM signal of 196Hz frequency.

The current sent to the wire is controlled by PWM and its duty cycle is calculated according to the fraction of the two values of light sensors as follows:

$$\left.\begin{aligned} p_l &= 100 \cdot (1 - \tfrac{s_r}{s_l}) \\ p_r &= 0 \end{aligned}\right\} \text{ if } s_r < s_l$$
$$\left.\begin{aligned} p_l &= 0 \\ p_r &= 100 \cdot (1 - \tfrac{s_l}{s_r}) \end{aligned}\right\} \text{ if } s_r > s_l \tag{C.1}$$

where s_r and s_l are the output values of the light sensors on the right and left side. p_r and p_l are the PWM duty cycle values sent to the SMA wire on the right and left side of the actuator. If the light source is in front of the glider, the rudder deflection is very little. However, if the light source is on one side, the ratio between the two sensory values is high and the resulting PWM duty cycle induces a stronger deflection of the rudder leading to a more pronounced direction change towards the light.

The actuator control has to be balanced with the response of the glider to rudder movements and its reaction time for perception. According to basic airplane dynamics, a too strong deflection leads to abrupt roll and sideways diving of the glider. In order to prevent this behavior, the maximal PWM duty cycle has been determined empirically to be 80 (corresponding to 80% high state of the PWM signal (equation C.1)), leading to a rudder deflection of 25°. In addition, an adjustment to the background light level has been implemented. Before the flight, the glider is calibrated by exposing it to the highest illumination difference that lead to the maximal ratio of the two sensor values in the particular environment. The maximal PWM duty cycle is then assigned to the maximal ratio of the two sensory values perceived.

Control Characterisation

In order to assess the quality of the control strategy and test the response to changes of light source location, we used a 75W light bulb placed at 50cm distance in front of the microglider with a varying angle α (figure C.4)). The rudder

deflection β was then measured by means of a 10cm pointer (figure C.4 (p)) attached to the rudder. Figure C.5 shows the output values of the two light sensors s_r and s_l and the PWM duty cycles p_r and p_l (according to (equation C.1)) versus the light source angle α. The field of view of each sensor spans 50° between 20° and 70° on each side (figure C.2).

The rudder movement (figure C.6) shows a deflection of up to 25° to the side of the light source gradually adjusting to the light source position. This characterization indicates proper functioning of the control mechanism in the static case. Further experiments were required to demonstrate this behavior in flight.

C.3 Results

In order to characterize the flying abilities of the microglider, a number of systematic in flight experiments were carried out and statistically analyzed. These experiments aimed at testing whether the microglider is actually able to detect the direction of a light source and fly towards it autonomously.

Launching Device

A launching device (figure C.7) has been built to minimize the error due to changes in launching conditions. It consists of a carbon tube attached to a spring made of synthetic gum. The microglider is prepared for launch by positioning the catcher (figure C.2.f) to the tip of the carbon tube. By manually pulling the glider backwards against the marker, the spring is charged and provides the required energy for launch. The launching parameters, i.e. launching angle and launching velocity, can be systematically and precisely adjusted by changing the marker position.

Aerodynamical Optimization

In order to improve in flight operation of our microglider, we needed to optimize the flight distance per given launching altitude, usually referred to as gliding

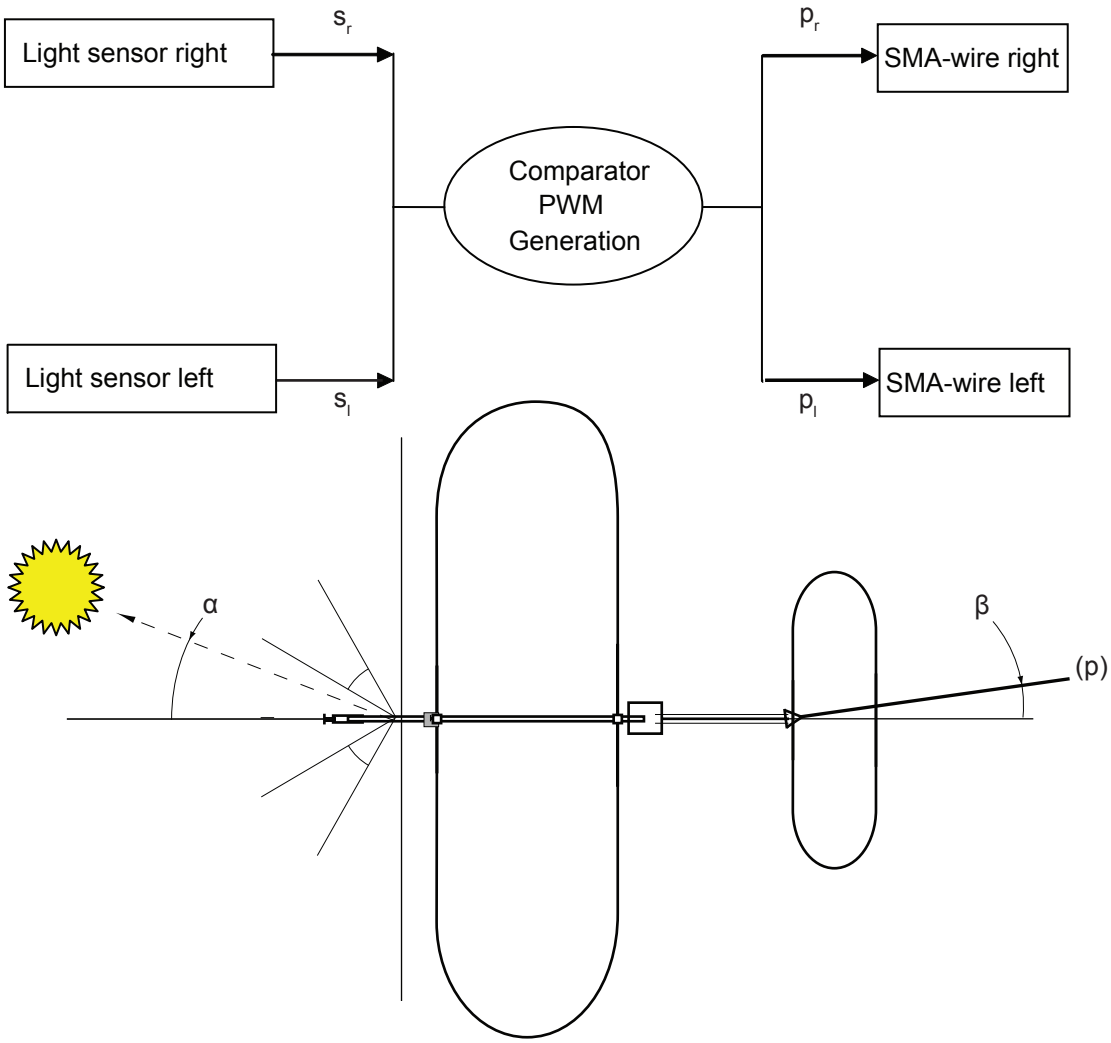

Figure C.4: Sensory actuator cycle scheme and characterisation setup. A 75W light source is positioned at 50cm distance (660lx) with varying light source angle α to measure the deflection angle β of the rudder (figure C.5 and C.6), (p) pointer for measurement of β

.

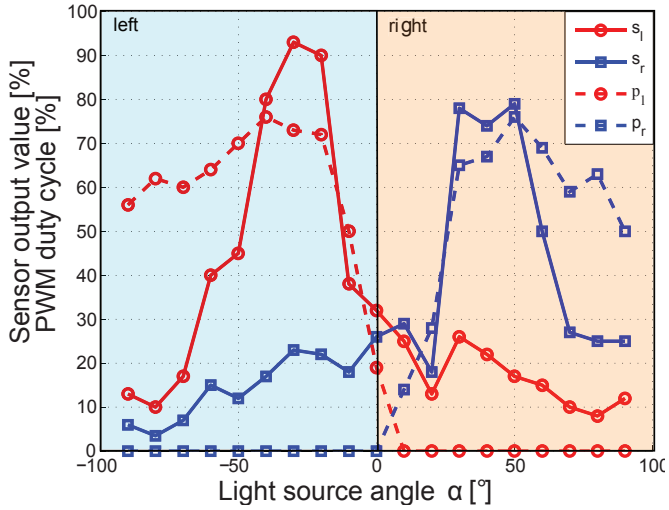

Figure C.5: Output values of the two light sensors s_l and s_r in percentage to saturation and PWM duty cycles p_l and p_r (equation C.1) versus the light source angle α (figure C.4)

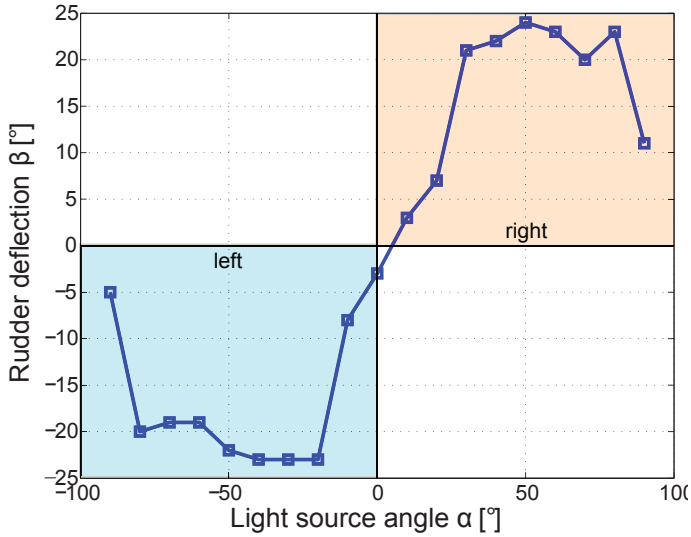

Figure C.6: Rudder deflection β depending on light source angle α (figure C.4)

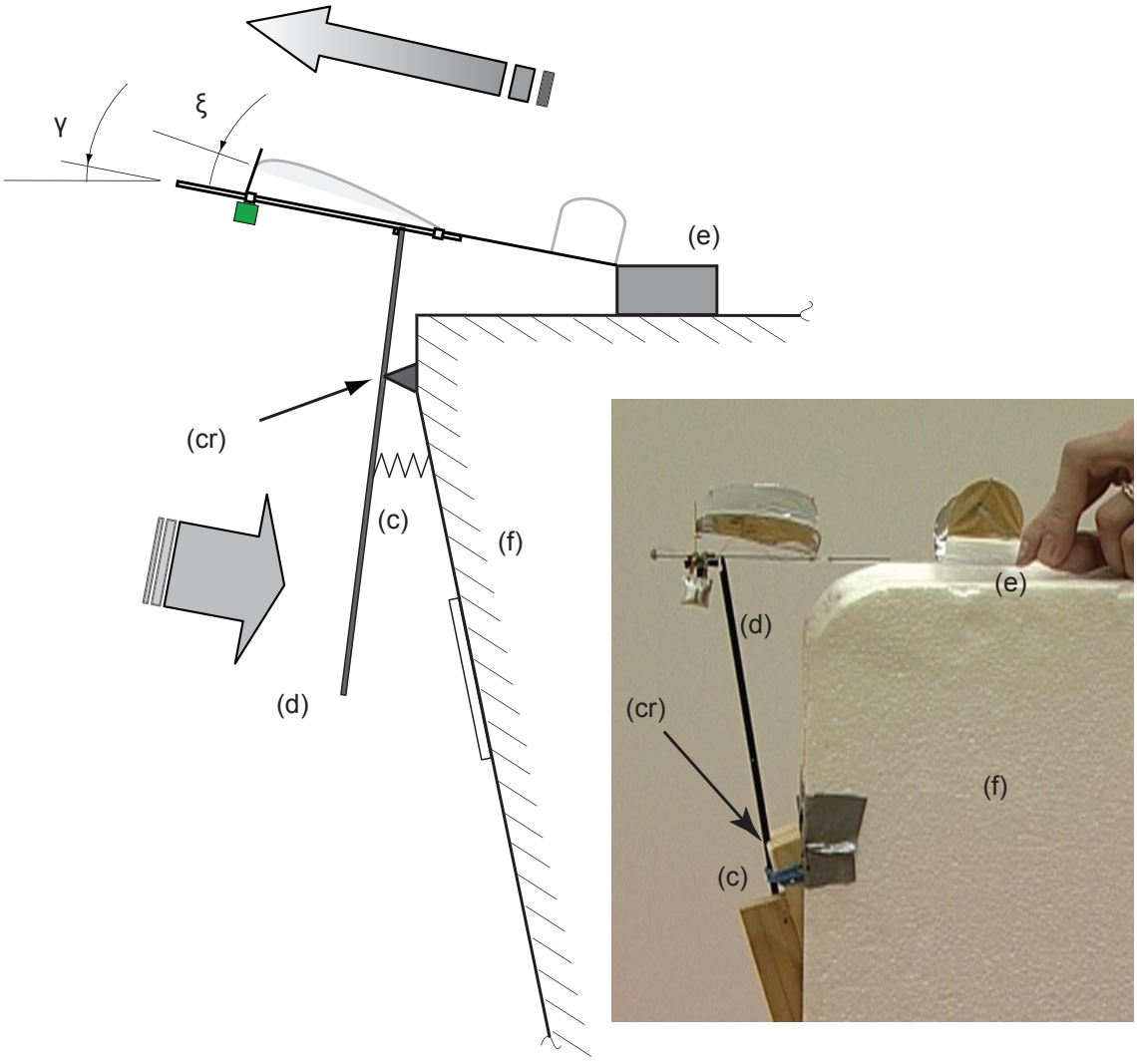

Figure C.7: Layout and picture of the launching device. γ launching angle, ξ angle of incidence, (c) spring, (d) carbon tube, (e) marker, (f) mounting, (cr) center of rotation. By pulling the glider backwards manually, the spring is charged and provides energy for the launching of the glider at a given launching angle

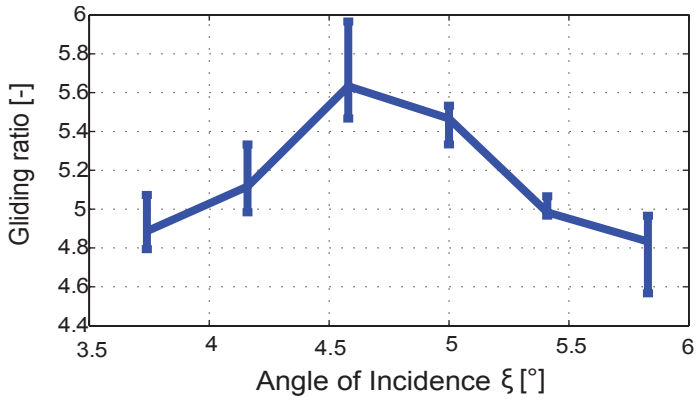

Figure C.8: Gliding ratio optimization. For every angle of incidence ξ, three subsequent launches have been carried out. Average values with error bars

ratio.

$$\text{Gliding ratio} = \frac{\text{Lift}}{\text{Drag}} = \frac{\text{Flight distance}}{\text{Launching hight}} \tag{C.2}$$

The easiest way to influence the flight performance for a given launching setup is to change the angle of incidence ξ, i.e. angle between the wing and the fuselage (figure C.7). In order to find the optimal angle of incidence, the microglider was launched with a velocity of 2m/sec and a fixed launching angle of 3.5°, whereby both values were measured optically using video and image processing (figure C.7 and C.9).

For each of the six different angles of incidence (figure C.8), three launches were carried out from a height of 1m and the flight distance was measured (figure C.9). The optimal angle of incidence has been found to be 4.6°, corresponding to a maximal average gliding ratio of 5.63 (figure C.8). This setting was used throughout the phototaxis experiments.

Phototaxis

We present a series of experiments where the glider was launched using the launching device to detect the direction of a light source and fly towards it. To this end, three series of launches were carried out, each with a different position of the light source (figure C.10). For every light source position, the microglider was launched 12 times using the same launching parameters. The landing posi-

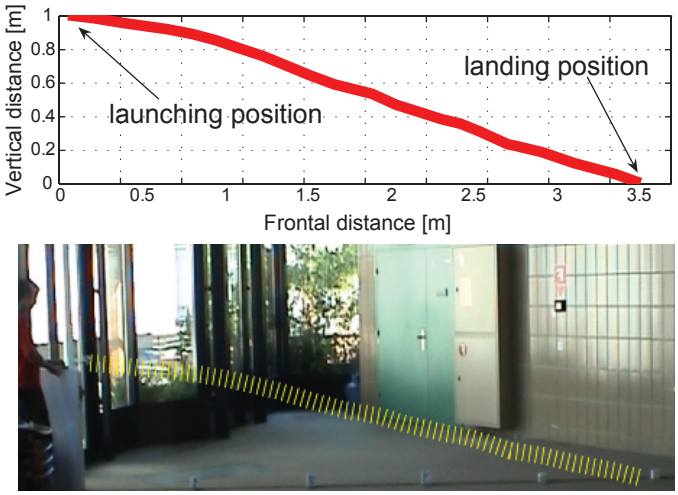

Figure C.9: Flight trajectory, launching velocity 2m/sec and launching angle $\gamma = 3.5°$

tions were measured and statistically analyzed. Due to time constrains these experiments have not been carried out with the latest, 1.5g microglider, but with an earlier prototype weighting two more grams with the same dimensions, control characteristics and a 25% lower gliding ratio of 4.3, flying at 1.7m/s. However, preliminary tests with the 1.5g version (see video attachment) show similar or improved behavior.

In order to test if the microglider actually displayed a phototactic behavior, a one-way analysis of variance (ANOVA) test was carried out on the three sets of landing positions. In our case, ANOVA was used to test if the microglider behaved differently when the light source was at a different position. The statistical evaluation was based on the lateral landing distance with respect to the launching axis (figure C.10).

For the three series of phototaxis experiments, the significance level p of the ANOVA test has been found to be less than 0.0001 (figure C.11). These experiments indicate that the EPFL microglider efficiently and reliably detects the light source and flies towards it.

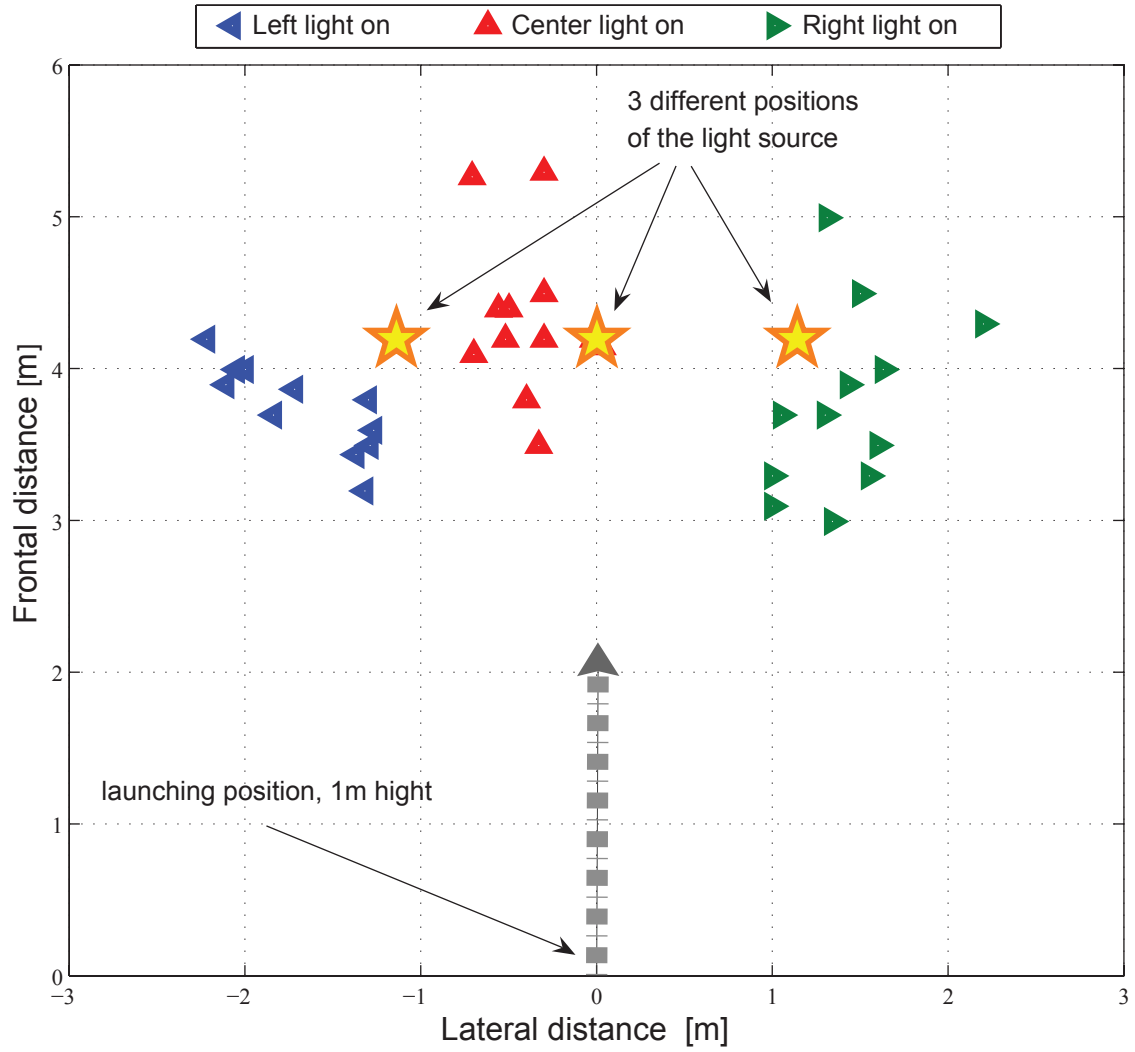

Figure C.10: Top view of the setup for the phototaxis experiments. Stars indicate the three possible light source locations. For every of the three locations, 12 subsequent launches have been carried out. The triangles mark the landing positions.

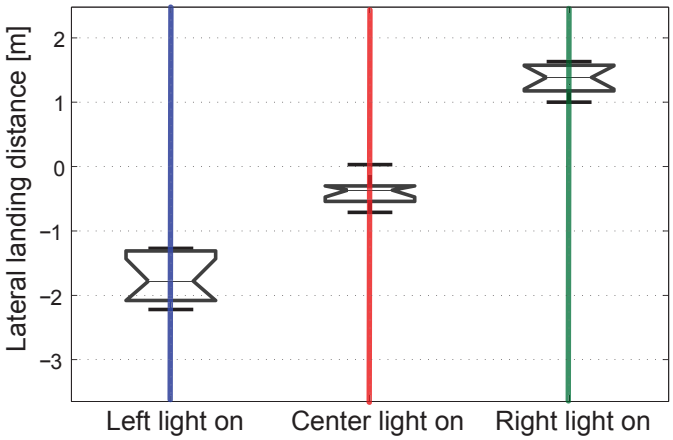

Figure C.11: Boxplot for the one-way ANOVA test on lateral distance of the landing points with respect to launching axis

C.4 Conclusion

We developed an ultra light weight microglider and demonstrated its capability of autonomous phototaxis. In order to keep the overall weight as low as possible and explore the potential of SMA for rudder control, we developed and integrated a novel 0.2g SMA actuator. The control mechanism for the sensory-motor cycle was characterized in the static case and the angle of incidence optimized, in order to maximize the gliding ratio. 36-sample in flight phototaxis experiments were performed and statistically analyzed showing that the microglider efficiently and reliably detects the light source and flies towards it.

The SMA actuator and the autonomous control strategy presented in this appendix could be used on the EPFL jumpglider. It would allow it to fly autonomously towards a light source, where it could charge its batteries using the solar cell based LiPo charger which is described in the tech report [49].

Compared to the magnetic coil actuators that are implemented on the EPFL jumpglider, using SMA based actuators allows to reduce the weight to a minimum, which is important for application where the payload of the jumpglider needs to be maximized.

D Perching to walls

Miniature Unmanned Aerial Vehicles (UAVs) such as the EPFL jumpglider could be extended with perching capabilities in order to efficiently place sensors in aloft locations. A major challenge for perching is to build a lightweight mechanism that can be easily mounted on an UAV, allowing it to perch (attach and detach on command) to walls of different materials. In this appendix, we propose a 4.6g perching mechanism that allows UAVs to perch on walls of natural and man-made materials such as trees and painted concrete facades of buildings. The mechanism is designed to translate the impact impulse when flying head-first to a wall into a snapping movement that sticks small needles into the surface. To detach from the wall, it uses a small electric motor for recharging the mechanism for the next perching sequence. Based on this principle, it damps the impact forces that act on the platform when perching out of flight to avoid damage of the UAV. We performed 110 sequential perches on a variety of substrates with a success rate of 100%[1].

Note: This chapter is based on the publication (Kovac et al. [82])

[1]See accompanying video at http://lis.epfl.ch/microglider/EPFLperchingMicroglider.mp4

D.1 Introduction

Flying robots such as the EPFL jumpglider presented in chapter 5 or other miniature Unmanned Aerial Vehicles (UAV) could be used in future for distributed sensing or environmental monitoring which is important in a variety of different scenarios [34, 94, 156]. In order to do that, one possible solution is to equip such UAVs with sensors and the ability to perch to natural and man made structures. We define perching as *the ability to attach to inclined surfaces or elevated positions out of flight and detach on command*. To date, only very few systems have been demonstrated recently that can attach to surfaces and only one system has been shown to be able to attach to and detach from vertical surfaces. The main difficulty in the design of such a perching robot is that it has to attach to the surface out of flight and subsequently detach from it to allow a reuse of the system or to change its location. All this needs to be achieved while maintaining small size and light weight to be implemented on a flying system.

In this appendix, we present the development and characterization of a working 4.6g perching mechanism. It is a perching module that can be integrated on any small UAV and allows it to attach head-first to vertical surfaces out of flight and detach from them again on command using a remote control. In order to fit the perching mechanism to different UAVs with different masses and flight velocities and to reduce the impact forces on attachment, we present a mathematical model that allows to dimension critical components of the mechanism. As a testbed to demonstrate the perching mechanism being successfully integrated on an UAV, we mount it on a microglider which is a gliding version of the commercially available MicroCeline [60].

Different approaches have been presented to date that tackle the challenge of perching for UAVs. Anderson et al [4] recently presented a variety of different perching concepts where the best solution consists of a small propelled UAV with a mass between 42g and 510g that crashes into the surface at stall speed and adheres to it using liquid glue. It then hangs down on a theater and uses a razor blade to cut the thread to free itself and retake flight. Although this is a very simple and innovative design, its main limitation is that the perching can be repeated only as many times as many sticky pads are integrated on the airplane.

Ideas are described how to store more than one sticky pad, but have not been implemented yet. The appendix mentions that it can perch succesfully, but no systematic characterization of the perching capabilities have been presented so far. Like other glue based attachment principles, this approach may as well not work on wet or dirty surfaces. Also is the 'rat-glue' used on the presented prototype in liquid state and detaches by itself after 60min, limiting the perching time. Depending on the UAV robustness, this approach may as well be limited to very light weight or slowly flying UAVs as the impact forces on crash with the wall are directly translated to the structure of the UAV. To reduce the risk for structural damage, damping devices or flight maneuvers would be required to reduce the impact velocity.

Another project has been recently presented by Desbiens and Cutkosky [91] where a glider is flying towards a wall, stalls and attaches to the wall using microspines. To do this autonomously, it incorporates an ultrasonic distance range sensor, a complete Paparazzi autopilot and suspension which is covered with microspines, similar to the ones used in [6]. Although this realization can attach to a variety of materials exploiting the surface asperity, it requires a relatively delicate dynamic stall maneuver of the entire UAV and adequate control, which reduces the success rate of attachment to 80% in the current early stage prototype. Detachment has not been demonstrated yet but could include concepts such as jumping off the surface or using propellers to reinitiate flight. The attachment has been demonstrated on a comparably heavy glider of 400g, which flies relatively fast at 9m/s. For smaller UAV, such as the very slowly flying and light weight microglider used in this appendix, stalling maneuvers may be even more delicate due to the low Reynolds number flight regime [104] which is difficult to control. Additionally, small or indoor flying UAVs impose strict weight requirements that do not allow the integration of heavy sensors or complex computation [167].

A similar concept has been described by Cory and Tedrake [35] who presented a glider that can successfully and precisely land on a string using a hook as the landing gear. To be able to do this, the glider is tracked in 3D in a lab environment using a VICON system with 6 cameras and is controlled off-board.

Wickenheiser and Garcia [151] aim at developing a perching aircraft that changes its tail configuration to decelerate in front of a vertical surface and attach to it. So far, the project has focussed mainly on aerodynamics and control and not on the attachment itself. Bayraktar and Feron [10] recently presented a helicopter that can land on inclined surfaces of up to 60
degree using velcro on its landing gear. Analogous to the previous two systems, this helicopter is tracked and controlled externally and has not been shown to be able to detach by itself after landing. Wright and Lind [156] are investigating sensor placement using a small UAV with morphing wings. The work so far has addressed the computational analysis of the aerodynamics of landing on a vertical surface without integrating mechanisms that would allow it to actually attach to it. Roberts et al. [119] recently presented a hovering platform that can autonomously attach to and detach from ceilings using actuated magnets. Its limitation to date is that it only works on horizontal and ferromagnetic ceilings.

Numerous other projects deal with the challenge of attachment and detachment from the perspective of applying it to climbing robots. All these systems however are not designed to fly and they have the tendency to be relatively slow and heavy, which limits their applicability to UAVs. The interested reader may be referred to [6, 103, 115, 125, 152] for an overview of existing state of the art robots that use different climbing techniques.

Several different adhesion methods, such as synthetic gecko tape, suction cups, magnets, needles etc., could be used to attach to the surface. In table D.1 we provide a summary evaluation of the advantages and limitations of the different methods that has been presented in the literature to date. We decided to base our design on penetration based clinging using needles due to its applicability for a wide range of prevalent surface materials, its ease of use and utility on smooth as well as rough surfaces.

As we will see later, our perching mechanism works successfully on vertical surfaces with a hardness between 24ShoreD and 89ShoreD. This range corresponds to materials such as tree barks, different kinds of wood, facades of buildings and painted concrete. Examples of the hardness of different prevalent man-made and natural materials where our mechanism can perch on are listed

in table D.2.

In the following sections we will first illustrate the process and design criteria that we applied for designing our mechanism. We will then present the modeling that allows to dimension the parts of the mechanism and describe the mechanical implementation. Finally, we will characterize the perching mechanism and demonstrate its integration with a microglider to successfully attach to walls of different materials and detach on command using a remote control. Video footage of its behavior indoors and outdoors can be seen in the accompanying video material.

D.2 Design

In order to design our perching mechanism, we assume that it will be mounted on the tip of an UAV which is flying at a constant forward velocity towards a vertical wall. Our perching mechanism has to fulfill two functions, i.e. autonomous attachment and detachment. In this section, we propose and discuss different design principles to fulfill these functions.

As the perching mechanism will be mounted on a UAV and has to work robustly, we define the design requirements to be (i) light weight, (ii) small size, (iii) effectiveness, (iv) structural simplicity and (v) exertion of little force on the UAV when perching to the wall. In line with these requirements, we choose the design principles to implement.

Surface attachment

For the attachment to the surface, we considered three attachment principles (figure D.1) and compare them using a standard engineering qualitative comparison as proposed in e.g. [147]. The first principle (A) consists of two needles (representing a symmetrical array of one or more needles) that are mounted in front of the glider and act like darts to stick to the surface. Since there are no moving or flexible parts required to implement this principle, it is very light weight, small and simple. Its drawback is that it is not very effective as it can stick only well if the impact of the UAV is exactly in line with the needles. An

Table D.1: Comparison of different adhesion methods for the application to perching robots

Adhesion method	Working principle	Advantages	Limitations
Synthetic gecko tape [7, 52, 53, 103]	Synthetic setae create a large contact surface with the substrate and adhere based on van der Waals forces.	Works on a variety of substrates, directional adhesion, light weight, no energy consumption	Does not work on dusty and dirty surfaces, adhesion depends strongly on roughness of substrate, to date only very limited life time, difficult fabrication process, preload force required, detachment requires peeling
Adhesive tape [37]	Chemical adhesion	Easy commercial availability, works on a variety of substrates, light weight, no energy consumption, depending on material, very strong adhesion	Does not work on dusty and dirty surfaces, dependance on roughness of material, limited lifetime, preload force required, detachment requires peeling
Suction cups [86, 117]	Vacuum creates force to hold it on the surface	Strong force on smooth surfaces, works on a variety of substrates	Works only on smooth surfaces, does not work well on dusty or dirty surfaces, requires a mechanism to create the vacuum, devices to date are relatively bulky and heavy
Magnets [119, 132]	Magnetic force	Very strong force, easy commercial availability, no preload force required to attach, light weight, no energy consumption	Works only on ferromagnetic materials
Electoradhesion [115]	Electrostatic attraction	Relatively strong adhesion, works on dusty and dirty surfaces, works on a variety of substrates	Requires a small amount of energy to stay attached, works only on smooth surfaces
Microspines (without penetration into the substrate) [6, 48]	Small spines act as hooks to attach to roughness on the surface	No energy consumption, Directional adhesion, works on a variety of substrates, no preload force required to attach	Does not work on very smooth or very rough surfaces, directional movement required to detach
Claws [152]	Grasping onto coarse structures on the surface	Works on a variety of substrates, potentially high adhesion through mechanical clinging	Works only on very rough surfaces, depends on friction of the substrate
Penetration based [116]	**Using needles to penetrate the substrate**	**Works on smooth and rough surfaces, works on different substrates, easy commercial availability of the needles, simple principle and easy to use, works on dusty and dirty surfaces, no energy consumption**	**Works up to a certain hardness of the substrate, leaves small holes in the surface**

Table D.2: Hardness of some prevalent man-made and natural substrates to which our perching mechanism can attach to

Substrate	Hardness [ShoreD]
Balsa wood	24
Poplar bark	36
Poplar wood	54
Okuome wood	61
Wallpaper	62
Spruce wood	65
Birch wood	69
Composite hardboard wood	76
MDF	87
Painted concrete facade	89

advantage of this principle is that the entire impact impulse is used to stick the needles into the surface. However, the deceleration distance is given by the protrusion depth of the needles, which is typically very short and therefore leads to very high forces acting on the structure of the UAV. For example, a very light weight UAV of 20g that is flying at 4m/s and sticks to the wall with a protrusion depth of the needles of 1mm would experience an average impact force of 160N, which is unacceptable for the structure of such a small UAV. Possibilities to deepen the protrusion depth by using different needles as a function of the substrate where the UAV shall attach to are very limited and would significantly add complexity to the system.

The second principle (B) consists of a grasping mechanism that is extended when the UAV impacts the surface and grasps subsequently, due to its elasticity, into the surface. This solution has the advantage that it can adapt well to the surface structure as the grippers extend first and then slide along the surface to grasp. The impact of the UAVs is first damped and the preloaded flexible arms then push the needles into the surface. This principle therefore exerts little forces on the structure of the UAV, but makes the penetration less effective due to the losses during damping.

The third and final principle that we considered (C) consists of two arms

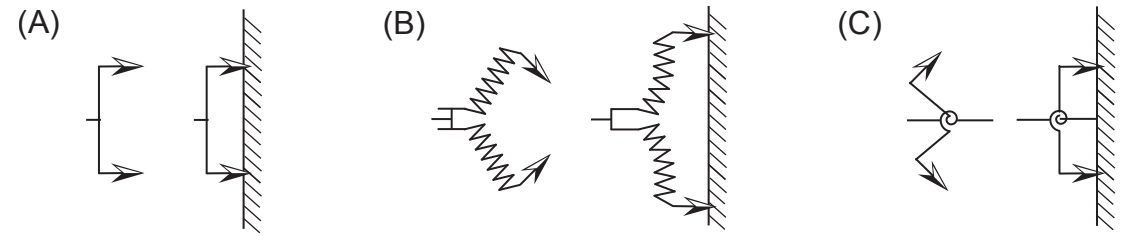

Figure D.1: Attachment principle for the perching mechanism. (A) sticks to the surface like a dart, (B) grasps to stick the needles into the surface, (C) snaps the arms to stick the needles into the surface

Table D.3: Qualitative evaluation summary of the three working principles for the attachment of our perching mechanism (figure D.1) (--: Very unfavorable, 0: Neutral, ++: Very favorable)

Criteria	(A)	(B)	**(C)**
Weight	++	0	**+**
Size	+	-	**0**
Effectiveness	-	-	**++**
Simplicity	+	-	**0**
Structural strain on the UAV	--	+	++

that are charged using a torsion spring. Once the UAV impacts the surface, the energy in the spring is released by a mechanical trigger and the two arms snap forward to stick the needles into the surface. Compared to the first two principles, (C) is more effective as the force that acts on the needles when the mechanism snaps can be adapted by using a different spring or mass of the arms. Depending of the arm length, the deceleration distance can easily be adjusted, which allows to keep the forces acting on the structure of the UAV low. The main drawback is that it requires the integration with a torsion spring which makes it structurally less simple compared to principle (A). Based on the comparison of these three possible attachment principles as qualitatively summarized in table D.3, we decided to use principle (C) for the attachment of our perching mechanism.

Detachment and recharging

Based on the surface attachment principle (C) we considered several possibilities to pull the arms backward to detach and recharge the mechanism for the next perching sequence. Ways to achieve this include small commercially available servos [62], Shape Memory Alloy (SMA) based actuators [77] or a small DC pager motor with a custom designed gearbox. The main advantage of the latter mechanism compared to the others is that it allows to dimension the motor and gearbox exactly to the needs of the perching mechanism which makes it a lighter solution than the commercially available servos. Compared to the SMA actuators, it is more effective as it avoids the small actuation length and hysteresis effects of SMAs.

We therefore decide to implement a DC motor actuated coil to pull back two strings that are attached to the arms. Once the arms are pulled back, a small magnet fixes them in their charged position. In case that the detachment would not succeed immediately, this mechanism could decharge and recharge again several times to pull the needles out of the wall.

Modeling of the perching mechanism

In this section we model the kinematics of the perching mechanism in order to dimension it for a given UAV. The goal is to dimension the torsion spring and the mass of the arms in a way that the UAV is decelerated while the arms are snapping forward and has zero velocity in the moment when the needles penetrate into the surface. This is a necessary condition to avoid that the UAV crashes into the surface or that the snapping would bounce it off the surface, both which would not allow a controlled and efficient perching to the substrate. Mathematically expressed, this requires that the impulse of the UAV is equal to the impulse generated by the snapping of the arms (figure D.2). For these calculations we assume that (i) the only mass of the arms is a point mass on its tips, (ii) the only contribution to the deceleration of the UAV is the snapping movement and (iii) that the spring force is perfectly linear with angular deflection.

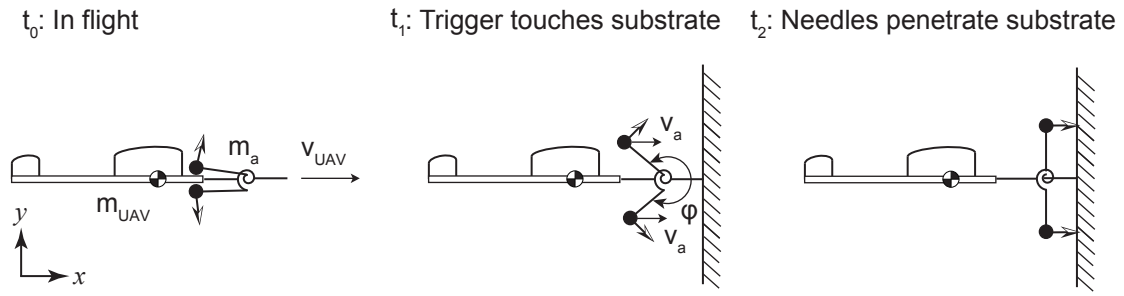

Figure D.2: Kinematic model of the perching mechanism mounted on an UAV. m_{UAV} mass of the UAV, v_{UAV} velocity of the UAV in x-direction, m_a mass of one arm, v_a velocity of the arms in x-direction. t_0 is the moment in flight before impacting on the surface, t_1 the moment when the trigger touches the surface and initiates the snapping movement, t_2 moment when the needles at the tip of the arms touch the surface

$$p_x(t) = m_{UAV} v_{UAV}, \qquad t = t_0 \tag{D.1}$$

p_x is the impulse of the entire system in the horizontal flying direction. m_{UAV} and v_{UAV} are the mass and velocity of the UAV. t_0 is the moment in flight before the trigger touches the substrate.

After time t_1, when the trigger touched the substrate and initiated the snapping, impulse is generated by the moving arms, each having a mass m_a, and the UAV is decelerated by the velocity $-v_d$ to satisfy the impulse balance.

$$p_x(t) = m_{UAV} v_{UAV} + 2 m_a v_a - m_{UAV} v_d, \qquad t_1 < t < t_2 \tag{D.2}$$

We dimension the mass m_a and the snapping velocity v_a in a way that the UAV is decelerated to zero velocity right before the time t_2 when the needles penetrate the substrate. In order to do this, we draw an energy balance and calculate the angular velocity $\omega(t)$ of the arms relatively to the UAV.

$$\frac{1}{2} c_s \varphi(t)^2 = -2 \cdot \frac{1}{2} J \omega(t)^2, \qquad t_1 < t < t_2 \tag{D.3}$$

$$\omega(t) = \sqrt{\frac{c_s}{2J} \left(\varphi(t_0)^2 - \varphi(t)^2 \right)}, \qquad t_1 < t < t_2 \tag{D.4}$$

With c_s being the spring constant of the torsion spring, φ the opening angle of the two arms, and J the moment of inertia of the two arms. Based on this, we can derive the velocity of the weights in x-direction v_a relative to the UAV.

$$v_a(t) = l_s \omega(t) \cos\left(90 - \frac{\varphi(t)}{2}\right), \qquad t_1 < t < t_2 \tag{D.5}$$

l_s is the length of the arms. Applying the parallel axis theorem $J = m_a l_s^2$ and giving the condition that the UAV has zero velocity when the needles penetrate the substrate $v_{UAV}(t_2) = 0$, we obtain the relation between the mass on the arms and the torsion spring.

$$m_a c_s = \frac{1}{2} \cdot \frac{v_{UAV}^2 \cdot m_{UAV}^2}{\varphi(t_0)^2 - \varphi(t_2)^2} \tag{D.6}$$

In order to maintain the impulse balance, we could therefore either use a smaller spring and a larger mass of the arms, or combine a stronger spring and a smaller mass of the arms. Using a large mass of the arms or a stronger spring may both increase the mass of the entire system. The goal is now to find the optimum in this trade-off and to chose a combination of spring and mass of the arms to keep the weight of the perching mechanism as low as possible. For simplicity we assume here that the gearbox and motor to charge the springs are identical for all the different combinations.

To determine the relationship between the spring mass m_s and the spring constant c_s, we measure the mass of ten standard steel torsion springs with a spring constant between 0.0137Nmm/° and 4.66Nmm/° that are commercially available at [61] (figure D.3). Performing a least square linear fit on these 10 points, we find the relation $m_s = 1.1 \cdot c_s + 0.014$. Based on this relation and equation D.6, we can plot the trade-off between the spring constant, the impulse of the UAV and the sum of the masses of the arms and the spring (figure D.4).

Our microglider testbed, with an entire system mass of 5g and a flight velocity of 2m/s has an impulse of 10mNs. We therefore choose a spring with a spring constant of 0.0854Nmm/° and a mass of 0.15g at the tips of each arm to satisfy the required conditions and minimize the weight of the entire perching mechanism. The best fit and resulting configuration is highlighted with a 'o' in

figure D.4.

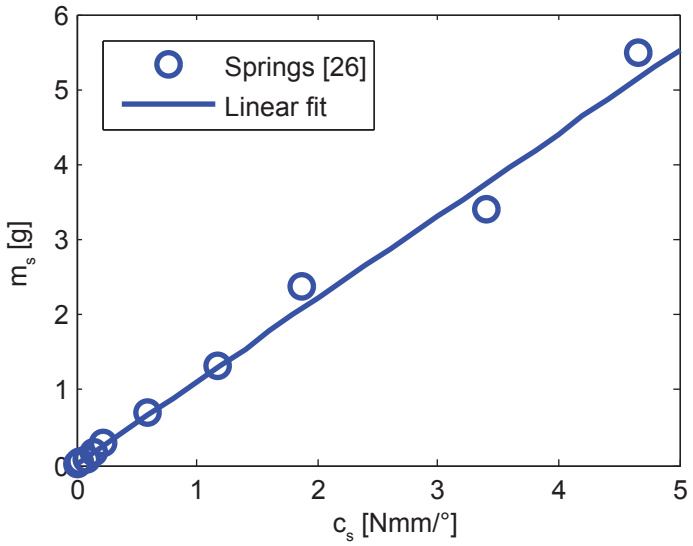

Figure D.3: Relation between the spring mass m_s and the spring constant c_s for a set of ten commercially available springs [61]

Implementation

As next step, we implemented the design principles as described above in Computer Aided Design (CAD) and fabricated the prototype. The details of the mechanical realization can be seen in the CAD view and the prototype in figure D.5.A-C, along with a picture of the realized prototype in figure D.5.D-E.

Realized is this perching sequence through a trigger (figure D.5.D.a) with a small linear spring on its end to push it back in position. When the trigger touches the surface, it separates the magnets (figure D.5.B.b), which allows the torsion spring (figure D.5.D.c) to snap its arms (figure D.5.D.d) forward and stick the needles (figure D.5.D.e) into the surface.

In order to satisfy the impulse balance, we add small weights (figure D.5.D.f) to each of the arms. In order to detach and recharge the mechanism, a small DC motor (figure D.5.A.g) and gearbox (figure D.5.A.h) pulls the arms backwards and positions the magnets that are mounted on the string (figure D.5.A.i) so that they keep the mechanism charged. The structural stability of the mechanism is ensured by using a stabilization bar (figure D.5.A.j). In order to keep the UAV

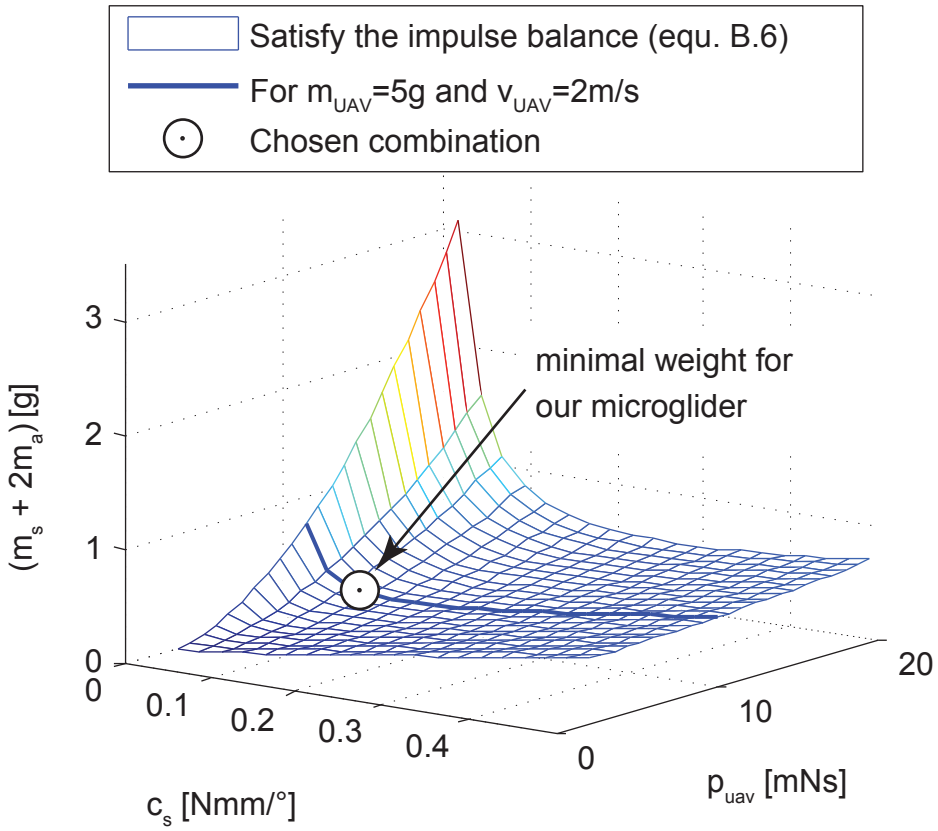

Figure D.4: The sum of the masses of the spring m_s and the arms m_a versus the impulse of the UAV p_{UAV} and the spring constant c_s of the torsion spring. For a microglider with a mass of 5g, flying at 2m/s, we choose the combination with minimal mass for the entire system (indicated with a 'o')

in a predefined position when perched to the wall, we add a support rod (figure D.5.A.k) to the mechanism. The carbon rod (figure D.5.A.m) ensures a stable position to be able to detach from the wall. The infra red receiver with battery (figure D.5.C.n), which is mounted on the gearbox, allows to remote control the mechanism to detach and recharge.

The attachment sequence is illustrated in figure D.6. In flight, the perching mechanism is in a charged state (figure D.6.A). Once it touches the surface, the trigger separates the magnets (figure D.6.B) and the arms snap forward and stick

the needles into the substrate (figure D.6.C). Finally, the mechanism settles in its stable position on the surface (figure D.6.D) and is then ready to detach from it on command to reinitiate flight.

Using the spring as calculated for the microglider, we need a force of 5.3N to recharge the perching mechanism. The smallest low cost motor that we found is a 4mm DC pager motor, which provides a torque of 0.038mNm at a motor speed of 8000t/min. This motor needs a gearbox with a transmission ratio of at least 178 to achieve the recharging. The implemented custom designed gearbox has four stages with a total transmission ratio of 833. This means that it provides a security factor of 4.6, which should be sufficient.

The two magnets that hold the mechanism in the charged position are commercially available Neodyme-Fer magnets with a diameter of 2mm and a pulling force of 1N. The spring which pushes back the trigger to its position has a spring constant of 0.09Nmm. At an acting distance of 2mm it exerts a force of 0.18N. This is high enough to push the trigger back after impact to its initial position, but does not significantly contribute to the deceleration of the UAV. In order to estimate its influence on the deceleration, we can calculate the impact force of a UAV to the wall. The energy of movement is defined as $E_{kin} = (1/2) \cdot m_{UAV} v_{UAV}^2$. For our rather light weight microglider, the kinetic energy in flight is 10mJ. Assuming a deceleration distance of 2mm, the force acting on the trigger and this spring when touching the surface is 5N, which is 28 times more than the force provided by the spring. This is the case for our light weight and slow flying microglider. For heavier or faster UAVs the influence would be even less. As implied in the modeling section, it is therefore justified to assume that the impulse of the snapping arms is the major contribution in the deceleration of the UAV. The needles that we use are commercially available steel sawing needles with a diameter of 0.5mm. The infrared remote control to control the motor is a commercial unit purchased at [60].

To keep the weight of the system as low as possible while ensuring strength, we use carbon for the trigger and the structural parts and print the connecting pieces and the gearbox out of ABS plus, using a 3D printer [65]. The gears are commercially available and made out of Polyoxymethylene (POM). The weight

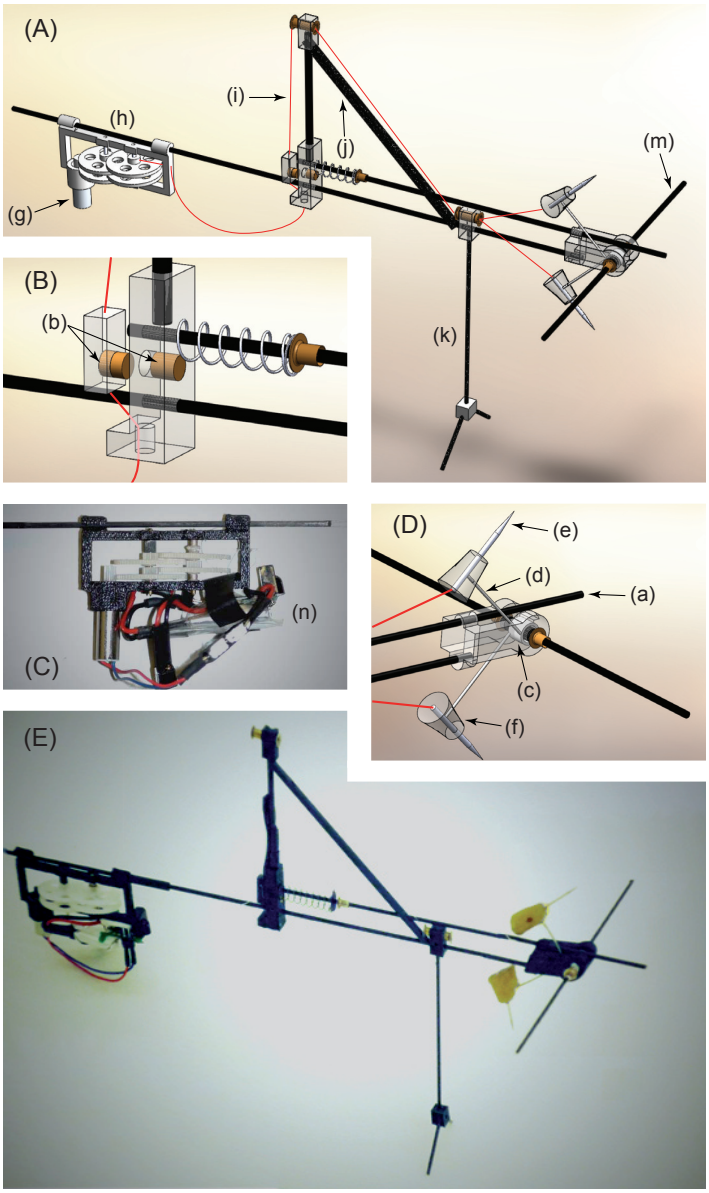

Figure D.5: Illustration of the details of the mechanical realization in CAD and on the realized prototype. (A) entire perching mechanism, (B) close up view of the release mechanism where the trigger separates the magnet to allow the arms to snap forward, (C) close up view of the front part of the mechanism, (D) close up photograph of the gearbox (E) photograph of the entire prototype

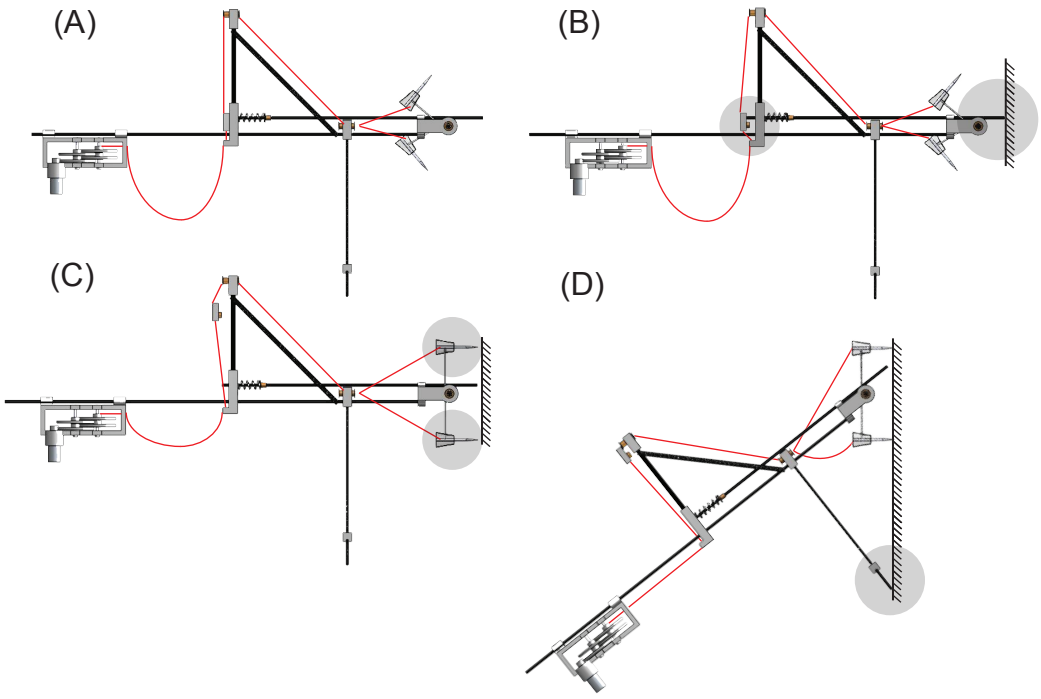

Figure D.6: Illustration of the attachment sequence. The grey circles indicate the areas of action. (A) charged state in flight, (B) the trigger touches the surface and separates the two magnets, (C) the arms snap forward and stick the needles into the substrate, (D) the mechanism settles in a stable position and is ready to be recharged and detach

Table D.4: Weight budget of the perching mechanism prototype

Part	Mass [g]
Motor	0.52
10mAh LiPo Battery	0.58
Gear box	0.76
Remote control receiver	0.7
ABS parts	0.61
Carbon pieces	0.69
Weight on arms	0.3
Spring	0.09
Connection pieces and cables	0.19
Total mass	**4.61**

budget is summarized in table D.4.

D.3 Results

In order to characterize our perching mechanism, we perform three sets of experiments to (i) evaluate how well the perching mechanism attaches to different substrates, (ii) test if our modeling of the perching mechanism is correct and (iii) characterize the reliability of attachment and detachment on different substrates. We add lead weights to the perching mechanism to simulate the mass of the UAV and launch it using a small linear catapult towards a wall (experimental setup in figure D.7). Using this setup, we film the perching sequence with a high speed camera [63] at 1000Hz. The shape and size of the needles that are used to attach have an influence on the attachment strength [116]. In order to keep this parameter constant, we sharpen the tips of the needles at an angle of 5° using a metal grinder. After ten launches, we replace the needles to avoid potential effect of wear.

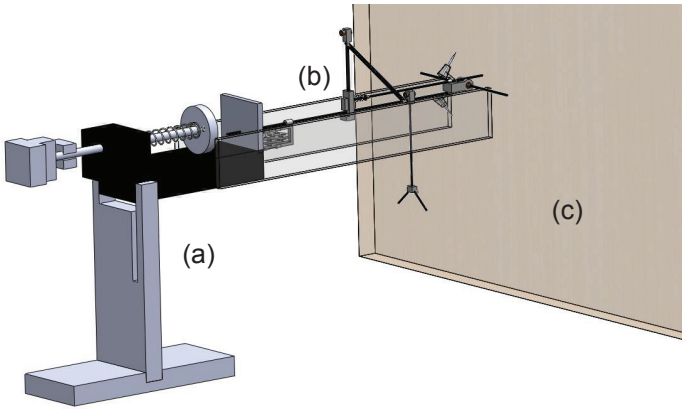

Figure D.7: CAD view of the experimental setup for the perching experiments. The catapult (a) accelerates the perching mechanism (b) to a desired impact velocity to the substrate (c)

Attachment security factor

In order to evaluate how well the perching mechanism attaches to different natural and man-made substrates, we launch the mechanism to four different substrates, i.e. a painted concrete facade, composite hardboard wood, poplar wood and poplar bark. By incrementally adding weights of 0.5g to the attached perching mechanism, we measure the weight that it can hold until it is torn off the substrate. We define the security factor S_F to be this maximal weight divided by the weight of our 5g mechanism (including the lead weight to simulate the UAV). It indicates the security margin of how well the perching mechanism can support the UAV when perched to the wall.

The mean S_F for every of the 10 launches per substrate is plotted in figure D.8 along with its standard deviation. We can observe that for harder substrates the security factor is lower than for softer substrates. However, in the case of the poplar bark, the security factor is one third of the poplar wood despite the fact that it is softer. As we will discuss in more detail later, this effect may be due to the substrate consistence of the poplar bark.

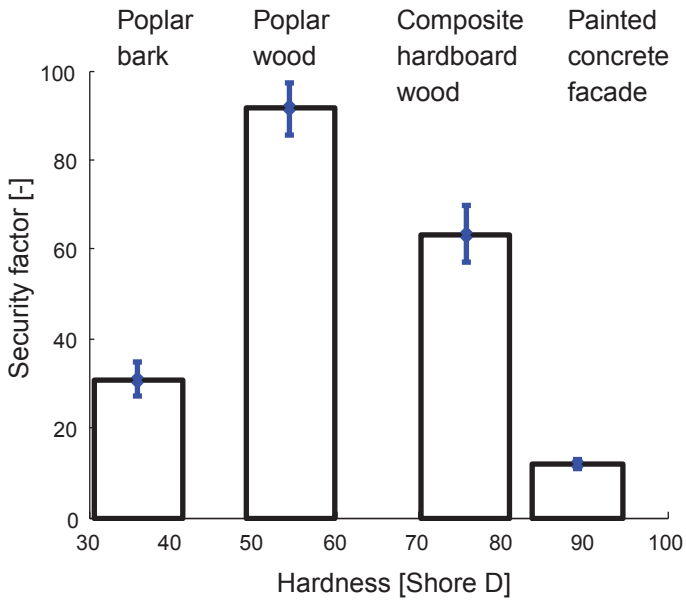

Figure D.8: Security factor for the attachment to the substrate for our system of 5g and its standard deviation

Impulse balance

This set of experiments aims at testing if our modeling of the perching mechanism as described in section D.2 is accurate and corresponds to reality. In order to do so, we adjust the weight of our perching mechanism for three different weight configurations, i.e. 2g, 5g and 8g, and launch it using the catapult at a velocity of 2m/s towards a wall. The spring constant and the weight of the arms are configured to fit a weight configuration of 5g at a flight velocity of 2m/s. We test the heavier and the lighter configurations to demonstrate what would happen if the choice of the spring and the masses of the arms would not be appropriate. For every configuration we perform ten sequential launches. Using a commercially available tracking software [67], we track the position of the front point of the perching mechanism behind the trigger.

The mean and standard deviation of the position versus time is plotted in figure D.9 for each of the three configurations. This set of experiments is performed using poplar wood as substrate material for the wall. It can be seen that for the

5g configuration (figure D.9.B) the oscillations right after impact are almost inexistent, which means that the system is decelerated to zero velocity just in the moment before the needles touch the surface. If we use a slightly too high mass of 8g (figure D.9.C), we see that the system is not decelerated sufficiently, crashes into the surface and bounces off. The needles penetrate the substrate at an angle ψ of 104° instead of 90° as in the case of the 5g configuration. In case that the mass is too low (figure D.9.A), the system remains further away from the surface and the needles penetrate the substrate at an angle of ψ=73°. Compared to the 8g configuration, the mechanism experiences higher frequency oscillations after attachment. The deceleration time Δt to zero velocity, which corresponds to the duration between the impact with the surface t_1 and the contact of the needles with the wall t_2 has been measured to be 4ms for all cases.

These experiments illustrate that the modeling truly does capture the dynamics of the perching mechanism and that the correct choice of the spring and weight of the arms is important to ensure proper perching.

Attachment and detachment reliability

In this set of experiments we evaluate the reliability of the perching mechanism for attachment and detachment on different substrates. We take the same four substrates as before and launch the perching mechanism in its 5g configuration towards the wall ten times for every substrate at a velocity of 2m/s. The result shows that the attachment to the substrate is successful for all of the 40 sequential launches on all the four substrates. The detachment as well is successful in all cases, but we observe that the effort to detach is different depending on the substrate. For the painted concrete facade substrate for example, the detachment is achieved already after around one half of the charging cycle, whereby for the softer poplar wood it takes in average 5.6 decharging-recharging cycles to detach. Since one charging cycle takes 1.5s, the detachment is achieved in average in less than 8.5 seconds even for the most difficult of the four substrates.

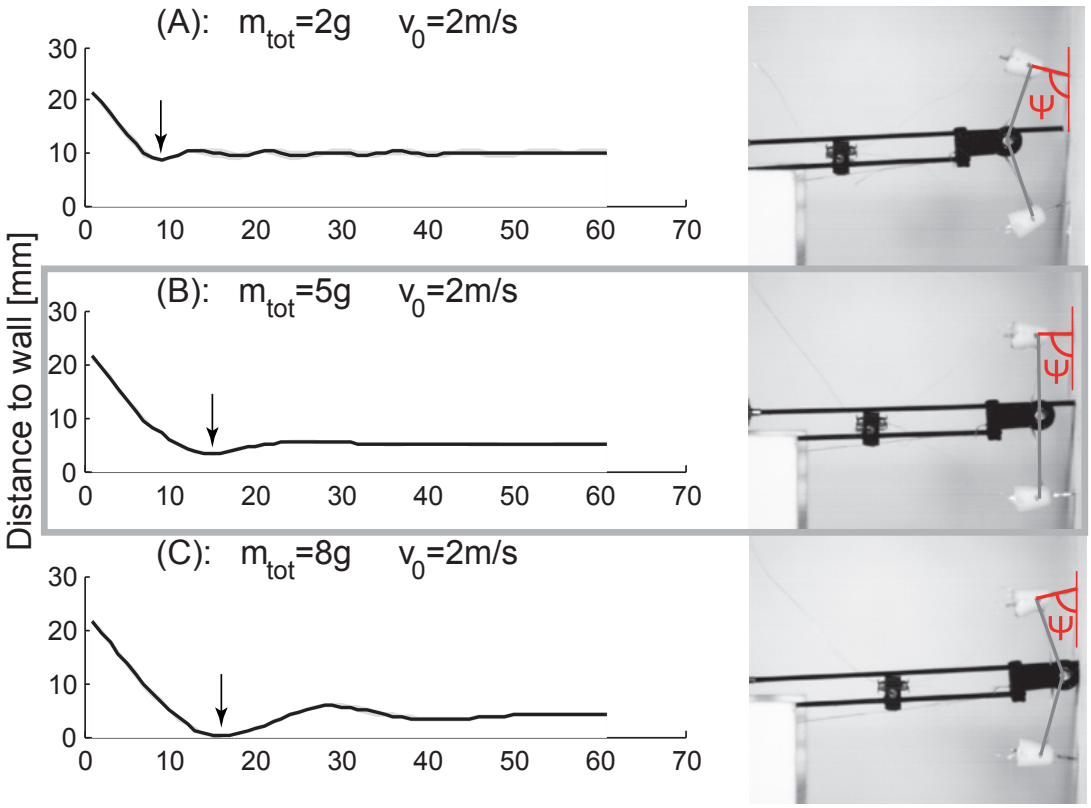

Figure D.9: Distance of the perching mechanism from the surface when perching for three different mass configurations. (A) the entire mechanism has a mass of 2g, (B) 5g and (C) 8g. The perching mechanism is designed to fit for the 5g configuration (boxed). ψ is the local penetration angle of the needles into the surface

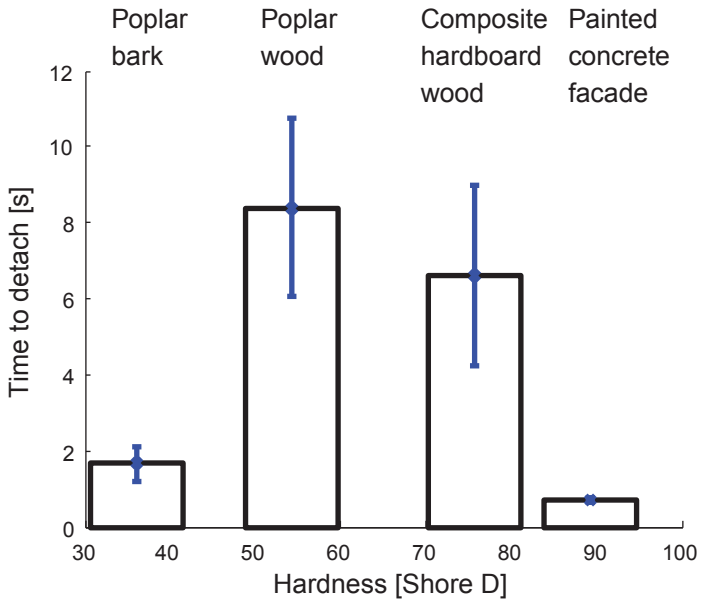

Figure D.10: Time it takes to detach from the four different substrates and its standard deviation

Integration with the microglider

To qualitatively demonstrate that the perching mechanism can successfully be integrated on an UAV, we illustrate a complete perching sequence to a wallpaper wall, a wooden facade of a building and a Marble tree in figure D.11. In order to balance the microglider, we added small weights to the tail, which reflected in the total weight of the complete system being 6g. To satisfy the impulse balance as described above, we increased the weight of each arm by 0.05g to 0.2g and launched the microglider by hand towards the object. Once the trigger touches the surface, it takes 4ms for the snapping movement until the needles stick into the surface. 0.26s later, the microglider settles in its final position and is ready to detach. Successful perching and detachment using this integrated microglider to different other walls, facades of buildings and trees can be seen in the accompanying video material.

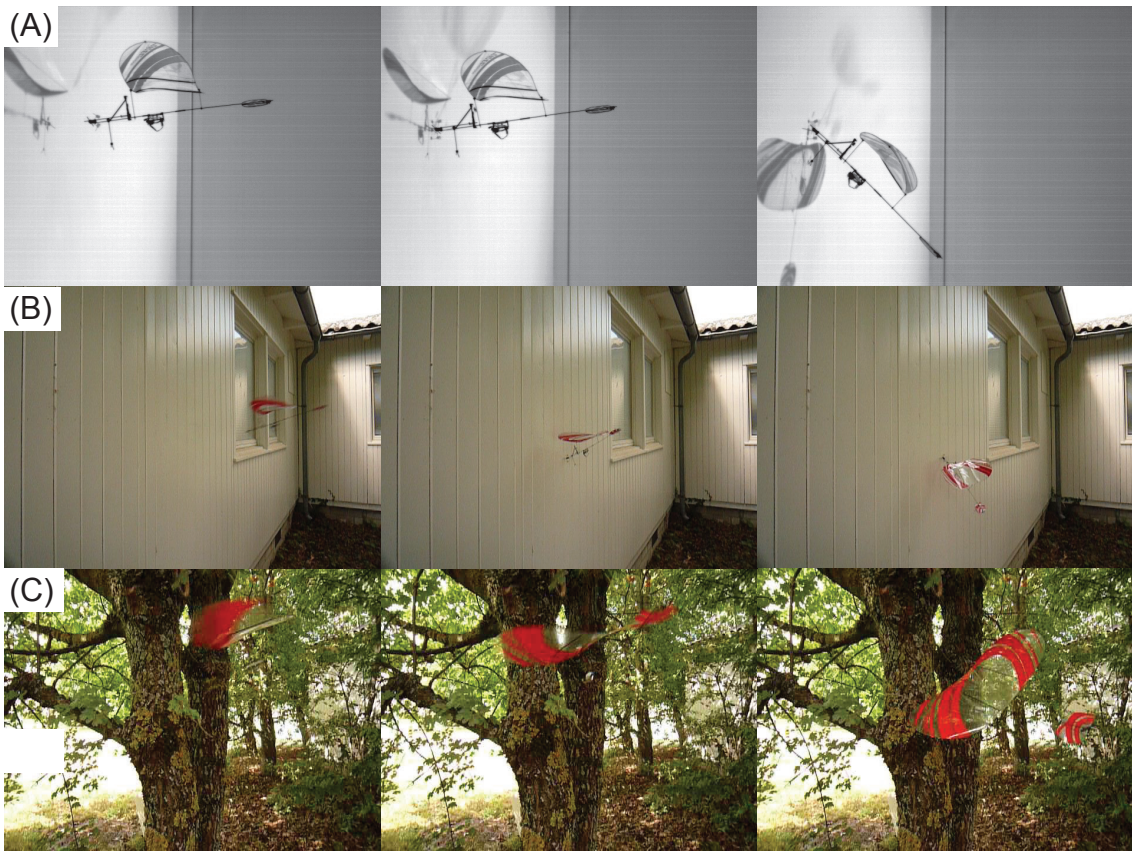

Figure D.11: Perching sequence of the microglider testbed to (A) a wallpaper wall, (B) a wooden facade and (C) a Marble tree

D.4 Conclusion

According to the results derived from the attachment security factor experiments, the attachment force is stronger for softer materials. In the case of the poplar bark, however, the attachment force is only around one third of the poplar wood despite the fact that it is softer. These results suggest that, in general, the hardness of the substrate is a major indication of how well the perching mechanism will stick to it. The somewhat surprising result with poplar wood implies that other material properties may play a role as well. The needle will enter deeper into softer substrates compared to harder ones and will provide the perching mechanism with more attachment force under the assumption that the only varying parameter is the hardness of the substrate. However, if the substrate is fibrous but of same hardness, it may allow greater attachment force compared to a non-fibrous substrate. On the other extreme, very brittle or porous materials may provide a much lower attachment force. For the experiments performed with our perching mechanism we can note that the security factor for the materials tested ranges between 12 and 91. These values are very high for an engineering system and are largely sufficient to reliably support the UAV for which the mechanism is designed. For the scope of this appendix we therefore do not explore in further detail how material properties interact with the needles while perching. Future work could address this question and aim at developing different needle geometries to optimize perching to different substrates.

Also, the cases tested include only substrates with a smooth surface. Depending on the rugosity of the surface, the perching strength may be influenced as the needles may penetrate the substrate locally from different angles, changing the force they can support [116]. Compared to other adhesion methods such as gecko inspired adhesion pads or similar surface attachment techniques, the penetration based adhesion that we use here is much less sensitive to surface rugosity and can function on very smooth as well as rough surfaces (see accompanying video material which shows successful perching to both relatively coarse tree barks and smooth wooden plates).

One limitation of the current design is that it cannot attach to very hard surfaces, such as glass or metal walls. A possible extension would therefore be to

combine the needle based adhesion with other adhesion methods, e.g. magnets or gecko pads, to enable attachment to these substrates as well. In the animal kingdom the combination of different adhesion methods is widely used: Wasps, for example, use a combination of van der Waals setae adhesion and spines [48]. In the current perching mechanism, combining it with other adhesion methods would require a partial redesign of the arms. The combination with magnets however can be done very easily without changing the perching mechanism by adding small magnets to the arms. It is noteworthy that one miniature Neodyme-Fer magnet with a diameter of 1.2mm and a mass of 0.006g can support a weight of up to 20g [60]. For very light weight UAVs one could consider magnetizing the needles themselves so that they can support the weight of the UAV when perching to ferromagnetic substrates.

As this appendix focusses on the development of the perching mechanism and the qualitative demonstration of its successful perching behavior on a microglider testbed, we do not further investigate integration issues with other flying platforms. Nevertheless, we wish to provide here a discussion of some aspects that need to be considered if one wants to adapt and use this perching mechanism for another UAV. According to the impulse based model, the perching mechanism can be adapted to any UAV if its mass and flight velocity is known, assuming that the UAV flies forward at a constant flight velocity and that the trigger of the mechanism touches the surface first. It may therefore be best to have the perching mechanism integrated on the most frontal tip of such a flying system. For propelled flight, platforms such as the MicroCeline follow up called Airburr [76] or the swift [88] may be adequate designs because they do not carry the propeller in front.

The main challenge is how to integrate the mechanism on the platform and how to combine it successfully with the global behavior of the UAV. On the microglider in this appendix, we attach the mechanism to the fuselage using superglue which is a very convenient and simple way to enable a small UAV with perching capabilities. The perching is achieved without requiring sensing or computation and is very robust: Out of 110 attachment and 40 detachment trials it showed a success rate of 100%. This perching mechanism could as well

be used for approaches that use dynamic maneuvers to detect the wall and decelerate or position the UAV before attaching to it. In such cases, one or several perching mechanisms could be mounted on the ventral part or on the wings of the UAV. In our microglider with a mass of 6g, the perching mechanism represents with 4.6g a significant fraction of the entire system mass. For larger, or other types of UAVs such as for example a quadrotor-like hovering platform, it could be possible to integrate several perching mechanisms on its outer periphery, since the mechanism weights only a few grams. The challenge in this case would be to ensure that the UAV approaches the wall at a sufficiently steep angle and that only one perching mechanism is released at once.

The cases that we tested in this appendix are performed perpendicular to the wall in both pitch and yaw. The attachment propensity may decrease with the angle at which the UAV flies to the wall such that below a certain threshold, attachment may no more be feasible. Based on the experience with the perching mechanism presented here, the limit for it to attach is in the order of $\pm 45°$ in pitch and $\pm 30°$ in yaw. This may vary depending on the substrate, the flight velocity and the mass of the UAV. A systematic characterization thereof is beyond the scope of this appendix. One possible solution how to ensure that the perching mechanism faces the wall perpendicularly in pitch could be to add a hinge between the mechanism and the UAV and add a small weight to the mechanism that would, due to gravity, keep the mechanism oriented vertically.

Depending on the UAV where the perching mechanism is integrated, the take-off after detachment from the wall may be a challenge as well and require a coordination of detachment and the propulsion of the UAV. For this, the support rod (figure D.5.A.k) could be adapted in shape and length to keep the UAV in a favorable position to ease the transition to flight after detachment. A possibility would be to use auto-stable UAV platforms that, after detachment from the wall, self-stabilize and navigate away from the wall in flight. Another way would be to jump off the wall using the EPFL jumpglider as presented in chapter 5. Using the combination of gliding, perching and jumping off the wall would allow the EPFL jumpglider to move in almost every terrain.

For UAVs that fly very fast or are very heavy, one needs to keep in mind that

the kinetic energy of a moving object is defined as $E_{kin} = (1/2) \cdot m_{UAV} v_{UAV}^2$. Assuming that the deceleration is constant, we can express the force during impact as $F_{impact} = E_{kin}/\Delta s$, where Δs is the deceleration distance. This means that the force acting on the UAV is linear proportional to its mass, quadratically proportional to its flight velocity and inversely proportional to the deceleration distance. For our case of a 6g microglider flying at 2m/s, and a deceleration time Δt of 4ms, the forces acting on the structure are $F_{impact} = m \cdot v_{UAV}/\Delta t = 2.5N$, which is acceptable. For comparison, a dart like design with a penetration depth of 0.5mm would lead to a very high and potentially hazardous force of $48N$. We can also assume that the deceleration distance is proportional to the arm length l_s of the perching mechanism. These basic scaling laws imply that for very fast and heavy UAVs, the arms of the perching mechanism need to be dimensioned proportional to $mv_{UAV}^2/\Delta s$ if the forces acting on the structure of the UAV should be constant.

Future work could include the integration of the perching mechanism on different UAVs such as the EPFL jumpglider and a more detailed assessment of the overall performance of perching enabled UAVs. Also, future work could include the combination of the penetration based clinging with other adhesion methods to enable it to attach to a larger variety of substrates.

Bibliography

[1] R. McN. Alexander. *Elastic Mechanisms in Animal Movement*. Cambridge University Press, 1988.

[2] R. McN. Alexander. Leg design and jumping technique for humans, other vertebrates and insects. *Philosophical Transactions: Biological Sciences*, 347 (1321):235–248, 1995.

[3] R. McN. Alexander. *Principles of Animal Locomotion*. Princeton University Press, 2003.

[4] M. L. Anderson, C. J. Perry, B. M. Hua, D. S. Olsen, J. R. Parcus, K. M. Pederson, and D. D. Jensen. The sticky-pad plane and other innovative concepts for perching uavs. *Proceedings of the 47th AIAA Aerospace Sciences Meeting*, 2009.

[5] R. Armour, K. Paskins, A. Bowyer, J. F. V. Vincent, and W. Megill. Jumping robots: a biomimetic solution to locomotion across rough terrain. *Bioinspiratoin and Biomimetics Journal*, 2:65–82, 2007.

[6] A.T. Asbeck, S. Kim, MR Cutkosky, W.R. Provancher, and M. Lanzetta. Scaling hard vertical surfaces with compliant microspine arrays. *The International Journal of Robotics Research*, 25(12):1165, 2006.

[7] K. Autumn, M. Sitti, Y. A. Liang, A. M. Peattie, W. R. Hansen, S. Sponberg, T. W. Kenny, R. Fearing, J. N. Israelachvili, and R. J. Full. Evidence for van

der waals adhesion in gecko setae. *Proceedings of the National Academy of Sciences*, 99(19):12252–12256, 2002.

[8] A. Azuma. *The Biokinetics of Flying and Swimming*. American Institute of Aeronatics and Astronautics, 2006.

[9] J. S. Bae, T. M. Seigler, and D. J. Inman. Aerodynamic and static aeroelastic characteristics of a variable-span morphing wing. *Journal of aircraft*, 42(2): 528–534, 2005.

[10] S. Bayraktar and E. Feron. Experiments with small helicopter automated landings at unusual attitudes. *Arxiv*, 2008.

[11] H. C. Bennet-Clark. The energetics of the jump of the locust *Schistocerca gregaria*. *Journal of Experimental Biology*, 63(1):53–83, 1975.

[12] H. C. Bennet-Clark and G. M. Alder. The effect of air resistance on the jumping performance of insects. *Journal of Experimental Biology*, 82(1):105, 1979.

[13] S. Bergbreiter, D. Mahajan, and K.S.J. Pister. Micromechanical energy storage with assembled elastomers. *Journal of Micromechanics and Microengineering*, 19:055009, 2009.

[14] M. D. Berkemeier and R. S. Fearing. Sliding and hopping gaits for the underactuated acrobot. *IEEE Transactions on Robotics and Automation*, 14(4): 629–634, 1998.

[15] M. C. Birch, R. D. Quinn, G. Hahm, S. M. Phillips, B. Drennan, A. Fife, H. Verma, and R. D. Beer. Design of a cricket microrobot. In *IEEE International Conference on Robotics and Automation*, volume 2, pages 1109–1114, 2000.

[16] P. Birkmeyer, K. Peterson, and R. S. Fearing. Dash: A dynamic 15g hexapedal robot. In *IEEE Int. Conf. Intelligent Robots and Systems*, 2009.

[17] K. L. Bishop. The relationship between 3-d kinematics and gliding performance in the southern flying squirrel, glaucomys volans. *Journal of Experimental Biology*, 209(4):689–701, 2006.

[18] F. J. Boria, R. J. Bachmann, P.G. Ifju, R.D. Quinn, R. Vaidyanathan, C. Perry, and J. Wagener. A sensor platform capable of aerial and terrestrial locomotion. In *IEEE/RSJ International Conference on Intelligent Robots and Systems*, pages 3959–3964, 2005.

[19] J. Brackenbury and H. Hunt. Jumping in springtails: mechanism and dynamics. *Journal of Zoology*, 229:217–236, 1993.

[20] V. Braitenberg. *Vehicles - Experiments In Synthetic Psychology*. The MIT Press, Cambridge, MA, 1984.

[21] A. K. Brodsky. *The Evolution of Insect Flight*. Oxford University Press, 1996.

[22] J. H. Brown and G. B. West. *Scaling in biology*. Oxford University Press, 2000.

[23] J. Burdick and P. Fiorini. Minimalist jumping robot for celestial exploration. *The Internation Journal of Robotics Research*, 22(7):653–674, 2003.

[24] H. Buri and Y. Weinand. ORIGAMI - folded plate structures, architecture. In *10th World Conference on Timber Engineering*, 2008.

[25] M. Burrows. Biomechanics: Froghopper insects leap to new heights. *Nature*, 424(6948):509, 2003.

[26] M. Burrows. Jumping strategies and performance in shore bugs (hemiptera, heteroptera, saldidae). *Journal of Experimental Biology*, 212(1): 106, 2009.

[27] M. Burrows and H. Wolf. Jumping and kicking in the false stick insect prosarthria teretrirostris: kinematics and motor control. *Journal of Experimental Biology*, 205(11):1519–1530, 2002.

[28] J. C. Butcher. *The numerical analysis of ordinary differential equations: Runge-Kutta and general linear methods*. Wiley-Interscience New York, 1987.

[29] G. Byrnes, N. T. Lim, and A. J. Spence. Take-off and landing kinetics of a free-ranging gliding mammal, the malayan colugo (galeopterus variegatus). *Proceedings of the royal society B*, 275(1638):1007–1013, 2008.

[30] G. Caprari and R. Siegwart. Mobile micro-robots ready to use: Alice. In *IEEE/RSJ International Conference on Intelligent Robots and Systems*, pages 3295– 3300, 2005.

[31] G. Card and M. Dickinson. Performance trade-offs in the flight initiation of drosophila. *Journal of Experimental Biology*, 211(3):341, 2008.

[32] E. Christian. The jump of the springtails. *Naturwissenschaften*, 65(9):495–496, 1978.

[33] J. Conrad and J. Mills. *Stiquito Advanced Experiments with a Simple and Inexpensive Robot*. IEEE Computer Society, 1997.

[34] J. Cortes, S. Martinez, T. Karatas, and F. Bullo. Coverage control for mobile sensing networks. *IEEE Transactions on Robotics and Automation*, 20(2):243–255, 2004.

[35] R. Cory and R. Tedrake. Experiments in fixed-wing uav perching. In *AIAA Conference on Guidance, Navigation, and Control*, 2008.

[36] F. A. Coyle, M. H. Greenstone, A. L. Hultsch, and C. E. Morgan. Ballooning mygalomorphs: Estimates of the masses of sphodros and ummidia ballooners(araneae: Atypidae, ctenizidae). *Journal of Arachnology*, 13(3): 291–296, 1985.

[37] K.A. Daltorio, A.D. Horchler, S.N. Gorb, R.E. Ritzmann, and R.D. Quinn. A small wall-walking robot with compliant, adhesive feet. *IEEE/RSJ International Conference on Intelligent Robots and Systems*, pages 3648–3653, 2005.

[38] J. Davenport. Allometric constraints on stability and maximum size in flying fishes: Implications for their evolution. *Journal of Fish Biology*, 62: 455–463, 2003.

[39] S. Dubowsky, S. Kesner, J. S. Plante, and P. Boston. Hopping mobility concept for search and rescue robots. *Industrial Robot: An International Journal*, 35(3):238–245, 2008.

[40] R. Dudley, G. Byrnes, S. P. Yanoviak, B. Borrell, R. M. Brown, and J. A. McGuire. Gliding and the functional origins of flight: Biomechanical novelty or necessity? *Annual review of ecology, evolution, and systematics*, 38: 179–201, 2007.

[41] G. J. Dyke, R. L. Nudds, and J. M. V. Rayner. Flight of sharovipteryx mirabilis: the world's first delta-winged glider. *Journal of Evolutionary Biology*, 19(4):1040–1043, 2006.

[42] S. B. Emerson and M. A. R. Koehl. The interaction of behavioral and morphological change in the evolution of a novel locomotor type:" flying" frogs. *Evolution*, 44(8):1931–1946, 1990.

[43] J. P. Entwistle and R. S. Fearing. Flight simulation of a 3 gram autonomous glider, 2006. Master Project, U.C. Berkeley.

[44] R. L. Essner. Three-dimensional launch kinematics in leaping, parachuting and gliding squirrels. *Journal of Experimental Biology*, 205(16):2469–2477, 2002.

[45] A.A. Faisal. Coordinated righting behaviour in locusts. *Journal of Experimental Biology*, 204(4):637–648, 2001.

[46] R. S. Fearing, K. H. Chiang, M. H. Dickinson, D. L. Pick, M. Sitti, and J. Yan. Wing transmission for a micromechanical flying insect. In *IEEE International Conference on Robotics and Automation*, pages 1509–1516, 2000.

[47] L. Frantsevich. Righting kinematics in beetles (insecta: Coleoptera). *Arthropod Structure and Development*, 33(3):221–235, 2004.

[48] L. Frantsevich and S. N. Gorb. Structure and mechanics of the tarsal chain in the hornet, vespa crabro (hymenoptera: Vespidae): implications on the attachment mechanism. *Arthropod Structure and Development*, 33(1):77–89, 2004.

[49] J.-P. Fuchs, M. Kovac, and D. Floreano. Solar cells for the self deploying microglider, 2008. Semester project, EPFL.

[50] R. Fukui, A. Torii, and A. Ueda. Micro robot actuated by rapid deformation of piezoelectric elements. In *International Symposium on Micromechatronics and Human Science*, pages 117–122, 2001.

[51] C. Galinski and R. Zbikowski. Some problems of micro air vehicles development. *Technical Sciences*, 55(1), 2007.

[52] H. Gao and H. Yao. Shape insensitive optimal adhesion of nanoscale fibrillar structures. *Proceedings of the National Academy of Sciences*, 101(21): 7851–7856, 2004.

[53] S.N. Gorb. Biological attachment devices: exploring nature's diversity for biomimetics. *Philosophical Transactions of the Royal Society A: Mathematical, Physical and Engineering Sciences*, 366(1870):1557, 2008.

[54] W. Gronenberg. Fast actions in small animals: springs and click mechanisms. *Journal of Comparative Physiology A: Sensory, Neural, and Behavioral Physiology*, 178(6):727–734, 1996.

[55] F. Haas and R. J. Wootton. Two basic mechanisms in insect wing folding. *Proceedings: Biological Sciences*, 263(1377):1651–1658, 1996.

[56] F. Haas, S. Gorb, and R. J. Wootton. Elastic joints in dermapteran hind wings: materials and wing folding. *Arthropod Structure and Development*, 29(2):137–146, 2000.

[57] M. Hollander and D. A. Wolfe. *Nonparametric Statistical Methods*. John Wiley. New York, 1999.

[58] G. Hoyle. The anatomy and innervation of locust skeletal muscle. *Proceedings of the Royal Society of London. Series B, Biological Sciences*, 143(911): 281–292, 1955.

[59] W. Hraiz, O. F. Torrent, M. Kovac, and D. Floreano. Wing folding implementation for the self deploying microglider, 2010. Master project, EPFL.

[60] http://www.didel.ch. Didel SA, 2008.

[61] http://www.durovis.ch/. Durovis steel torsion springs, 2009.

[62] http://www.falconmodels.uk.com. Falcom mk iv 1.6g servo, 2009.

[63] http://www.fastecimaging.com. Troubel shooter 1000 high speed camera, 2007.

[64] http://www.faulhaber.com. Faulhaber SA, 2008.

[65] http://www.funtech.com. Dimension elite 3d printer, 2008.

[66] http://www.memory metalle.de. Info-sheet No. 13, Nitinol Alloy Types, Conditions and Surfaces, 2007.

[67] http://www.xcitex.com. Proanalyst motion analysis software, 2008.

[68] J. Y. Huang, X. D. Wang, and Z. L. Wang. Controlled replication of butterfly wings for achieving tunable photonic properties. *Nano Letters*, 6(10):2325–2331, 2006.

[69] F. Iida, R. Dravid, and C. Paul. Design and control of a pendulum driven hopping robot. In *IEEE/RSJ International Conference on Intelligent Robots and Systems*, pages 2141–2146, 2002.

[70] S.M. Jackson. Glide angle in the genus petaurus and a review of gliding in mammals. *Mammal Review*, 30(1):9–30, 1999.

[71] J. Jones. Inflatable robotics for planetary applications. In *Proceedings of the 6th National Symposium on Artificial Intelligence and Robotics and Automation in Space*, pages 18–22, 2001.

[72] A. Jusufi, D. I. Goldman, S. Revzen, and R. J. Full. Active tails enhance arboreal acrobatics in geckos. *Proceedings of the National Academy of Sciences*, 105(11):4215–4219, 2008.

[73] R. T. Kaftka and Z. Gürdal. *Elements of Structural Optimization*. Kluwer Academic Publishers, 1992.

[74] M. Kaspari and M. D. Weiser. The size-grain hypothesis and interspecific scaling in ants. *Functional Ecology*, 13(4):530–538, 1999.

[75] M. T. Keennon. Muscle wire technology for micro and indoor models. In *NEAT micro seminars*, 2004.

[76] A. Klaptocz, G. Boutinard Rouelle, A. Briod, J.-C. Zufferey, and D. Floreano. An indoor flying platform with collision robustness and self-recovery. In *IEEE/RSJ International Conference on Intelligent Robots and Systems*, 2010.

[77] M. Kovac, A. Guignard, J.-D. Nicoud, J.-C. Zufferey, and D. Floreano. A 1.5g sma-actuated microglider looking for the light. In *IEEE International Conference on Robotics and Automation*, pages 367–372, 2007.

[78] M. Kovac, M. Fuchs, A. Guignard, J.-C. Zufferey, and D. Floreano. A miniature 7g jumping robot. In *IEEE International Conference on Robotics and Automation*, pages 373–378, 2008.

[79] M. Kovac, J.C. Zufferey, and D. Floreano. Towards the self deploying microglider, a biomimetic jumping and gliding robot. In *Proceedings of the 4th International Symposium on Adaptive Motion of Animals and Machines*, pages 41–42, 2008.

[80] M. Kovac, M. Schlegel, J.-C. Zufferey, and D. Floreano. A miniature jumping robot with self-recovery capabilities. In *IEEE/RSJ International Conference on Robotics and Automation*, pages 583–588, 2009.

[81] M. Kovac, J.C. Zufferey, and D. Floreano. Towards a self-deploying and gliding robot. In Dario Floreano, Jean-Christophe Zufferey, Mandyam V. Srinivasan, and Charlie Ellington, editors, *Flying Insects and Robots*, chapter 19. Springer, 2009.

[82] M. Kovac, J. Germann, C. Hurzeler, R. Siegwart, and D. Floreano. A perching mechanism for micro aerial vehicles. *Journal of Micro-Nano Mechatronics*, 2010.

[83] M. Kovac, M. Schlegel, J.-C. Zufferey, and D. Floreano. Steerable miniature jumping robot. *Autonomous Robots*, 28(3):295–306, 2010.

[84] I. Kroo and P. Kunz. Mesoscale flight and miniature rotorcraft development. In *Fixed and Flapping Wing Aerodynamics for Micro Air Vehicle Applications*, volume 195, pages 503–517. AIAA, 2001.

[85] P. K. Kundu and I. M. Cohen. *Fluid Mechanics*. Academic Press, 2004.

[86] G. La Rosa, M. Messina, G. Muscato, and R. Sinatra. A low-cost lightweight climbing robot for the inspection of vertical surfaces. *Mechatronics*, 12(1):71–96, 2002.

[87] B. G. A. Lambrecht, A. D. Horchler, and R. D. Quinn. A small, insect-inspired robot that runs and jumps. In *IEEE/RSJ International Conference on Robotics and Automation*, pages 1240– 1245, 2005.

[88] S. Leven, J.-C. Zufferey, and D. Floreano. A simple and robust fixed-wing platform for outdoor flying robot experiments. In *International Symposium on Flying Insects and Robots*, pages 69–70, 2007.

[89] P. P. Li, K. Q. Gao, L. H. Hou, and X. Xu. A gliding lizard from the early cretaceous of china. *Proceedings of the National Academy of Sciences*, 104(13): 5507, 2007.

[90] L. Lostan, M. Kovac, and D. Floreano. Passive wing folding mechanism for a microglider, 2008. Semester project, EPFL.

[91] A. Lussier-Desbiens and M.R. Cutkosky. Landing and perching on vertical surfaces with microspines for small unmanned air vehicles. *Journal of Intelligent and Robotic Systems*, 57(1):313–327, 2010.

[92] S. Macia, M. P. Robinson, P. Craze, R. Dalton, and J. D. Thomas. New observations on airborne jet propulsion (flight) in squid, with a review of previous reports. *Journal of Molluscan Studies*, 70(3):297–299, 2004.

[93] L. Mahadevan and S. Rica. Self-organized origami. *Science*, 307(5716):1740, 2005.

[94] A. Mainwaring, D. Culler, J. Polastre, R. Szewczyk, and J. Anderson. Wireless sensor networks for habitat monitoring. In *Proceedings of the 1st ACM international workshop on wireless sensor networks and applications*, 2002.

[95] D. P. Maitland. Locomotion by jumping in the mediterranean fruit-fly larva ceratitis capitata. *Nature*, 355:159–161, 1992.

[96] J. Maynard Smith. The importance of the nevous system in the evolution of animal flight. *Evolution*, 6(1):127–129, 1952.

[97] M. G. McCay. Aerodynamical stability and maneuvrability of the gliding frog polypedates dennysi. *Journal of Experimental Biology*, 204:2817–2826, 2001.

[98] J. A. McGuire. Allometric prediction of locomotor performance: an example from southeast asian flying lizards. *The American Naturalist*, 161(2): 337–9, 2003.

[99] J. A. McGuire and R. Dudley. The cost of living large: Comparative gliding performance in flying lizards (agamidae: Draco). *The American Naturalist*, 166(1):93–106, 2005.

[100] J. Meng, Y. Hu, Y. Wang, X. Wang, and C. Li. A mesozoic gliding mammal from northeastern china. *Nature*, 444:889–893, 2006.

[101] J. M. Morrey, B. Lambrecht, A. D. Horchler, R. E. Ritzmann, and R. D. Quinn. Highly mobile and robust small quadruped robots. In *International Conference on Intelligent Robots and Systems*, pages 82–87, 2003.

[102] T.J. Mueller. *Fixed and Flapping Wing Aerodynamics for Micro Air Vehicle Applications*, volume 195 of *Progress in Astronautics and Aeronautics*. AIAA, 2001.

[103] M. P. Murphy and M. Sitti. Waalbot: An agile small-scale wall-climbing robot utilizing dry elastomer adhesives. *IEEE/ASME Transactions on Mechatronics*, 12(3):330–338, 2007.

[104] J.-D. Nicoud and J.-C. Zufferey. Toward indoor flying robots. *IEEE/RSJ International Conference on Robots and Systems*, pages 787–792, 2002.

[105] R. Niiyama, A. Nagakubo, and Y. Kuniyoshi. Mowgli: A bipedal jumping and landing robot with an artificial musculoskeletal system. In *IEEE International Conference on Robotics and Automation*, pages 2546–2551, 2007.

[106] U. M. Norberg. Bat wing structures important for aerodynamics and rigidity (mammalia, chiroptera). *Zoomorphology*, 73(1):45–61, 1972.

[107] U. M. Norberg. *Vertebrate Flight: Mechanics, Physiology, Morphology, Ecology and Evolution*. Springer, 1990.

[108] A. Norman. Adaptive changes in locust kicking and jumping behaviour during development. *Journal of Experimental Biology*, 198(6):1341, 1995.

[109] J. A. Oliver. "gliding" in amphibians and reptiles, with a remark on an arboreal adaptation in the lizard, anolis carolinensis carolinensis voigt. *The American Naturalist*, 85(822):171–176, 1951.

[110] K. E. Paskins, A. Bowyer, W. M. Megill, and J. S. Scheibe. Take-off and landing forces and the evolution of controlled gliding in northern flying squirrels glaucomys sabrinus. *Journal of Experimental Biology*, 210(8):1413, 2007.

[111] K. G. Pearson, I. C. Gynther, and W. J. Heitler. Coupling of flight initiation to the jump in locusts. *Journal of Comparative Physiology A: Neuroethology, Sensory, Neural, and Behavioral Physiology*, 158(1):81–89, 1986.

[112] T. J. Pedley. *Scale effects in animal locomotion*. Oxford University Press, 1977.

[113] S. Pellegrino. *Deployable Structures*. Springer, 2002.

[114] M. Picard, M. Kovac, and D. Floreano. Sensor and control set for the self deploying microglider, 2010. Semester project, EPFL.

[115] H. Prahlad, R. Pelrine, S. Stanford, J. Marlow, and R. Kornbluh. Electroadhesive robots - wall climbing robots enabled by a novel, robust, and electrically controllable adhesion technology. In *IEEE International Conference on Robotics and Automation*, pages 3028–3033, 2008.

[116] W.R. Provancher, J. E. Clark, B. Geisler, and M.R. Cutkosky. Towards pentration-based clawed climbing. In *7th International Conference on Climbing and Walking Robots*, pages 22–24, 2004.

[117] Z. Qian, Y. Zhao, and Z. Fu. Development of wall-climbing robots with sliding suction cups. In *IEEE/RSJ International Conference on Intelligent Robots and Systems*, pages 3417–3422, 2006.

[118] M. H. Raibert, H. B. Brown Jr, and M. Chepponis. Experiments in balance with a 3d one-legged hopping machine. *The International Journal of Robotics Research*, 3(2):75, 1984.

[119] J. F. Roberts, J.-C. Zufferey, and D. Floreano. Energy management for indoor hovering robots. In *IEEE/RSJ International Conference on Intelligent Robots and Systems*, pages 1242–1247, 2008.

[120] T. J. Roberts and R. L. Marsh. Probing the limits to muscle-powered accelerations: lessons from jumping bullfrogs. *Journal of Experimental Biology*, 206(15):2567–2580, 2003.

[121] M. Rothschild, J. Schlein, K. Parker, C. Neville, and S. Sternberg. Execution of the jump and activity. *Philosophical Transactions of the Royal Society of London. Series B, Biological Sciences*, 271(914):499–515, 1975.

[122] H. F. Rowell. Drymophilacris bimaculata. In *Costa Rica Natural History*, pages 714–716. University of Chicago Press, 1983.

[123] R. Santer, P. Simmons, and F. C. Rind. Gliding Behaviour Elicited by Lateral Looming Stimuli in Flying Locusts. *Journal of Comparative Physiology*, 191(1):61–73, 2004.

[124] R. D. Santer, Y. Yamawaki, F.C. Rind, and P. J. Simmons. Motor activity and trajectory control during escape jumping in the locust locusta migratoria. *Journal of Comparative Physiology A: Neuroethology, Sensory, Neural, and Behavioral Physiology*, 191(10):965–975, 2005.

[125] D. Santos, B. Heyneman, S. Kim, N. Esparza, and M. R. Cutkosky. Gecko-inspired climbing behaviors on vertical and overhanging surfaces. In *IEEE International Conference on Robotics and Automation*, pages 1125–1131, 2008.

[126] G. Savioz, M. Kovac, and D. Floreano. Wing folding mechanism for flying microrobots, 2007. Semester project, EPFL.

[127] U. Scarfogliero, C. Stefanini, and P. Dario. Design and development of the long-jumping" grillo" mini robot. In *IEEE International Conference on Robotics and Automation*, pages 467–472, 2007.

[128] M. Schlegel, M. M. Woodward Kovac, M. Sitti, and D. Floreano. A minimalist jumping and climbing robot, 2010. Master project, CMU.

[129] J. Scott. The locust jump: an integrated laboratory investigation. *Advances in Physiology Education*, 29(1):21–26, 2004.

[130] R. A. Serway, R. J. Beichner, and J. W. Jewett. *Physics for scientists and engineers with modern physics*. David Harris, 2000.

[131] M. Shafizadeh Khoolenjani, M. Kovac, and D. Floreano. Wing design for the self deploying microglider, 2010. Semester project, EPFL.

[132] W. Shen, J. Gu, and Y. Shen. Permanent magnetic system design for the wall-climbing robot. *Applied Bionics and Biomechanics*, 3(3):151–159, 2006.

[133] G. T. Sibley, M. H. Rahimi, and G. S. Sukhatme. Robomote: A tiny mobile robot platform for large-scale ad-hoc sensor networks. In *IEEE International Conference on Robotics and Automation*, pages 1143–1148, 2002.

[134] J. Socha and M. LaBarbera. Effects of Size and Behavior on Aerial Performance of two Species of Flying Snakes (Chrysopelea). *The Journal of Experimental Biology*, 208:1835–1847, 2005.

[135] J. Socha, T. O'Dempsey, and M. LaBarbera. A 3-d kinematic analysis of gliding in a flying snake, chrysopelea paradisi. *Journal of Experimental Biology*, 208(10):1817–1833, 2005.

[136] C. Stefanini, A. Menciassi, and P. Dario. Modeling and experiments on a legged microrobot locomoting in a tubular, compliant and slippery environment. *International Journal of Robotics Research*, 25(5-6):551–560, 2006.

[137] S. A. Stoeter, P. E. Rybski, and N. Papanikolopoulos. Autonomous stair-hopping with scout robots. In *IEEE/RSJ International Conference on Intelligent Robots and Systems*, volume 1, pages 721–726, 2002.

[138] Y. Sugiyama, M. Yamanaka, and S. Hirai. Circular/spherical robots for crawling and jumping. In *IEEE International Conference on Robotics and Automation*, pages 3595–3600, 2005.

[139] R. B. Suter. Ballooning: data from spiders in freefall indicate the importance of posture. *Journal of Arachnology*, 20(2):107–113, 1992.

[140] T. Tanaka and S. Hirose. Development of leg-wheel hybrid quadruped "airhopper" design of powerful light-weight leg with wheel. In *IEEE/RSJ International Conference on Intelligent Robots and Systems*, pages 3890–3895, 2008.

[141] R. J. Templin. The spectrum of animal flight: insects to pterosaurs. *Progress in Aerospace Sciences*, 36(5-6):393–436, 2000.

[142] H. Tennekes. *The Simple Science of Flight*. MIT Press, 1997.

[143] A. L. R. Thomas, G. Jones, J. M. V. Rayner, and P. M. Hughes. Intermittent gliding flight in the pipistrelle bat (pipistrellus pipistrellus)(chiroptera: Vespertilionidae). *Journal of Experimental Biology*, 149(1):407–416, 1990.

[144] D. Thompson. *On growth and form*. Cambridge University Press, 1992.

[145] H. Tsukagoshi, M. Sasaki, A. Kitagawa, and T. Tanaka. Design of a higher jumping rescue robot with the optimized pneumatic drive. In *IEEE International Conference on Robotics and Automation*, pages 1276–1283, 2005.

[146] M. J. Tyler and T. Michael. *Frogs*. Cornell University Press, 1997.

[147] D. G. Ullman. *The mechanical design process*. McGraw-Hill, 2002.

[148] J. F. V. Vincent. Deployable structures in biology. In *Morpho-Functional Machines: The New Species: Designing Embodied Intelligence*, pages 23–40. Springer, 2003.

[149] V. Vitanov, M. Kovac, and D. Floreano. Jump to glide transition, 2007. Semester project, EPFL.

[150] P. Weiss. Hop... hop... hopbots!: designers of small, mobile robots take cues from grasshoppers and frogs. *Science News*, 159:88, 2001.

[151] A.M. Wickenheiser and E. Garcia. Optimization of perching maneuvers through vehicle morphing. *Journal of Guidance Control and Dynamics*, 31(4): 815–823, 2008.

[152] G. D. Wile, K. A. Daltorio, E. D. Diller, L. R. Palmer, S. N. Gorb, R. E. Ritzmann, and R. D. Quinn. Screenbot: Walking inverted using distributed inward gripping. In *Robotics and Automation, IEEE International Conference on*, pages 1513–1518, 2008.

[153] R. S. Wilson, C. E. Franklin, and R. S. James. Allometric scaling relationships of jumping performance in the striped marsh frog limnodynastes peronii. *Journal of Experimental Biology*, 203(12):1937–1946, 2000.

[154] R. J. Wood, S. Avadhanula, E. Steltz, M. Seeman, J. Entwistle, A. Bachrach, G. L. Barrows, S. Sanders, and R. S. Fearing. Design, fabrication and initial results of a 2g autonomous glider. In *IEEE Industrial Electronics Society Meeting*, 2005.

[155] R. J. Wootton, K. E. Evans, R. Herbert, and C. W. Smith. The hind wing of the desert locust (schistocerca gregaria forskal). i. functional morphology and mode of operation. *Journal of experimental Biology*, 203(19):2921, 2000.

[156] K. Wright and R. Lind. Investigating sensor emplacement on vertical surfaces for a biologically-inspired morphing design from bats. In *AIAA Atmospheric Flight Mechanics Conference and Exhibit*, 2007.

[157] A. Yamada, M. Watari, H. Mochiyama, and H. Fujimoto. A robotic catapult based on the closed elastica with a high stiffness endpoint and its application to swimming tasks. In *IEEE/RSJ International Conference on Intelligent Robots and Systems*, pages 1477–1482, 2008.

[158] S. Yanoviak, R. Dudley, and M. Kaspari. Directed Aerial Descent in Canopy Ants. *Nature*, 433:624–626, 2005.

[159] S. P. Yanoviak and R. Dudley. The role of visual cues in directed aerial descent of cephalotes atratus workers (hymenoptera: Formicidae). *Journal of Experimental Biology*, 209(9):1777–1783, 2006.

[160] M. Yim, K. Roufas, D. Duff, Y. Zhang, C. Eldershaw, and S. Homans. Modular reconfigurable robots in space applications. *Autonomous Robots*, 14(2): 225–237, 2003.

[161] B. A. Young, C. E. Lee, and K. M. Daley. On a flap and a foot: Aerial locomotion in the "flying" gecko, ptychozoon kuhli. *Journal of Herpetology*, 36(3):412–418, 2002.

[162] J. Zettler, U. Zettler, and B. Egger. Jumping technique and climbing behaviour of the collembolan ceratophysella sigillata (collembola: Hypogastruridae). *European Journal of Entomology*, 97(1):41–46, 2000.

[163] P. Zhang and Q. Zhou. Voice coil based hopping mechanism for microrobot. In *IEEE international conference on Robotics and Automation*, pages 1783–1788, 2009.

[164] J. Zhao, M. Wang, X. Zang, and H. Cai. Biological characteristics analysis and mechanical jumping leg design for frog robot. In *First International Conference on Intelligent Robotics and Applications: Part I*, page 1080, 2008.

[165] J. Zhao, R. Yang, N. Xi, B. Gao, X. Fan, M. W. Mutka, and L. Xiao. Development of a miniature self-stabilization jumping robot. In *IEEE/RSJ International Conference on Intelligent Robots and Systems*, pages 2217–2222, 2009.

[166] J.-C. Zufferey. *Bio-inspired Vision-based Flying Robots*. PhD thesis, Ecole Polytechnique Fédérale de Lausanne (EPFL), 2005.

[167] J.-C. Zufferey and D. Floreano. Fly-inspired visual steering of an ultralight indoor aircraft. *IEEE Transactions on Robotics*, 22:137–146, 2006.

[168] J.-C. Zufferey, A. Klaptocz, A. Beyeler, J.-D. Nicoud, and D. Floreano. A 10-gram vision-based flying robot. *Advanced Robotics, Journal of the Robotics Society of Japan*, 21(14):1671–1684, 2007.

Publications

Journal publications:

M. Kovač, M. Schlegel, J.-C. Zufferey, and D. Floreano. Steerable miniature jumping robot. *Autonomous Robots*, 28(3):295-306, 2010.

M. Kovač, J. Germann, C. Hurzeler, R. Siegwart, and D. Floreano. A perching mechanism for micro aerial vehicles. *Journal of Micro-Nano Mechatronics*, 2010.

M. Kovač, W. Hraiz, O. Fauria, J.-C. Zufferey, and D. Floreano. Jump-gliding locomotion for miniature robots. *In preparation*, 2010.

Full conference publications:

M. Kovač, A. Guignard, J.-D. Nicoud, J.-C. Zufferey, and D. Floreano. A 1.5g SMA-actuated microglider looking for the light. In *Proceedings of the IEEE International Conference on Robotics and Automation*, pages 367-372, 2007.

M. Kovač, M. Fuchs, A. Guignard, J.-C. Zufferey, and D. Floreano. A miniature 7g jumping robot. In *Proceedings of the IEEE International Conference on Robotics and Automation*, pages 373-378, 2008.

M. Kovač, M. Schlegel, J.-C. Zufferey, and D. Floreano. A miniature jumping robot with self-recovery capabilities. In *Proceedings of the IEEE/RSJ International Conference on Robotics and Automation*, pages 583-588, 2009.

M. Schlegel, M. Kovač, M.Woodward, M. Sitti, D. Floreano. A minimalist jumping and climbing robot, *In preparation*, 2010.

Conference abstract publications:

M. Kovač., G. Savioz, J.-C. Zufferey, and D. Floreano. Towards the Self Deploying Microglider; Gliding Flight and Bioinspired Wing Folding Mechanism. *Proceedings of the International Symposium on Flying Insects and Robots*, pages 61-62, 2007.

M. Kovač, J.C. Zufferey, and D. Floreano. Towards the self deploying microglider, a biomimetic jumping and gliding robot. In *Proceedings of the 4th International Symposium on Adaptive Motion of Animals and Machines*, pages 41-42, 2008.

Book chapter:

M. Kovač, J.C. Zufferey, and D. Floreano. Towards a self-deploying and gliding robot. In Dario Floreano, Jean-Christophe Zufferey, Mandyam V. Srinivasan, and Charlie Ellington, editors, *Flying Insects and Robots*, chapter 19. Springer, 2009.

Patent:

M. Kovač, M. Piorkowski, Dynamic steering methods for jumping robots. *Patent pending*, 2010.

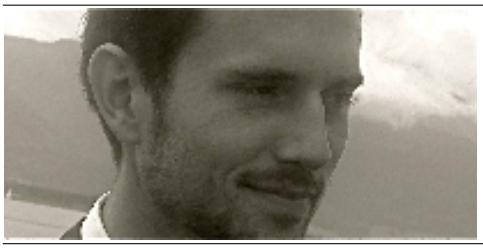

Curriculum Vitae

Mirko Kovač is PhD candidate at the Laboratory of Intelligent Systems within the School of Engineering at Ecole Polytechnique Fédérale de Lausanne (EPFL). He received his M.S. degree in Mechanical Engineering from the Swiss Federal Institute of Technology in Zürich (ETHZ) in 2005 with his master thesis carried out at University of California in Berkeley, USA. During his studies he was research associate with RIETER Automotive Switzerland, the WARTSILA Diesel Technology Division in Switzerland, and CISERV in Singapore. He has presented his work at several international conferences and in journals and has supervised 20 B.A./M.S. level student projects, one of which received the 2008 Foundation Annaheim prize for the best student project. In 2009 he won the JTCF Novel Technology best paper award at the IEEE/RSJ International Conference on Intelligent Robots and Systems (IROS'2009) and the 2009 runner up best poster award at the research day at EPFL. His research interest is the conception and design of novel locomotion and control methods for mobile robots and their analogy in biological systems.